From structure to dynamics and back: The interplay between topology and activity in brain networks

by

Troy Matthew Lau

A dissertation submitted in partial fulfillment
of the requirements for the degree of
Doctor of Philosophy
(Physics)
in The University of Michigan
2011

Doctoral Committee:

Associate Professor Michal R. Zochowski, Chair
Professor Robert S. Savit
Associate Professor Joshua Damien Berke
Assistant Professor Victoria Booth
Assistant Professor Robert David Deegan

To Mom and Dad, who have supported me in everything I have done in life, and who this education would not be possible without

ACKNOWLEDGEMENTS

There are so many people I would like to thank for supporting with me throughout graduate school and the past nine years of my higher education. Most importantly I would like to thank my parents. Mom, you have been by my side since the day I was born. I have always been able to talk to you, whether it be for advice, encouragement, or just somebody to vent to. I'm not sure I could have made it though all of this school without you. Dad, you've always given me the confidence, caring, and strength I've needed. You have been so supportive of everything I have done in school and in life. I owe you two everything. I would also like to thank my step-parents Lori and Dan, you have been nothing but kind and caring to me, and for that I am extremely grateful.

Steph, you are my best friend and my partner. I cannot imagine what the past two years would have been like without you. You've been a shoulder to rest on, a friend to talk to, someone to rant and rave to, a confidant, and always there to give me a hug when I needed one. And to all my wonderful friends; Jordon, Wen, Jon, Candice, Kristen, Gordon, Eric, Dan, Steph M., Tiffany, and Katie, you have all made my last 5.5 years so enjoyable. We have had so many good times together, graduate school would simply not have been the same without you. And a special thanks to Abbie, who I've watched grow from an infant to a wonderful little girl. Your incredible strength, determination, and adorable smile has taught me to always be happy, no matter what you face. Most importantly you've taught me the things and people that really matter in life.

I would also like to thank my lab and in particular my advisor Michal Zochowski, without whom my Ph.D research would not be possible. And to all my lab mates, Sarah, Ben,Jack, Jane, Tony, Liz, and Chris, who have each offered wonderful insight and discussion into my research. I would also like to thank Professor Joshua Berke who's work, advice, and input was vital to my first paper.

Finally I would like to thank the Physics and Biophysics Departments at the University of Michigan for the great curriculum, direction, and financial support. Additionally I would like to thank the NIH and the NIH Molecular Biophysics Training grant (T32 GM008270) for providing two years of support for my research.

TABLE OF CONTENTS

LIST OF FIGURES

Figure

LIST OF ABBREVIATIONS

MPC Mean Phase Coherence

FSI Fast-Spiking Interneuron

STDP Spike-timing Dependant Plasticity

GJ Gap Junction

LAS Localized Activation State

RAS Random Activation State

GSS Globally Synchronous State

CV Coefficient of Variation

GABA Gamma-aminobutyric Acid

PSD Power Spectral Density

RAF Resonate and Fire

IAF Integrate and Fire

CHAPTER I

Introduction

The brain is one of the most remarkably complex systems in nature. Yet, despite the enormous amount of research dedicated to it, it is probably the least understood system. There are 100,000,000,000 neurons in the brain and approximately 7000 connections per neuron. At the fundamental level of a single neuron, it already begins to get complicated; there are hundreds of different types of neurons, each with their own distinct biological properties and functions, with more discovered with every month of new journal articles. Neurons are supported and nourished by an equal number of glial cells, which for a long time, were thought to play only a supporting role in the brain; however, recent research has shown that these cells are integral to cognitive and functional processes [1, 2, 3, 4, 5].

At the next level are the connections between neurons. Connections can be excitatory, inhibitory, modulatory, or otherwise, depending on the cell types involved. On small scales within ensembles of neurons, specific neuronal subtypes form connections to other specific subtypes, within certain distances, and sometimes in specific directions. Other types of neurons innervate (and connect to) all other neuron types, integrating a wide range of input characteristics. On a larger scale, some regions route the flow of information and processing throughout the brain. For example, the basal ganglia is able to 'select' the strongest functional inputs by combining feed-

forward/feed-back connections between layers and utilizing the various arrangements of neuronal subtypes within each layer [6, 7, 8, 9].

To make matters even more complicated, the brain is constantly changing. On the cellular level, through a process called neurogenesis, new neurons are being born in the olfactory bulb[10, 2, 11] and hippocampus well into adulthood [12, 13, 11]. A growing and expanding area of research, the study of neurogenesis has helped overturn the widely held assumption that a brain contains all the cells it will ever need at birth. In the hippocampus, these cells integrate with existing neuronal ensembles and are believed to assist in the formation of new memories [14, 15]. Changes on the network level occur through synaptic plasticity, the strengthening and weakening of connections between neurons. Again in the hippocampus, where short term memories are stored, memory traces are constantly being modified and overwritten with new ones via the modification of synapses [16, 17, 18, 19]. Over the past 60 years, after the concept of the modification of neuronal connections was introduced by Hebb, the understanding of the brain as a highly adaptable and modifiable system has only grown. These ideas are now essential to our understanding of learning and adaptation through experience.

Beyond all the biological components and network structure lies the true complexity of the brain, in that the brain is constantly changing over time, both rapidly and in the long term. These dynamics arise from shifts in activity on the neuonal firing rate level, all the way to the routing or flow of information between brain regions. This is in contrast to other networks such as social and computer networks, which remain static over periods of time that allow for study. In the simplest reduction, the brain is a network of coupled oscillators (neurons)... about 100 billion of them. Then to say that the brain would be chaotic and unpredictable would be an immense understatement. To make things even more complicated, the brain's activity is continuously being altered by its surroundings. When awake, the brain is interacting

with the environment, acquiring sensory and cognitive data, and processing this information to respond with appropriate actions. From autonomic functions, motor responses, and cognitive processes, changes in the brain's activity allow an individual to perform a diverse and complex range of tasks. It is this range of dynamics that allows a child to learn math in a classroom at one moment and play soccer at recess the next moment. The brain is just as active when asleep, as it uses this state to encode memories and experiences [20]. Research has even shown that the hippocampus and neocortex replay the same patterns of activity from the previous day while asleep to store memories [21, 22, 23]. This introduction will briefly discuss some of the experimental methods used to measure these dynamics, as well as the different time and length scales relevant to them.

Many of the questions about the brain posed 50 years ago still remain. What is the cellular/structural foundation of a memory, and how is it stored and recalled? How are different things such as colors, sounds, faces, and locations integrated into complete images? How does the brain effectively determine what aspects of everyday experience to learn and record and which to not? How are decisions made quickly and effectively, utilizing (and learning from) past experiences? What we have learned is that structure and dynamics play a much bigger role than neuroscientists once considered. The utilization of the mathematical concepts of graphs/networks is rapidly becoming appreciated as a way to understand the structure of the brain [24, 25, 26]. The use of measures previously designed for other complex physically interacting systems has given us insight into and allowed us to resolve interactions and brain states we would have never seen previously.

The goal of the work in this dissertation is to first understand the interactions between the cellular and network levels in the brain and second to understand how the resultant neuronal activity plays a role in function. This is primarily done though computational (computer) models with some analysis of *in vivo* data. Chapter II

investigates the network topology of gap-junction coupled cells and the resultant dynamics. The results are put in the framework of the basal ganglia, the brain region associated with action selection and decision making [27]. The results from these simulations are shown to compare well with novel data from the Berke lab regarding the basal ganglia [28]. Chapter III demonstrates the drastically different dynamics that are possible when varying network properties are combined with oscillatory currents in a heterogeneous neuronal network. These results are very pertinent as the role of oscillations in the brain is a major active area of research today. Finally, chapter IV presents a novel mechanism where neurons with the ability to classically resonate and shift this resonance frequency in response to a depolarization, can provide the ideal basis for efficient learning. This occurs because the spatio-temporal patterning of network activity is highly specific and uniform for these neurons, providing the ideal conditions for spike-timing dependent plasticity-based learning.

The following sections are only a brief introduction to the biology and physics used in this dissertation; the specifics are left to the chapters themselves. The biology will cover the basics of neurons, synapses, axons, dendrites, and neurotransmitters. The physics and mathematics will cover the basics of networks and their usefulness in understanding the brain. The final sections will give an introduction to three open questions in neuroscience today that will be addressed by the chapters.

1.1 The neuron

The neuron is the fundamental cell of the brain. It can be thought of as a single processing unit, where larger and larger groups of neurons/units are able to carry out more and more complex computations. Figure 1.1 shows the basic structure of a typical neuron, though there are numerous different types that can look very different from this model. When the neuron receives no inputs, the cell body of the neuron, or soma, is in a state of electrochemical equilibrium where the ionic concentrations

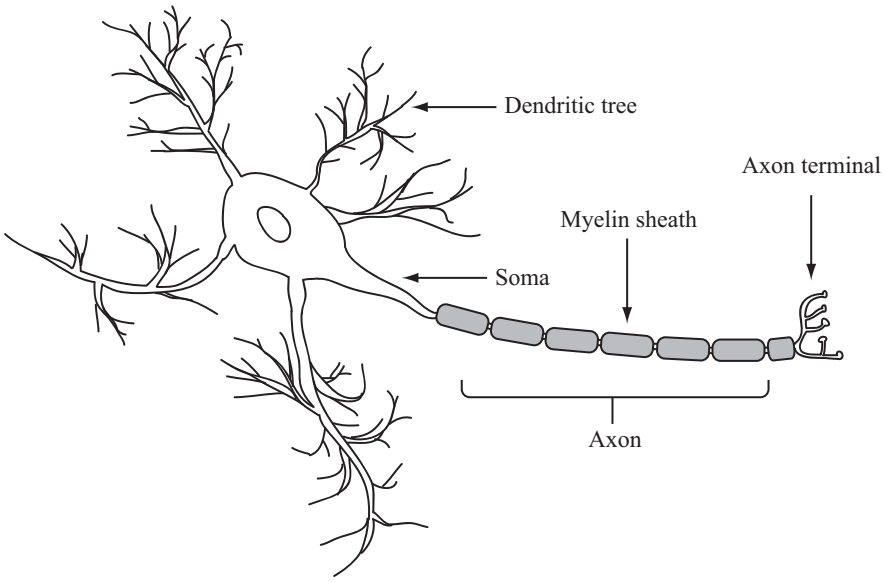

Figure 1.1: Model of a typical neuron. The dendritic tree is where the neuron receives input from other neurons. This structure can vary greatly in size and complexity and correspondingly can influence the functional properties of the neuron. The soma is where inputs from the dendrites are integrated and the action potential is generated. The action potential then travels down the axon, the output component of the neuron. The speed and efficiency of the action potential is greatly enhanced by the myelin sheath and nodes of Ranvier insulating around the axon.

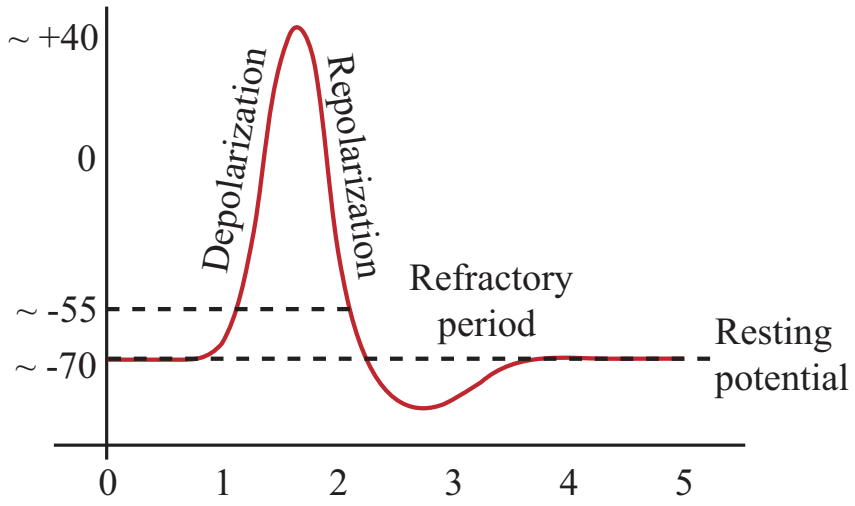

Figure 1.2: Action Potential. Initially a neuron is in electrostatic equilibrium at 70 mV. If sufficient excitatory input current is received, the neuron depolarizes via an inward flow of sodium ions. This occurs until an outflow of potassium ions causes the neuron to repolarize. The neuron overshoots its original resting potential and requires 3 ms to come back to rest. During this refractory period the neuron is not able to receive any input or fire action potentials. Certain neurons, like fast-spiking interneurons, have much faster action potentials and briefer refractory periods.

of sodium, potassium, calcium, and chloride rest at 70 mV. The soma is also where synaptic inputs from the dendrites are integrated and this equilibrium is broken, generating an action potential. An action potential is characterized by the rapid depolarization, via the inflow of sodium ions, and repolarization, via the outflow of potassium ions, of the cell followed by a refractory period where it is not able to fire another action potential (Figure 1.2). The influx and outflux of these ions are gated by conductance channels. For example, Na has two conductances, one near the resting potential and one near the top of the action potential. The in/outflux of these ions switch at their reversal potential, preventing runaway hyperpolarization or depolarization. In a typical neuron this entire process takes 4-5 ms, but for certain neurons, such as the fast spiking interneuron, it may happen much more quickly [29, 30].

One of the most complete mathematical models used to describe the anatomy and

dynamics of a neuron is the Hodgkin and Huxley Model [31, 32, 33]. There are many variants, which can include an arbitrary number of ion channels and compartments, but a relatively common one is presented below. It is a two compartment (s - soma, d - dendrite) model where,

the somatic compartment is described by:

$$C\frac{dV^s}{dt} = -I_L - I_{Ns} - I_{Kdr} - g_c(V^s - V^d) + I_{noise}, \tag{1.1}$$

the dendritic compartment is described by:

$$C\frac{dV^d}{dt} = -I_{L,d} - g_c(V^d - V^s) + I_{ext}, \tag{1.2}$$

where the currents are $I_L = g_L(V^s - V_L)$ is the somatic leak current, $I_{L,d} = g_L(V^d - V_L)$ is the dendritic leak current, $I_{Na} = g_{Na}m_\infty^3 h(V^s - V_{Na})$ is the sodium current, and $I_{Kdr} = g_K n^4(V^s - V_K)$ is the delayed potassium current. V_L, V_{Na}, and V_{Kdr} represent the leakage, sodium, and potassium reversal potential respectively while g_L, g_{Na}, m, h, g_K, and n control the conductance channels for those currents. Chapter 3 uses this model briefly to study the interaction between single neuron and network resonances.

1.1.1 Anatomy

1.1.1.1 Chemical and electrical synapses

The most common type of neuron to neuron connection is the chemical synapse. It is formed between the axon of the pre-synaptic cell and the dendrite of the post-synaptic cell at a junction called the synaptic cleft (Figure 1.3A). The chemical synapse is only activated when a pre-synaptic neuron fires an action potential (Figure 1.2), triggering a cascade of neurotransmitters to be released across the synaptic cleft. There are three primary types of chemically-mediated synapses: excita-

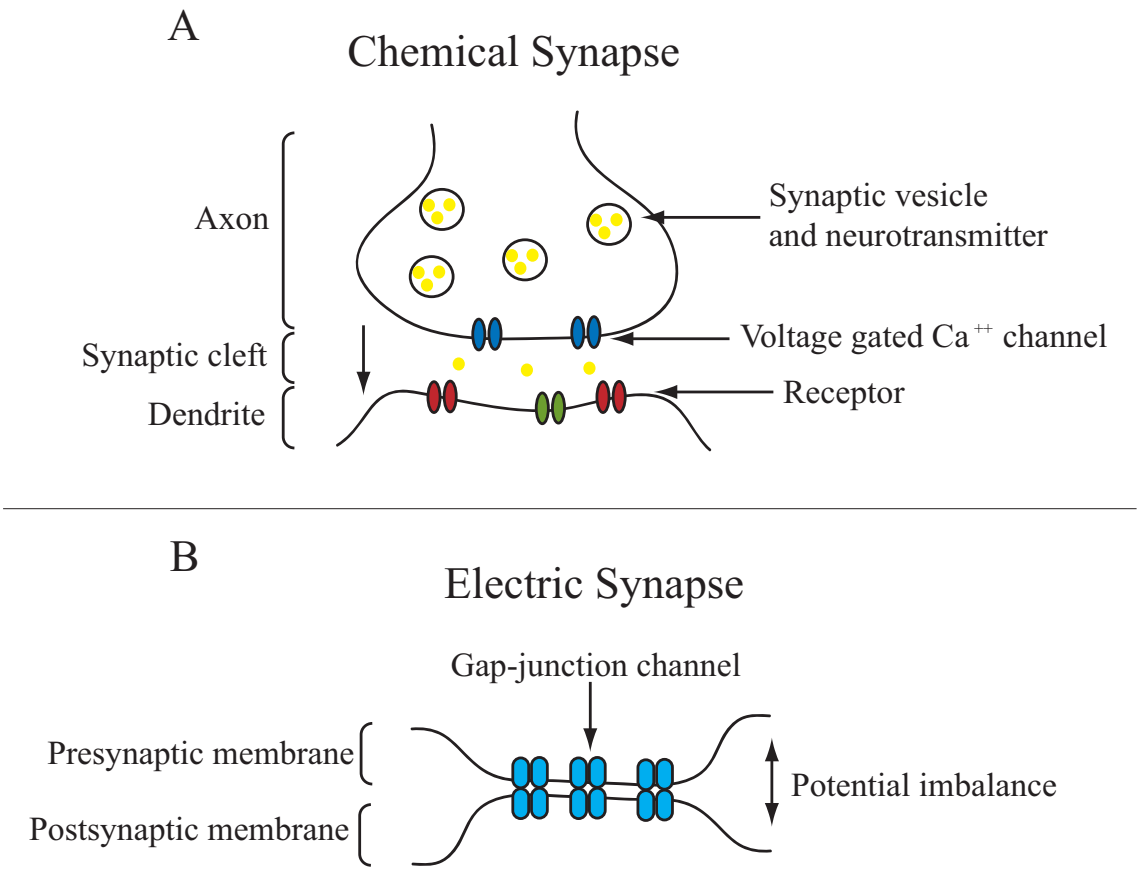

Figure 1.3: Chemical and electrical synapses. A - The chemical synapse is shown. During an action potential, the neurotransmitters travel in vesicles across the synaptic cleft from the pre-synaptic axon to the post-synaptic dendrite. The pre-synaptic cell determines whether the connection is excitatory, inhibitory, or modulatory. The action potential may backpropogate down both the axon and dendrite of the pre- and post-synaptic cells, a vital mechanism in neuronal plasticity. B - The electrical synapse or gap-junction is shown. Here ions travel freely across the channel, allowing the contacting cells to equilibrate their membrane potentials. This connection is bi-directional and occurs in the absence of any action potential.

tory, inhibitory, and modulatory. Excitatory connections, commonly mediated by glutamate, depolarize the post-synaptic neuron leaving it more likely to fire. Inhibitory connections, commonly mediated by gamma-aminobutyric acid (GABA), cause a post-synaptic cell to polarize, leaving it less likely to fire. All of the chemical synapse-specific work in this dissertation focuses on these two types of connections. The third type of connection covers a wide family of neurotransmitters/channels associated with modulatory effects on post-synaptic cells. One of the most common of these is dopamine, a neurotransmitter that can affect the sensitivity of specific channels [34]. In addition to the type of connection being specific to the pre-synaptic neuron, each neuron typically expresses one type of neurotransmitter, meaning it can only mediate one type of chemical connection.

The second type of connection between neurons is the electrical synapse or gap-junction [35, 36, 37, 38]. The gap-junction is a direct connection between two cells' membranes or proximal dendrites, by which ions can freely pass Figure 1.3B [39, 40]. A diagram of the gap-junction connection is shown in Figure 1.3b. The gap-junction is distinct from the chemical synapse in three important ways. First, the activation of this synapse does not require an action potential but is instead caused by an imbalance of the membrane potentials of the two neurons, causing ions to flow to equilibrate this imbalance. The second distinction is that there is no defined permanent pre/post synaptic cell; the gap-junction is bi-directional. The third distinction follows from the first two, and is that there is no excitatory/inhibitory distinction. Whether one cell will depolarize or hyper-polarize another is simply dependent on their relative membrane potentials. All together, these properties have an important influence over brain activity. The most significant effect is that these cells encourage synchronization of firing activity, not only amongst themselves but between other neuronal types that they are connected to [41]. Historically, gap-junction connections were thought to be rare in the brain, but recent studies have demonstrated that they are far more

prevalent and important that once believed. This makes understanding the behavior of these connection types that much more important [42]. Chapter II will discuss them extensively and present computational work using them.

1.1.1.2 The axon

The axon is the primary output mechanism of the cell through which the action potential travels. It is characterized by a long, thin projection that may stretch anywhere from $< 1mm$ to one meter, as in the case of spinal cord motor neurons. To overcome the potential for signal loss over long distances, axons are usually coated with a myelin sheath which is broken into sections by the nodes of Ranvier. These myelinated sections act as insulated capacitor-like segments, causing the action potential to 'jump' along the axon and propagate faster than it would continuously.

At the end of the axon is the axon terminal, where it makes a connection with the dendrites of other neurons. While each neuron may have only one axon (some have zero) the terminal(s) allow for connections to multiple post-synaptic cells. An extensive discussion and quantitative detail on the electrophysiology of axonal fibers can be found in Hodgkin and Huxley's seminal work [31, 32, 33].

1.1.1.3 The dendrite

Post-synaptic to the axon, the dendrite is the primary receiving mechanism of the neuron. It has a branched tree-like shape and each neuron may have numerous dendritic projections, with the entire structure called the dendritic tree. Some neuron types, like the granule cell, may have small and simple dendritic trees, while others, like the Purkineje cell, may have large, complex, and highly innervating trees. The size of these trees is not random but serves distinct functional purposes in their specific brain regions.

Each dendrite receives input from the axon of another cell via the synapse (see

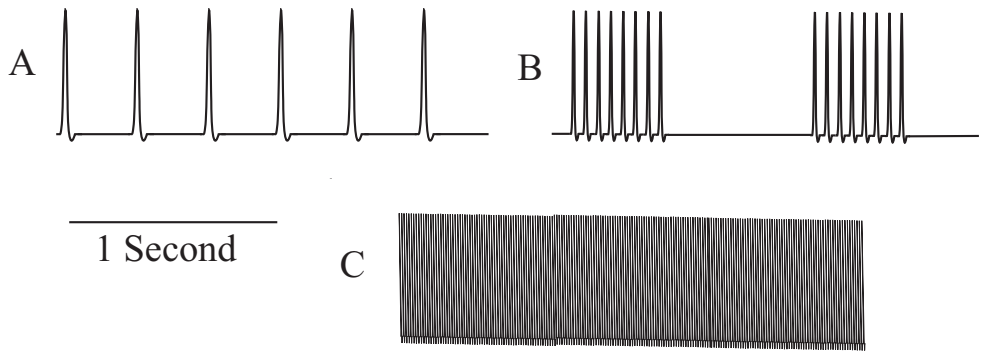

Figure 1.4: Neuronal Firing Patterns. A - Tonic or regular spiking pattern. B - Phasic or bursting spiking pattern. C - Fast-spiking pattern

Synapse). The input is transformed into an electrical cascade and travels down the length of the dendrite from the synapse to the soma. The electrical transmission through the dendrite is well described by passive cable theory, first developed by Hermann and Cramer in the late 19th century, and further refined by numerous other scientists [43]. When the combined input from all synapsed dendrites reaches the soma, it is integrated.

1.1.2 Neuronal dynamics

The neuron is capable of a wide range of voltage dynamics in response to the synaptic current it receives from other neurons. These dynamics are dependent on both the properties of the neuron itself, and characteristic of the current it receives. Starting with the output of a neuron, there are three common classifications of neuronal discharge (action potential) patterns. Tonic or regular spiking neurons [44, 45] fire constantly in response to uniform input currents, and typically have the slowest firing rates. Accordingly, these neurons are capable of a wide range of different firing rates, dependent on the specific value of the input current they receive [46]. Phasic neurons fire in rapid bursts in response to a current [47]. Phasic firing patterns can create shifting states of excitation and inhibition which may generate some of the oscillations seen in the brain [48, 49]. Finally, fast-spiking neurons are able to fire

at constantly high firing rates which can provide a constant inhibitory suppression of large populations of neurons [30, 50, 45, 51]. Figure 1.4 shows qualitative examples these three firing patterns.

In addition to the variety of spiking patterns a neuron is capable of, the dynamic properties of the extracellular current input to a neuron also greatly influence the activity of the neuron. Among the most prevalent and well studied of these, especially from a physical perspective, are the resonant properties of neurons and the external oscillations they may produce [52, 53]. In this section, I will discuss two classifications of neurons, non-resonating and resonating neurons, and the computational models that can be used to describe these types. The resonance response has been attributed to the generation of many of the oscillations measured throughout the brain [54, 55, 52].

1.1.2.1 Oscillations and the resonance properties of neurons

In a real neuron, or equally complex biological model, a number of voltage gated channels control the outflux and influx of ions into the cell. These channels act like the resistor, inductor, and capacitor elements in a circuit, giving the neuron the dynamic properties of an oscillator. These oscillatory properties are not transient effects, but play a significant role in the functioning of the brain [56, 57, 58, 59, 52, 56, 60, 61, 62, 63, 64]. At the sub-threshold/sub-firing level, oscillatory input current can coordinate the voltages of larger populations of neurons through phase synchronization of the oscillatory neurons. This coordination can provide windows of activity to gate cognitive function and other processes.

An even more interesting phenomenon can occur if this input frequency matches the neuron's fundamental frequency set by the properties of the ion channels. In this range, the neuron can exhibit a classical resonance frequency. Not every neuronal subtype exhibits a resonance frequency, but there is significant evidence that some

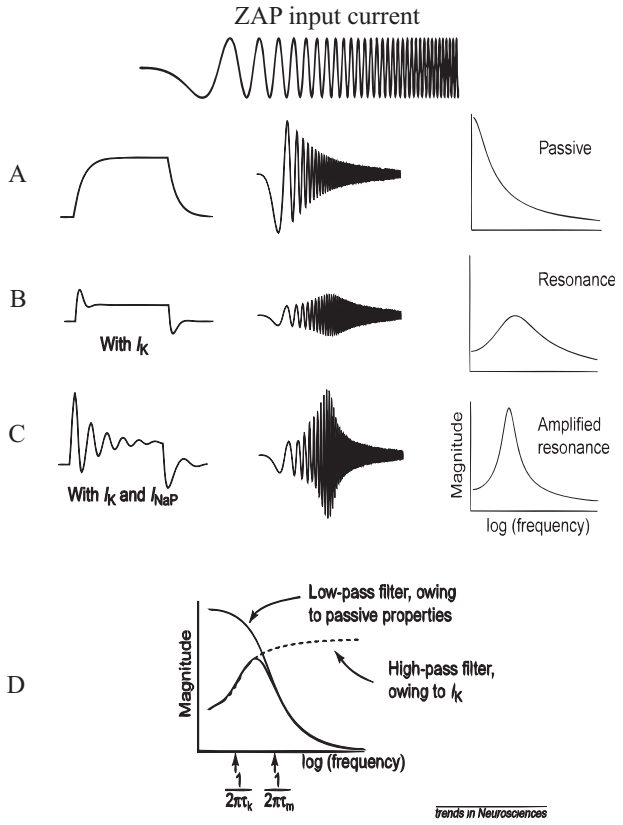

Taken from 'Resonance, oscillation, and the intrinsic frequency preferences of neurons' by B. Hutcheon and Y. Yarom.
Trends in Neurosciences, Vol. 23 No. 5, 2000

Figure 1.5: Properties of Neuronal Resonance. Left column - Response to a constant subthreshold depolarizing current. Center column - Response to ZAP current. Right Column - Impedance profile. A - Passive response of neuron. B - Weak resonance condition. C - Enhanced resonance condition D - Determining the frequency window of resonance. This figure was taken from [52]

neurons can resonate classically [54, 65, 66, 67]. The resonance properties of real and simulated neurons are commonly investigated via ZAP and patch-clamp ZAP currents [68, 65, 69]. The ZAP current is a frequency-space based analysis where the frequency of an input current is increased over time to elucidate any impedance responses and help us understand the different damping effects that the currents can have. The resulting voltage response is then the impedance of the neuron, and any bounded peaks in this impedance suggest a resonance effect. Here we will investigate the properties of a neuron necessary to generate these resonances. This discussion is drawn from work by Hutcheon and Yarom [52] and Izhikevich [53].

The first step to inducing resonance in a neuron is that it must exhibit the properties of a low-pass filter. This is achieved via the leakage current and membrane capacitance. Figure 1.5A demonstrates the impedance profile of such a neuron. If a neuron is dominated by the membrane and leakage time scales, or if the model is designed with only these properties, then this alone will not allow it to resonate. A commonly used model, and one used in Chapters 2 and 3 of this thesis, which displays these properties is the leaky integrate and fire model [70],

$$\tau_m \frac{dV}{dt} = -V(t) + RI(t) \tag{1.3}$$

where τ_m is the membrane time constant, V is the membrane voltage, R is the resistance, and I is the current. Such a neuron's impedance will decay with increasing frequency of current input (Figure 1.5A right) and act as a low-pass filter. This is because the membrane cannot respond to fast changes in the external current, thus increasing frequencies will only serve to lower the voltage response of the neuron.

In order to achieve a weak resonance condition, the properties above must be coupled with a current that actively opposes and activates slowly in response to a change in voltage (Figure 1.5B). Here the impedance peaks at a specific intermediate frequency range. In the neuron, the delayed potassium current (I_K) provides this

mechanism. This current is analogous to the gravitation force on a pendulum and the spring constant, except that its response is delayed. I_K allows the neuron to equilibrate its voltage in an oscillatory fashion, thus setting the time scale for the resonance frequency itself.

Unfortunately (to those who really desire resonance in neurons) the I_K makes achieving resonance more difficult while concurrently making it possible. This is because I_K significantly dampens the voltage response of a neuron, making the resonance response weak and intrinsically difficult to achieve. Fortunately, the neuron has mechanisms to enhance this resonance as well. This is achieved through 'persistent' I_{Na} channels or I_{NaP} channels that act in a similar way to the depolarizing typical I_{Na} current by activating and enhancing the voltage changes in a neuron. Figure 1.5C demonstrates how this current enhances resonance.

In computational neuroscience, these properties can be achieved through a model like the Resonate-and-Fire neuron [71], or through a properly parameterized Hodgkin and Huxley neuron [32, 33] amongst a variety of other models. I use the resonate and fire model in Chapter 4 of this thesis. The equation for such is,

$$\frac{dx}{dt} = bx - \omega y \tag{1.4}$$

$$\frac{dy}{dt} = \omega x + by \tag{1.5}$$

where x and y are the internal state variables, ω scales the resonance frequency, and b the voltage response. It is important to understand the distinction between 'integrators' (Equation 1.3) and 'resonators' (Equations 1.4, 1.5). Integrators simply add up the input current at some rate dependent on the leakage. Resonators oscillate from input current changes and have intrinsic frequency preferences. The use of either will introduce a different set of dynamics into the neuronal network system, and

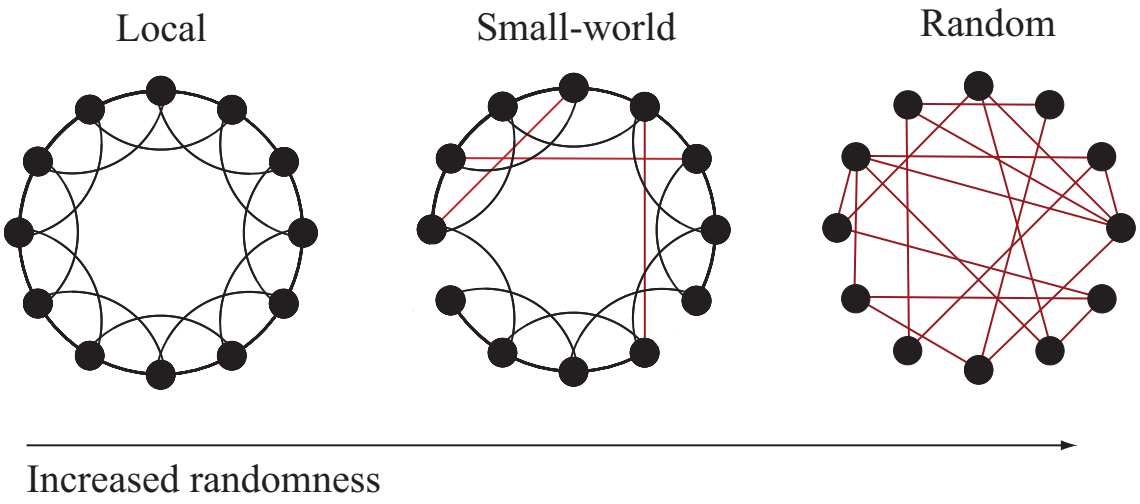

Figure 1.6: The Watts and Strogatz paradigm for small-world network design. First a network with periodic boundary conditions is connected locally (to its two nearest neighbors on each side in this case). The network is then partially rewired satisfying a small-world condition dependent on its initial rewiring radius. Finally a network is completely rewired leaving a randomly coupled network.

selecting the proper model is dictated by the properties one is trying to understand.

It is important to note however, that these properties are only valid for oscillatory currents where the mean input is zero, $\langle I_{oss} \rangle = 0$. In an interesting paper by Izhikevich [53], he studied the response of neurons to periodic depolarizing 'bursts'. These bursts have positive currents, and hence only depolarize neurons. In this case the integrate and fire type of neuron will in fact depolarize more with higher frequency currents because the more frequent the spikes, the more the current behaves like a constant. Alternatively, a periodic burst into a resonating neuron will still resonate with spiking at the proper frequency. Such a distinction is important because both depolarizing bursts and oscillations are prevalent throughout the brain.

1.2 Complex networks

Large scale interacting networks are common across biology, physics, technology, finance, and society. Whether it be the brain, spin-glasses, the Internet, the stock

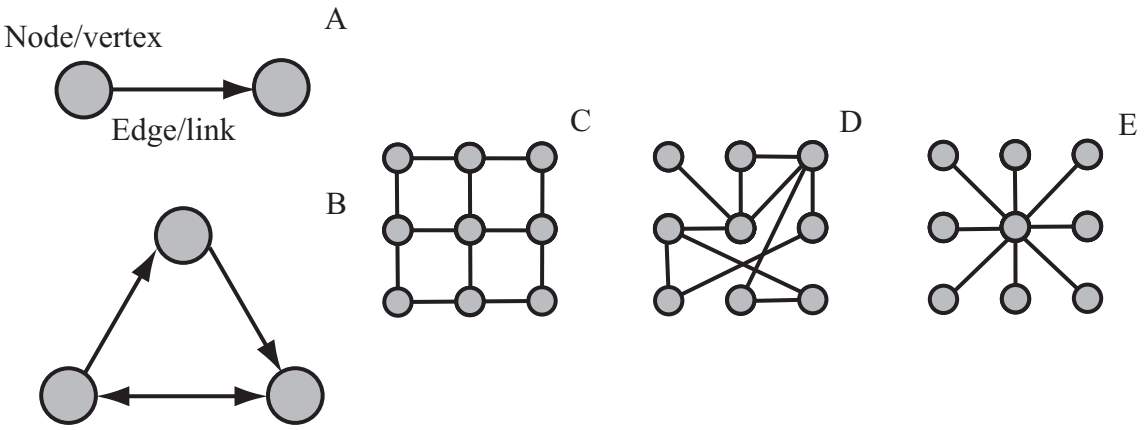

Figure 1.7: Basic network design concepts. A - A directional connection between two verticies via a link. B - One and two way connections between a trio of verticies. C - A locally coupled network. D - A randomly coupled network. E - A network featuring a hub vertex.

market, or a senior class in high school, interacting elements form systems with complex activities [72]. Understanding the behavior of these systems, called graph theory in mathematics, has been gaining more and more prevalence in the scientific community, especially with advances in computers and the complicated models that can be tested on them. Work in this field is approached by designing complexity at the nodes of these networks (i.e. a 17 compartment Hodgkin-Huxley neuron model) and/or in the complexity of the connections themselves (i.e. social networks). Furthermore, by including large numbers of nodes and connections in computer simulations of theses networks, population dynamics can be measured directly rather than inferred from smaller scale approximations. The work in this thesis focuses on the intersection between these three approaches. In the following sections, we will give an overview of previous work in this field as well as the biological basis we have used in modeling the neuronal networks of the brain.

1.2.1 Basic network design

In graph theory the basic element of a network is called a *vertex* or *node* and the *edges* are the links between them Figure 1.7A. In the case of a brain network model,

these vertices are neurons and the edges are the axonal and dendritic connections. Network connections may be independent of direction (such as social networks of friends or gap-junction networks in the brain) or have distinct directionality between them (like epidemiological networks or chemical synapses). Such specifications are important because the dynamics of these networks depend greatly on the flow and direction of information (Figure 1.7B).

Beyond connections between pairs of vertices is the larger scale connectivity in the network. The network topology, architecture, or structure as it is typically called, refers to the overall arrangement of connections. The 'degree distribution' is used to quantify this connectivity and is defined as the number of connections (N) per vertex plotted against the probability that a vertex will have N connections. Figure 1.7C demonstrates a simple network with regular or local connectivity. Here connections are only made between 'nearest neighbor' vertices. Figure 1.7D demonstrates another common topology with random connectivity. Here vertices have equal probability of being connected anywhere within the network. Finally, Figure 1.7E demonstrates a hub topology. Here all vertices are linked via a single hub, or central vertex. A common example of this would be the airport network in the United States. Recent work by Perc [73] demonstrated that single oscillating hub cells can act as pacemakers and set the frequency of the entire network. An extension of this architecture is called a scale-free network where the degree distribution follows a power law, with only a few vertices making many connections. Since the work in this thesis does not cover this type of topology, we refer the reader to [74, 72] for further discussion.

1.2.2 Small-world networks

In the seminal work by Watts and Strogatz, they present a methodology of not only designing networks, but defining their structure by those design parameters [75]. This idea was based on the small-world experiment performed by Stanley Milgram in

1967 [76]. Milgram sent out letters to random people across the United States with the explicit instructions to mail the letter to a specific individual in New York, if they happened to know him. If they didn't know him, they were instructed to send the letter to an acquaintance they thought might know him (i.e a friend in New York or another mail carrier). Milgram found that, on average, it took only six mailings of the letter, or six connections, to reach this specific person. These are called small-world networks, and this paradigm is the foundation for the design of the brain networks in this thesis. In building a small-world network, one begins with completely local connectivity and rewires a percentage of these connections anywhere in the network. Within an intermediate range of rewiring probability, depending on the initial wiring parameters, the network achieves small-world properties. This means that there are a large number of local connections and a small number of random connections that stretch across the network. This creates a topology where it will only take a few number of links to trace from one vertex to any other vertex in the network. In the brain, many different areas have been classified as small-world networks. These include regions of the cortex, hippocampus, and the basal ganglia to name a few [77, 78, 79]. In Boccaletti's review on complex networks, he classifies the parameters of a number of small world brain networks [72]. I will leave a technical discussion of this to Chapter II, however Figure 1.6 demonstrates this design.

1.2.3 The network dynamic: Synchronization and oscillations

What happens when goods/money change hands at different rates in an economic system? How long did it take Milgram's letters to reach the mail carrier in New York? How long does it take information to filter through the basal ganglia? All of these become realistic considerations once we realize that not all networks are static systems. In the brain, the neurons/nodes are dynamic and their states shift over time. Milgram's letters took a longer time to reach their destination if they had further to

travel, meaning the vertices were time dependent. One phenomenon that can result from this is synchronization. Imagine if I, in Ann Arbor, MI, decided to mail two sets of letters. The first set went to everybody in San Francisco, CA and second went to everyone in New York City, NY. If I mailed these letters on the same day, then (assuming a uniform mail service) everybody in New York would simultaneously receive a letter in a couple of days, and everybody in San Francisco would receive their letters a few days after that. Therefore, there will be a synchronous receipt of letters by everybody in New York and, a few days later, a synchronous receipt in San Francisco.

Consider again New York City and San Francisco. Now imagine I mailed everybody in New York and told them to send a letter to everybody in San Francisco, who, in return, would send letters back to New York. This process would repeat itself every time somebody received a letter, and say it took five days for these letters to travel across the country. What I would have generated is an oscillation of mail flowing across the country with a period of ten days, where the travel delay sets the frequency of the oscillations. This concept of network-generated oscillations is fundamentally different than those generated by individual units. It has been proposed as the generator of a number of rhythms in the brain, especially slower rhythms that are longer than the time constants of individual neurons [80, 81, 82]. This subject will be of significance to the work in Chapter IV.

1.3 Neuronal network dynamics: The anatomical vs. functional structure at different scales

In reality the brain cannot be understood by simply mapping a network topology or by determining the properties of a single neuron. The true nature of the brain's biological structure lies at the intersection of the two. Neurons are integrated into

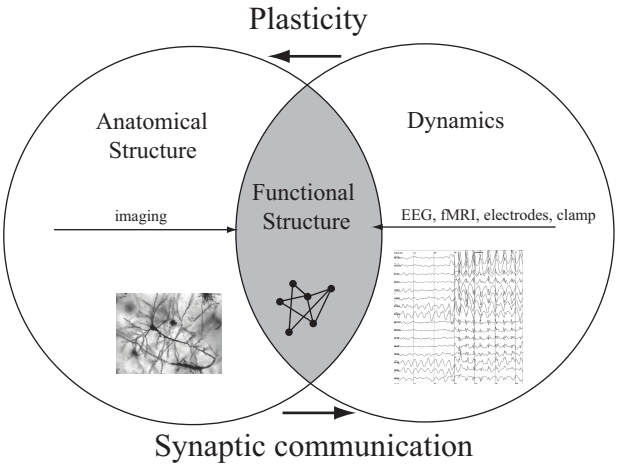

Figure 1.8: Functional Structure Diagram. Diagram showing the overlap and interplay between anatomical structure, dynamics, and functional structure.

complex networks that can behave drastically differently with modifications to either. In fact, the brain's proper functioning is so intricately dependent on both that the failure of either cellular or structural/connectivity mechanisms result in the neurological diseases we are so familiar with today. The problem is that, in trying to combine already biologically complicated neurons with equally complicated networks leaves us with an immensely complex neuronal network structure. To surmount these challenges we must make simplifications and reductions about the brain system we seek to understand. This will allow us to construct reasonable models on which simulations and analyses can be performed on appropriate time scales and computing power.

One of the most effective ways to simplify the understanding of the brain is to differentiate between anatomical and functional structure. Firstly, anatomical structure is just that, the actual network structure that the axons and dendrite makes in the brain. Every image that is published regarding fixed (fluorescent) stained neurons and connections, shows the anatomical connections within networks of the brain. In the context of this thesis, much work has been dedicated to the understanding of anatomical structure in the striatum [40, 83], the hippocampus [36, 84, 85], and the cortex [37, 86, 87, 88, 89].

The anatomical structure is not the whole story. Physical synapses may be silent, others may be significantly stronger than others, and neurons can have strong influences over others while not being physically connected. These considerations have lead researchers to study the functional connectivity in the brain [90, 79, 78, 91, 92, 93]. Functional connectivity is measured by methods that consider the dynamics of the brain networks themselves. The underlying paradigm is that neurons, networks, or regions that are functionally coupled will either have correlated or causal dynamics indicating a connection between the two. A vast array of different measures has been designed to understand the functional relationship between two neurons/networks/regions. These include mean phase coherence [94], causal entropy [95], information integration [96], functional clustering [97], and transfer entropy [98], to name a few. It is important to understand the differences between these two types of connectivities because, while the anatomical connectivity lays the structural framework throughout the brain, it is the functional connectivity that determines the overall activity. Figure 1.8 qualitatively describes this relationship.

1.3.1 Scales and regions in the brain

By dividing the brain into different functional regions and subregions, and understanding how these regions interact between different size scales, we can further simplify our understanding of the brain. The classifications have obviously become more refined over time but the concept remains the same. They arise because of historically difficult experimental/clinical challenges in recording whole brain activity and the more modern computational challenges of simulating the brain. Experimentally, it is impossible to measure the behavior of the entire brain while concurrently measuring the activity of each individual neuron. Computationally, with even the most complex computers, it is (nearly) impossible to model every single neuron and connection, while completing this task in a reasonable amount of time (though re-

searchers are trying, see Whole Brain Project). Conceptually, or theoretically, the behavior of even the smallest subunits of the brain seems to vary so greatly that the integration of these units has proven an immense challenge to understand. Here I will discuss the four major size scales commonly delineated in research, and how I use some of them in my computational work. I will also discuss their relevance both anatomically and functionally; however, note that these size distinctions are purely transient, and can vary greatly in their actual physical sizes.

To start at the biggest scale, the whole brain is itself a network of four classically anatomically and functionally defined regions. The brainstem can be thought of as an output and input node. It receives sensory input from the peripheral nervous system and controls movements downstream of the spinal cord. The diencephalon contains components such as the thalamus that regulate and filter activity. The cerebellum is the primary motor control area of the brain. Finally, the cerebrum contains the cortex, frontal lobes, and basal ganglia regions responsible for cognitive processing, decision making, and memory storage, amongst other processes. At this scale, brain regions are not connected randomly, instead each connection serves a particular purpose to route information throughout the brain. In the lab or clinically, these large-scale regions are typically recorded via electroencephalography (EEG) [99] or magnetic resonance imaging (MRI) techniques [100]. The former benefits from high temporal resolution while the latter from spatial resolution. Even an MRI however, is spatially limited to sub-regions of the cortex while the EEG cannot distinguish single spikes due to noise and filtering. These limitations only allow us to average the activity and interaction of large-scale regions; however, often times, as in the case of the basal ganglia or hippocampus, important processes are occurring at smaller scales and shorter times.

The next step down in size is the level of certain brain regions. Experimentally, the functional connectivity can be determined by applying measures using data from

intracranial EEG [101, 102, 103, 104], fMRI [105, 106, 107] or similar techniques. On the other hand, the anatomical connectivity is often determined by examining slice preparations. From the functional recordings we can determine the interactions between subregions like the CA3, CA1, and dentate gyrus of the hippocampus with invasive techniques that still allow the subject to freely interact with its environment. Coupling these interactions with the anatomical connectivity allows the development of corresponding network models. These models can even begin to include single neurons and their complicated dynamics. But typically, these models are still greatly reduced, for example modeling 1000 neurons in place of 1 million. Regardless of this, recent computational modeling work at this scale has contributed greatly to our understanding of these subregions.

The next scale is the level of groups of neurons, or neuronal ensembles, which is where most of the research in this thesis lies. It is also the scale where we can most easily classify the anatomical topology of neuronal networks (e.g. small-world). Within each structure of the brain lie different layers or areas, depending on the overall design. These layers or areas typically contain a limited diversity of neurons, some of which interact with other layers/regions, and others where connections remain within those areas. At these scales, statistical mechanics describe the network topology, and connectivity is understood via percentages and probabilities. *in vitro* slices and cultures have provided much insight into the anatomy of these groups of neurons. To measure dynamics, these areas may be studied *in vivo* via the use of tetrodes [108] and *in vitro* via multi-electrode arrays [109, 110]. These measurements can then lead to various determinations of the functional structure, as discussed above. From a modeling perspective, this scale is quite tractable. Many computational studies have been performed on these scales with varying complexities of neurons. In Chapter II, I will specifically investigate the striatal subregion of the basal ganglia to understand the properties of gap-junction coupled networks. I will demonstrate how the anatom-

ical structure of the gap-junction connections clearly dictates the resultant dynamics, transforming a homogeneous anatomical structure into a heterogeneous functional structure and activity pattern.

Finally, we arrive again at the scale of individuals or pairs of neurons. Via patch clamping techniques, the membrane potential interactions between cells can be performed at very precise levels. Anatomical structure is relatively simple at this level, but the different interactions between similarly connected neurons can provide enormous insight into different functional connections. Computationally, immensely complex and realistic neuron models can be employed to study the interactions between pairs of neurons. While these studies may be valuable in understanding the effects of firing rate, phase responses, and modulations, they lack the network structural complexity to elucidate any advanced functioning that occurs in the brain.

1.3.2 Selecting specific properties of brain activity

From the discussion above, it is clear that there are a tremendous amount of interactions going on at all scales of the brain. Arising from all these interactions are numerous properties and characteristics of activity that can be measured. Determining which characteristics are important will dictate the necessary complexity of the neuron and network model to be designed. For example, it may not be necessary to integrate neuronal subtypes into the network structure that consists of only a fraction of a percent of the total population physiologically. Unfortunately, such reductions are not always as simple as percentages, as you will see in Chapter II, where a single interneuron can enervate and influence hundreds of other neurons. These decisions, while necessary, must be done cautiously and with a thorough understanding of the biology involved and mechanisms utilized.

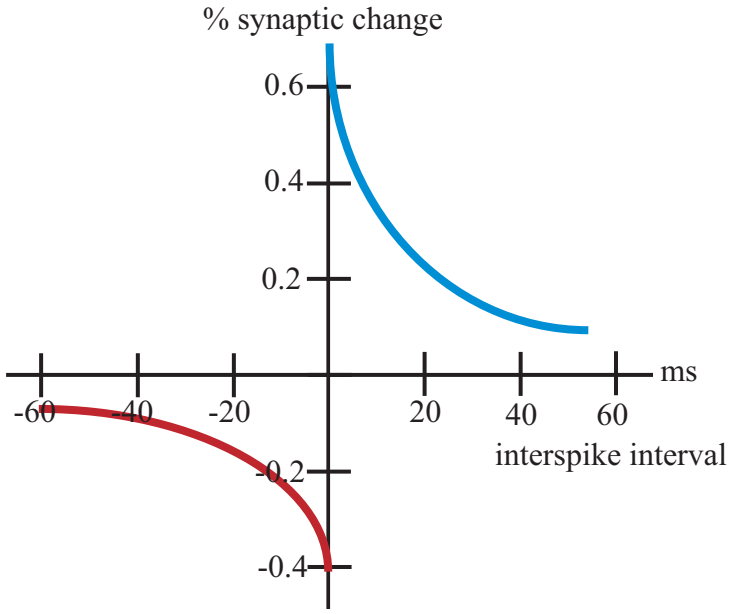

Figure 1.9: STDP learning rule. Shown is a characteristic, non-symmetric, decaying exponential STDP learning rule. When the presynaptic neuron fires before the postsynaptic neuron the synapse is strengthened. Alternatively, if the presynaptic neurons fires after the synapse is weakened.

1.4 Synaptic plasticity and how dynamics modify topology

The introduction of Hebbian learning was revolutionary to the field of neuroscience. The idea that 'neurons that fire together, wire together' gave scientists a basis by which connections in the brain could be modified and adapted. Through this principle, dynamics are able to modify the structural connectivity, and therefore the current activity, of the brain shape and its future shape. Subsequent research has built on this concept and we now have a much more concrete understanding of this rule. Work by Henry Markram and others has shown that the temporal order of this firing dictates whether connections are straightened or weakened, and by what amounts [111, 112, 113, 19, 114, 115, 116, 17]. Despite this great progress, neuroscientists have yet to answer how the brain translates spike-timing dependent plasticity (STDP) to cognitive learning.

The basis of STDP relies on the concept that two neurons that fire closer in time

are linked by some cognitive or functional process and therefore should be linked physiologically. Let us take neuron A and B as an example, STDP rules state that the closer in time that A and B fire, the stronger the synaptic change should be between them. Additionally, STDP indicates that there should be a causal relationship between the neurons. For example, if neuron A fires slightly before neuron B, then the causal relationship is A $\rightarrow$ B and the uni-direction connection from A to B should be strengthened. Alternatively, if B fires before A, then A cannot have caused B and the synaptic connection should be weakened. As these time differences become smaller and smaller, the synapses will strengthen or weaken more and more. A significant amount or research (see above) has demonstrated that this is in fact true. Figure 1.9 and Equations 1.6 and 1.7 demonstrate the most commonly used decaying exponential relationship between the firing time difference and the % synaptic change,

$$\%Change = A_{+}e^{\frac{-t_{diff}}{\tau_{+}}} \tag{1.6}$$

$$\%Change = -A_{+}e^{\frac{t_{diff}}{\tau_{-}}} \tag{1.7}$$

where the top(bottom) equation is for positive(negative) time differences t_{diff}, $\pm A$ scales the % synaptic change, and $\tau_{\pm}$ is the time constant for synaptic change. It is the goal of much research in neuroscience to now take the well understood properties of STDP and translate them to rules that dictate the learning and encoding of memories in the brain. Such an achievement would mark a significant leap in our understanding of such a fundamental property of cognition.

1.5 The network topology and dynamics: Pattern formation, oscillations, resonance, and learning in the brain

The preceding sections have discussed the framework to combine network topology and neuronal models to understand how they affect the dynamics of neuronal systems. In the following sections, I will introduce specific brain systems and properties that exemplify these interactions and discuss how they are tied together. I will also introduce a specific mechanism of how dynamics can 'go-back' and influence topology via spike-timing dependent plasticity. A recurring theme in these sections will be the emergence of unique spatio-temporal patterns of activity that may be generated by the network topology itself, or by the current dynamics of the input the neurons receive. These patterns include the formation of spatial heterogeneities in overall network activity, the emergence of oscillations in overall firing rates, and the emergence of classical resonance-like properties in otherwise non-resonating networks of neurons.

1.5.1 Gap-junction networks and the basal ganglia

Recent studies have shown gap-junctional connections to be far more prevalent in the brain than once thought. One region where they may play a vital role in functioning is in the striatum of the basal ganglia [40, 117, 27]. The basal ganglia is one of the most complex areas in the brain (Figure 1.10), acting as a filter to eliminate or select certain actions or decisions. The malfunctioning of this region is associated with movement disorders such as Parkinson's disease, Huntington's disease, and Tourette's syndrome [118, 119, 120]. The striatum is the largest and primary gateway component of the basal ganglia, receiving input directly from the cortex. In the striatum, gap-junctional connections are present on fast-spiking interneurons (rapidly repolarizing inhibitory neurons whose connectivity is limited to within the

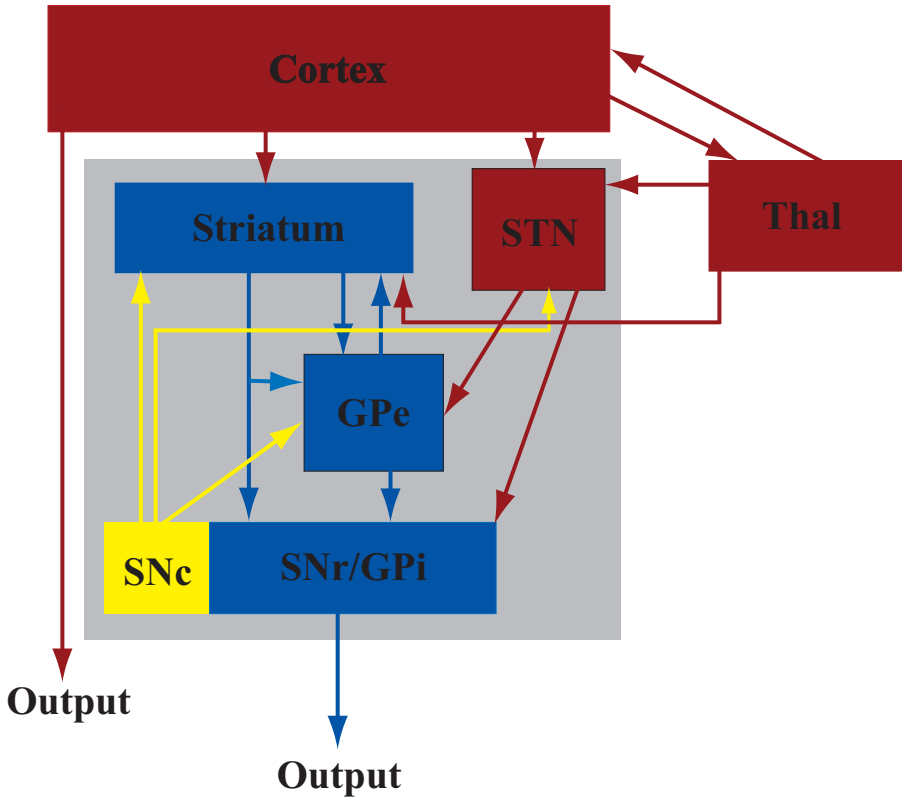

Figure 1.10: A connectivity diagram for the basal ganglia (inside the gray box). Input is received from the cortex into the striatum and the subthalamic nucleus (STN). Globus pallidus external (GPe), Globus pallidus internal, substantia nigra pars reticulata (SNr), and substantia nigra pars compacta (SNp). Excitatory connections/area are denoted in red, inhibitory in blue, and modulatory in yellow. Within each region however, there may be a diverse range and multiple types of connections. The output of the basal ganglia is to the spinal cord, brainstem, thalamus, and feedback pathways into the basal ganglia.

striatum). These interneurons receive excitatory input from the cortex and form electrical connections between themselves and GABAergic connections with medium spiny neurons.

The cellular and network basis for this action selection and filtering is still an active area of research. One common theory is that, through a large amount of inhibition, the basal ganglia is able to restrict all but the strongest and most coherent inputs [6, 121, 8]. Another common theory is that the precise timing of activity in the various components of the basal ganglia allows for 'gating' of sensory input through oscillation windows and synchronous inhibition [118, 56]. The work in Chapter II investigates the network basis for such activity that may support these ideas. The gap-junction inhibitory network provides a fascinating basis of study because of the two connection topologies, a type of network that is not often studied. I show that there is a strong dependence of the interneuron network activity on the specific topology of that network. From varying the connectivity from local to random, and changing the strength of both types of connections, the network activity passes though numerous regimes. The most interesting of these regimes is a range of spatio-temporal pattern formations that allow specific, spatially localized, subsets of neurons to be synchronously active while others are quiet. Changing the inhibitory connectivity from local to random further modifies the activity pattern from one synchronized area to multiple synchronized areas. This spatially heterogeneous activity provides a potential basis for the specific inhibition, or dis-inhibition of downstream neurons. These results give us insight into how the network topology influences how decisions may be made and what can go wrong when the topology of the striatum is disturbed. The results are then compared to *in vivo* experimental data from Joshua Berke's lab, and it is shown that the simulations correspond well to their novel results. This work was published in Physical Biology in 2010 [27].

1.5.2 Oscillations in the brain and interaction with network topology

Oscillations are ubiquitous throughout nearly all regions of the brain. Categorically broken down into alpha(8-12Hz), delta(1-4Hz), theta(4-8Hz), beta(13-30Hz), and gamma(30-70Hz) bands, they are generated by the overall modulation of activity of a neuronal population to a specific frequency. In the basal ganglia, oscillations are integral to motor control, and the alterations of the oscillations have been shown to be associated with Parkinson's disease and other movement disorders [118, 56]. In the hippocampus and cortex, theta rhythms are thought to play a role in learning and memory retrieval [58, 81, 122, 123, 57]. In those same areas, gamma rhythms are though to be important to synaptic strengthening via spike-timing dependent plasticity (see next section) because the high frequency provides the ideal time windows for firing and modification [124] between the peaks and troughs. In the motor circuitry, EEG measurements have shown that specific frequencies from certain regions are associated with movements [8**?** , 125]. During the whole movement these measured frequency changes correspond to a highly coordinated sequence of events from planning to execution.

The mechanism for the generation of these oscillations is one area currently undergoing study. As I have already discussed, one proposal is that they are generated from the networks themselves, as opposed to individual neurons and their properties. Synaptic transmission delays between excitatory neuronal ensembles can generate reverberation between the two groups, just like the mailed letters across the country. Another mechanism, proposed especially for higher frequency oscillations, is by an inhibitory fast-spiking interneuron network [123, 30]. The synchronization of these networks is known to be enhanced by gap-junction connectivity, and the work in Chapter II has demonstrated the dependence of this synchronization and these oscillations on network topology.

Chapter III will cover a much less investigated area on oscillations, how the net-

work structure interacts with dynamic oscillations when they are *input* into neuronal ensembles. I present data from a computational study in which oscillating currents of varying frequencies and amplitudes are input into a network of neurons. The network is heterogeneous in that a subset of neurons are coupled more strongly (i.e. a memory trace) than the rest of the network. The overall connectivity strength of the network is changed along with the amplitude and frequency of the input oscillation. The results demonstrate a network-resonance condition, or the ability for the synaptically strengthened subset to selectively fire in response to certain frequencies. The mechanisms behind this activity are a unique interplay between the dynamics of the individual neurons (i.e. time constant), the dynamics of the network (i.e.synaptic delay), and the topology of the network itself (i.e. number of connections).These result suggests that certain frequency ranges can have specific effects on neuronal activity dependent on the properties of the network itself.

1.5.3 STDP learning via and oscillations and resonance

Chapter IV introduces a possible mechanism by which the brain may convert subthreshold input signals into coherent spatio-temporal patterns of network activity and then consistent STDP learning. This is done in the framework of STDP learning, presented above, and input oscillations that we know are prevalent throughout the brain. In these simulations, a neuronal network receives subthreshold oscillations at the classical resonance frequency of the neurons, causing the network to be active. The specific resonance responses are then additionally shifted by another subthreshold signal current. I demonstrate that the combination of these input oscillations, resonance, resonance frequency shift, and STDP provide an ideal mechanism for converting correlated input signals to coherent learning. This learning modifies the topology of a previously random network to reflect the temporal relationships of the different patterns they receive. Specifically, one region of the network receives a

time varying current with a Gaussian profile, while another receives a slightly delayed Gaussian current. I observe that strong unidirectional connections form between the two regions with the region receiving the preceding (following) Gaussian forming outputting (receiving) connections from the other region. Additionally, this model is shown to naturally demonstrate the properties of frequency related phase precession which is gaining notice in experimental neuroscience today [57, 126].

All together, the work I will present to you in this thesis will focus around the concepts of oscillations, spatio-temporal pattern formation, and synchronization, as they relate to network topology. I will demonstrate how the network structure can govern dynamics, how structure and dynamics can interact, and how dynamics can govern structure. The goal of this thesis is not to decipher and explain every bit of observed activity or structure in the brain, but to explain and quantify the underlying the physical properties that govern these processes and formations, and to provide insight into the interactions between them.

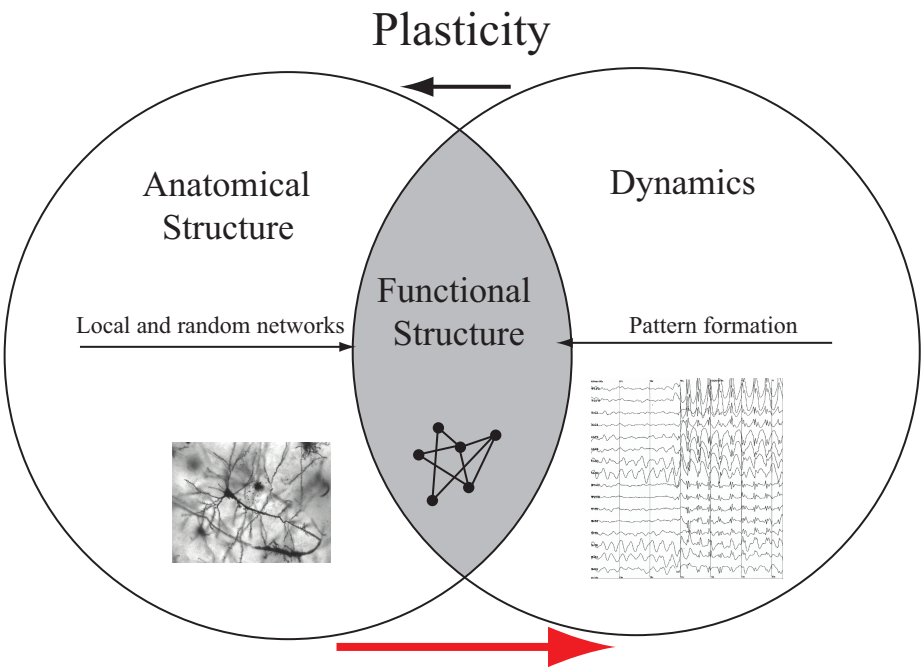
Plasticity
Anatomical
Structure
Dynamics
Functional
Structure
Local and random networks
Pattern formation
Synaptic communication -
GJ and inhibitory network topologies

CHAPTER II

Local dynamics of gap-junction-coupled interneuron networks

2.1 Introduction

At any scale in the brain, the neuronal network structure plays a significant role the the resultant dynamics. In particular, local connectivity, where connections are formed only with neighboring neurons, can have completely different functionality than connections which stretch long distances across regions. For example, short range connected neuronal subsets may function as local processors while long range connections may serve to integrate these processors. Another layer of complexity can be added if neurons have two types of connections simultaneously, one that has local connectivity properties and one that has global properties. This chapter investigates such a network topology, in the context of electrical gap-junction and inhibitory connections, and how their connectivity structure completely dictates the dynamic spatio-temporal patterns of activity formed.

Networks of interneurons coupled by electrical gap-junctions (GJs) and inhibitory electrical synapses are vital features of many brain circuits. Interneurons in the neocortex [127], visual cortex [86], and hippocampus [60] serve to coordinate and synchronize the activity of larger populations of neurons [30], and this synchronizing

role is well described by computational models of interneuron networks [128, 129, 130, 131, 132]. However, the activity of interneuron networks does not simply serve to set the pace of brain circuits. For example, recent studies have demonstrated unexpectedly asynchronous firing of GJ-coupled striatal fast-spiking interneurons (FSIs; [28]), and how such activity emerges from and is constrained by network connectivity is not well understood [117].

We wish to extend the computational study of interneuron networks by systematically investigating the effects of network topology and GJ connection strength on the spatio-temporal activity patterns of interneuron networks. Differences in network and connection properties may allow interneuron networks to have distinct functions, and corresponding distinct activity patterns, in different brain regions. The first half of this chapter is a general study on interneuron dynamics that covers a wide range of connection topologies and connection strengths. We introduce our reduced network model and the metrics we employ to quantify the observed patterns of network activity. We then use these metrics to study spatial network patterns and their temporal stability as a function of connectivity levels, connectivity strength, and network macrostructure. The intent is for these studies to be applicable to any GJ-coupled networks of inhibitory neurons.

In the second half of this chapter we use our computational analysis of interneuron networks to gain insight into observed firing patterns of striatal FSIs [133]. We show that subtle alterations in the input to the network can cause transitions from unstable to stable patterns, and we compare these observed transitions to results obtained in electrophysiological studies of striatum during action selection. *In vivo* these neurons receive direct inputs from the cortex [134], are coupled together by GJs on their dendrites [135] and provide strong perisomatic GABAergic inputs to > 100 nearby striatal projection neurons [121]. FSI-mediated inhibition appears to play an important role in the selection and suppression of actions (discussed in [28]),

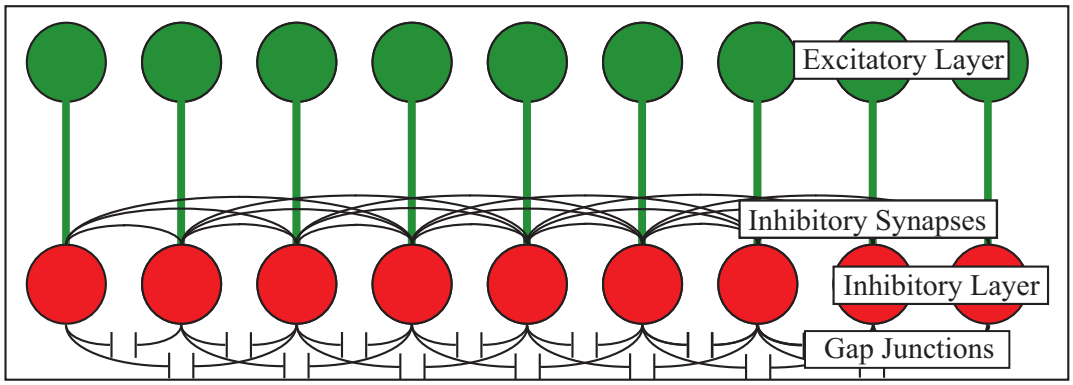

Figure 2.1: Network architecture. General network layout of the FSI interneuron layer (red) and coupled excitatory input layer (green). The interneuron layer is internally coupled via both inhibitory connections and GJ connections. The excitatory input layer has direct connections to corresponding neurons in the network.

and a deficit in this cell population may contribute to Tourette Syndrome [136]. Understanding the relationships between FSI anatomical connectivity, firing patterns and behavioral functions is therefore an important area of current research.

2.2 Modeling

2.2.1 Simulations

2.2.1.1 General network architecture

The interneuron network consists of 200 neurons arranged on a 1-D lattice Figure 2.1. The network has periodic boundaries, forming a ring structure. The neurons were connected using the Small World paradigm [75], where neurons are initially connected

to all neighbors within a distance r, then connections are removed randomly and reconnected anywhere in the network with a probability of p. Thus, on average, every neuron has a $1-p$ probability of connecting to its neighbors and a probability p of connecting to any other neurons in the network. Thus, for $p = 0$ we obtain solely local network connectivity, for $p = 1$ the connectivity is fully random.

To investigate the relative contributions of electrical and chemical networks, we modified connectivity parameters for the inhibitory and the GJ networks separately. For the synaptic inhibitory component, the wiring radius of inhibitory connections was set to $(r_i) = 5$, 10, or 30 with a rewiring probability (p_i) ranging from 0-1 in increments of 0.05. For the GJ component, radii started smaller, with the wiring radius of GJ connections $(r_g) = 3$, 5, 10, or 30, and the rewiring probability (p_g) again ranged from 0-1 in increments of 0.05.

Each simulation was run over 2 seconds and all measurements, unless otherwise stated, are the averaged values over 10 independent simulations. Each independent simulation had distinct connectivity due to separate rewiring, random initial voltages, and driving patterns.

2.2.1.2 External network input

For homogenous driving (section 2.3.1), the interneuron network was stimulated by a layer of 200 uncoupled excitatory neurons, unidirectionally connected 1-to-1 with the interneurons. Each excitatory neuron fired as a random Poisson process with mean of 20 Hz. For non-homogeneous driving (section 2.3.2), in addition to the driving described above, a subpopulation of 20 contiguous excitatory neurons (id# 90-110) were given additional properties. Either we increased the firing rate of this subset of neurons, by a factor ranging from 1 to 16, or we kept the firing rate identical to the rest of the population while increasing the correlation of firing times within this subset. The amount of correlation is quantified by a jitter (ms) which is the

Gaussian deviation in firing times from the mean firing of neurons in this subset. A jitter of 0 will give perfectly correlated firing while a width near the average firing rate will return the same random firing pattern as all other neurons.

2.2.1.3 Inhibitory connections

To model the dynamics of the neuron we used the leaky integrate-and-fire neuron model:

$$\tau_m \frac{dV^j}{dt} = -\alpha_j V^j + R_s I - \sum_k w_{syn}^{jk} S^{jk} I_{syn}^k \tag{2.1}$$

Here, V^j is the membrane potential of the j^{th} neuron, $\tau_m = 0.5$ms is the time constant; α is a leakage coefficient which is different for every cell, $\alpha \in [1{:}1.3]$; I_{syn}^k is the synaptic current generated at the time of the spike, w_{syn}^{jk} defines the chemical synapse coupling strength; S^{jk} is the synaptic connectivity (adjacency) matrix; I is a uniform external current which keeps the neurons readily excitable, $I = 0.5$; R_s is the neuron resistance $R_s = 1$.

The synaptic current is activated after the pre-synaptic neuron reaches a threshold $V_{thresh} = 1$ and fires an action potential. The pre-synaptic neuron is then returned to $V = 0$ and remains there for a refractory period $t_{ref} = 5$ms. The synaptic current is of the form

$$I_{syn}^k(t) = e^{\frac{-(t-t_{spike}^k)}{\tau_s}} - e^{\frac{-(t-t_{spike}^k)}{\tau_f}} \tag{2.2}$$

where $(t - t_{spike}^k)$ is the time since the last firing of the presynaptic neuron, $\tau_s = 3$ms is the slow time constant, and $\tau_f = 0.3$ms is the fast time constant. The variables τ_s and τ_f are chosen such that the post-synaptic potential lasts approximately 2ms.

2.2.1.4 Electrical connections

The GJ connections differ from synaptic connections in several important ways. First, GJ connections are bi-directional: current can flow in either direction between two neurons. Second, they have no activating threshold: voltage-equilibrating ion flow occurs even at membrane voltages subthreshold for spiking. When spikes do occur, GJs can partly communicate this event in the form of a spikelet [42, 38], which is modeled via the addition of a excitatory term to the leaky-integrate-and-fire equation:

$$\tau_m \frac{dV^j}{dt} = -\alpha_j V^j + R_s I - \sum_k w_{syn}^{jk} S^{jk} I_{syn}^k + \sum_m g_{gap}^{jm} G^{jm} (I_{syn}^m(t) + \sigma_{gap}(V^m - V^j)) \quad (2.3)$$

Here, g_{gap}^{jm} denotes the efficacy of GJ connections; G^{jm} is the gap junction connectivity matrix, V^m is the potential of the m^{th} pre-synaptic neuron and V^j is the potential of the post-synaptic neuron. The $I_{syn}^m(t)$ represents the spikelet and the $\sigma_{gap}(V^m - V^j)$ is the voltage equilibrating, dissipative term. In all our simulations $\sigma_{gap} = 1$.

Inhibitory coupling constant $w_{syn} = 2$ for all simulations while the GJ coupling constants g_{gap} ranged from 0-0.5, chosen to match the relative synaptic efficiencies observed in GJ interactions [132].

2.3 Analysis

2.3.1 Definitions of spatial and temporal metrics

2.3.1.1 Spatially localized activation metric, Ω

To measure spatial pattern formation within the network, we computed the degree to which the firing of locally grouped subsets of neurons deviated from the mean

population firing rate. Specifically, we calculate the average spike rate, R, for every neuron in the time window of $b_t = 400$ ms. We then take a spatial sliding window of varying size $b_n \in [1, N]$ along the neuron number axis. The R denotes the time-binned and neuron population-binned cell firing rates. We then compute the variance of these binned firing rates:

$$\sigma^2(b_n) = \frac{\sum_N (R' - \langle R' \rangle)^2}{N} \tag{2.4}$$

Thus the variance will be large if there are localized neural groups that have significantly higher/lower mean spiking rates. Conversely, if the spiking frequency is uniform, the variance will tend to zero. Since we do not know the size of the localized groups a priori, the variance will depend on the spatial bin size b_n , i.e the maximum value of variance ($\sigma^2(b_n)$) will be reported for the bin size corresponding to the average size of activated groups. Thus our measure of spatially localized activation is defined to be:

$$\Omega = MAX_{b_n}(\sigma(b_n)). \tag{2.5}$$

Figure 2.2 demonstrates different values of Ω for different activity patterns.

2.3.1.2 Temporal Stability metric

To assess network stability we first measured the coefficient of variation ($\bar{CV}$) of firing rates for each individual neuron over the time course of the simulation. This was defined as the standard deviation of inter-spike intervals (ISIs) divided by the mean ISI:

$$CV_{neuron} = \frac{1}{\langle ISI \rangle_{neuron}} \sqrt{\frac{\sum_i (ISI_{i,neuron} - \langle ISI \rangle_{neuron})^2}{N_{ISI}}} \tag{2.6}$$

Here i is the index of each ISI and N_{ISI} is the total number of ISIs for a specific

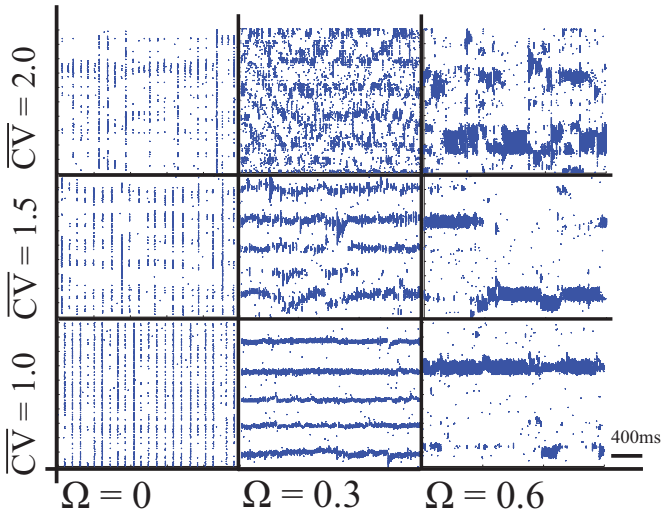

Figure 2.2: Illustration of how the Ω and $C\bar{V}$ metrics can describe key features of network activity. For each subplot, the neuron number is along the y-axis and timesteps along the x-axis with dots where the neuron has fired. In cases where locally distinct spatial patterns form, Ω has a correspondingly higher value. The subplots also show that more stable patterns are associated with lower $C\bar{V}$ values. In addition, all plots in the left column show examples of globally synchronous states (GSS), while the central and right columns demonstrate localized activation states (LAS).

neuron. The overall stability measure is simply the mean $C\bar{V}$ for all neurons in the network. If the neurons show stable firing rates $C\bar{V}$ will be lower (Figure 2.2).

2.3.2 Electrophysiological data acquisition and analysis

2.3.2.1 Recording striatal FSIs

The recordings in this section were performed in the Berke Lab at the University of Michigan by Professor Joshua Berke and Dr. Gregory Gage.

Individual neurons were recorded extracellularly from the striatum of four rats implanted with tetrodes (four 12.5 m nichrome wires twisted together) during performance of a simple choice task [137]. Thirty-nine striatal FSIs were identified using previously established waveform and activity criteria [138, 28]. Neural signals were sampled with high temporal precision (31,250 samples/sec) and wide-band filtering (1-9,000 Hz) to minimize distortions of waveform shape [137]. During daily recording sessions, rats were placed in a dimly illuminated operant behavior box with an array of five nosepoke holes on one wall. The simple choice task required hungry rats to nose-poke an illuminated hole and hold there until receiving a go signal (a white noise burst). During the hold period, an instruction cue was delivered to a speaker inside the operant box: a 250 ms tone of either high (4 kHz) or low (1 kHz) pitch. If the rats chose to move leftwards after hearing the low tone, or rightwards after the high tone, they were rewarded with a 45 mg sucrose pellet, which they collected from the wall opposite the nosepoke holes. The total hold time required to correctly complete the trial was pseudo-randomly selected to be between 900-1250 ms (uniform distribution) while the tone delay varied from 250-350 ms after initial nosepoke. If the rats failed to hold until the go signal, trials were aborted and a 10-15 s timeout period began (with houselights on). All recording sessions were made from rats that had already learned the task (mean: 74.4 % correct trials).

2.3.2.2 Cumulative stability analysis of rat striatal FSIs and simulated data

To assess the stability of firing as rats were instructed which way to go, we examined spike times within 500ms of the instruction cue. For each neuron, only trials with at least five spikes before and five spikes after event onset were included in the analysis. Altogether we included 828 trials in which rats were cued to make a rightward movement, with 22/39 neurons providing sufficient stability shifts, and 1/2 of the neurons accounting for more than 95% of the recorded trials. For leftward movements we included 818 trials, with 22/39 neurons providing more than 10 stability shifts, and 1/2 of the neurons accounting for 94% of the recorded trials. For each of these trials we calculated the pre- to post-cue shift in temporal stability, $\Delta\bar{CV}_i$:

$$\Delta\bar{CV}_i = 2\frac{\bar{CV}_{i,before} - \bar{CV}_{i,after}}{\bar{CV}_{i,before} + \bar{CV}_{i,after}} \tag{2.7}$$

where i denotes the trial index. A positive $\Delta\bar{CV}_i$ thus represents an overall stabilization of the network after the cue, while a negative $\Delta\bar{CV}_i$ its destabilization. We then calculated the mean stability shift over all trials for left and right movement choices:

$$\Delta\bar{CV} = \langle\Delta\bar{CV}_i\rangle \tag{2.8}$$

To compute statistical significance of the observed mean shift in stability ($\Delta\bar{CV}$) we created 1000 surrogate trials by randomly exchanging the sequences of pre- and post- cue spike trains for each trial. This process was repeated 1000 times, allowing us to obtain randomized distributions of the mean stability shift of the surrogate trials ($\Delta\bar{CV}_{surrogate}$). We then computed the surrogate mean and standard deviation. The significance levels and scores were established assuming a Gaussian distribution around the surrogate mean. This analysis allowed us to determine whether the ob-

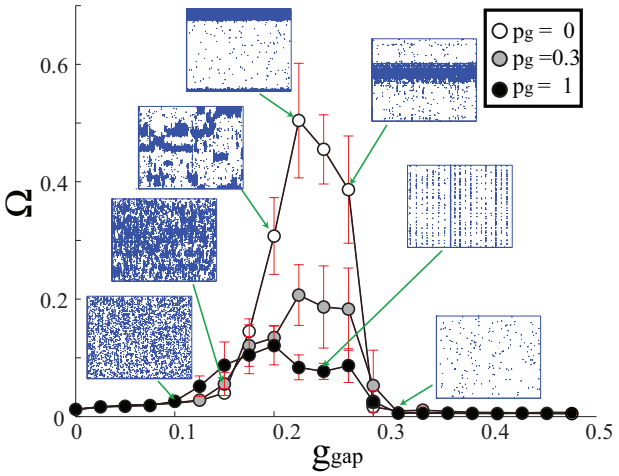

Figure 2.3: Qualitative changes in network activity arising from the topology of GJ connectivity. g_{gap} vs. Ω for $r_i = 30$, $p_i = 1$, $r_g = 5$, and $p_g = 0$ (white circles), 0.3 (gray circles), 1 (black circles). Selected raster plots depicts examples of network dynamics for different values of p_g. As g_{gap} increases so does Ω , to a peak value, before the network fails to sustain a pattern and Ω declines. The highest value of Ω occurs when $p_g = 0$ (local connectivity) and declines as p_g approaches 1 (random connectivity).

served mean stability shifts are merely due to random fluctuations or represent a statistically significant event. For comparison, an identical calculation was performed on the spike trains obtained from the simulation and we repeatedly recorded activity of a single (and the same) neuron on different simulation runs.

2.4 Dynamics of FSI networks

To better understand the dynamics of interneuron networks with both inhibitory synapses and GJ channels we used two separate connection topologies converging on the same neurons (Figure. 2.1). We observed that, contrary to many previous results that demonstrated the formation of predominantly synchronous states of activity [128, 129, 130, 131, 132], these interneuron networks are capable of a wide range of dynamical regimes and activity patterns. We show that by changing the topology of both the inhibitory and GJ connectivity, in addition to spatially uniform and synchronous activity, the network also exhibits highly non-uniform spatio-temporal

patterns (Figure 2.3). These states can be grossly divided into three groups:

Localized activation state (LAS) There are one or more well defined groups exhibiting synchronous high frequency firing, while other regions of the network remain nearly silent (Figure 2.3 center). These regions may be temporally stable throughout the simulation or change their position rapidly.

Random activation state (RAS) The network exhibits low firing rates and random patterning predominantly driven by the input layer (Figure 2.3, left).

Globally synchronous state (GSS) A high fraction of the cells fires synchronously, with varying frequency dependent on overall network excitation (Figure 2.3).

We investigated the emergence of these spatio-temporal patterns as a function of the underlying networks topologies, connectivity strength, and connectivity density. We assessed the spatial non-uniformity of network response, and the temporal stability of network activity, using the Ω and $C\bar{V}$ metrics respectively (defined in section 2.2.1).

Finally, we compared the activity patterns obtained in our computational model with those observed experimentally, obtained from striatal FSI recordings of freely moving rats performing a decision task.

2.4.1 FSI network dynamics driven by homogenous input

2.4.1.1 Properties of electrical synapses, and spatial pattern formation in the electrical-inhibitory network

In this section we investigated the spatial activation pattern of the network as a function of electrical connectivity parameters. We monitored changes in the SLA metric (Ω) as a function of connection topology (lines with colored circles) and electrical coupling strength g_{gap} (x-axis; Figure 2.3).

We observe that for fixed connectivity r_g and for weak electrical coupling the network exhibits the RAS. This is due to the fact that the network activity is solely driven

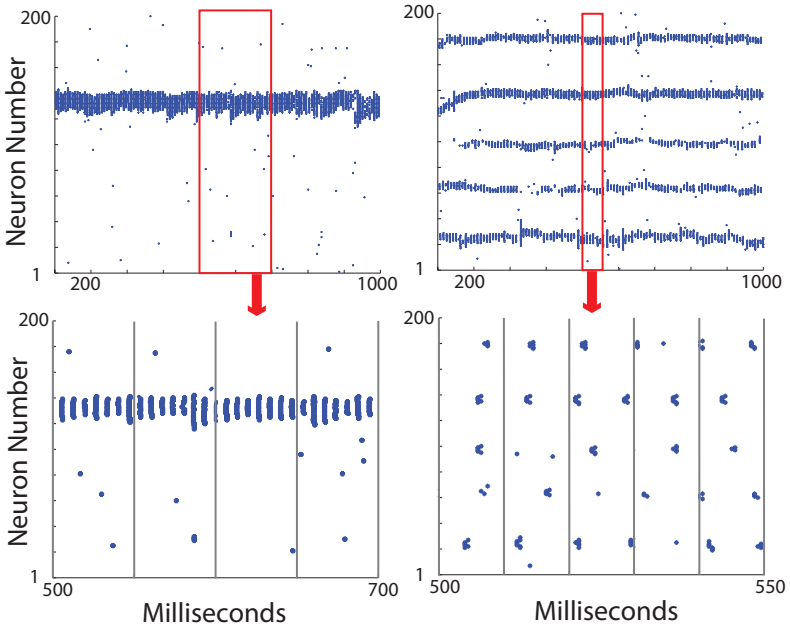

Figure 2.4: Inter-domain synchrony and lack of synchrony between domains. $r_i = 30$, $p_i = 0$ (right column),1(left column), $r_g = 5$, and $p_g = 0$ For the LAS regime the neurons within active regions are synchronous. However, if multiple regions are active (right column) the population subsets are not necessarily synchronous across the entire network

by the input layer that exhibits random homogenous activity patterns. When the GJ connectivity of the network increases to intermediate values of coupling strength, the network activity exhibits the highly non-uniform spatial pattern characteristic of the LAS. The observed pattern forms because of a GJ-mediated equilibration of the potentials, of locally connected interneurons, These local groups of neurons then become collectively active (quiescent) when a significant amount of excitation(inhibition) is input. Specifically, the local connectivity of GJs mediates the formation of discrete, high activity domains that inhibit other regions of the network. The firing frequency of neurons within these domains is well above mean input frequency, while the rest of the network is relatively quiescent, firing significantly below the input frequency. Additionally, the neural activity is highly synchronized within each activated domains, with neurons firing within 3ms of each other, but the multiple domains remain unsynchronized amongst each other (Figure 2.4). The locations and sizes of the activated

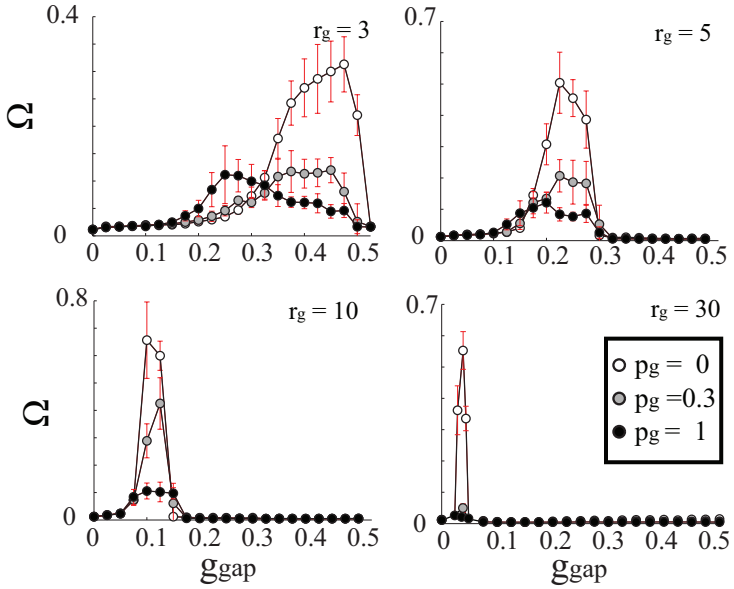

Figure 2.5: Ω values obtained for various values of GJ coupling strength g_{gap}, connection topology (p_g = 0.0 (white), 0.3 (gray), 1 (black); r_g = 3, 5, 10, 30), and connection distance r_g. The chemical connectivity remains constant with parameters are r_i = 30,p_i = 1). As r_g increases, the corresponding g_{gap} range that produces high values of Ω decreases and narrows. The top right panel is the same as Figure 2.3.

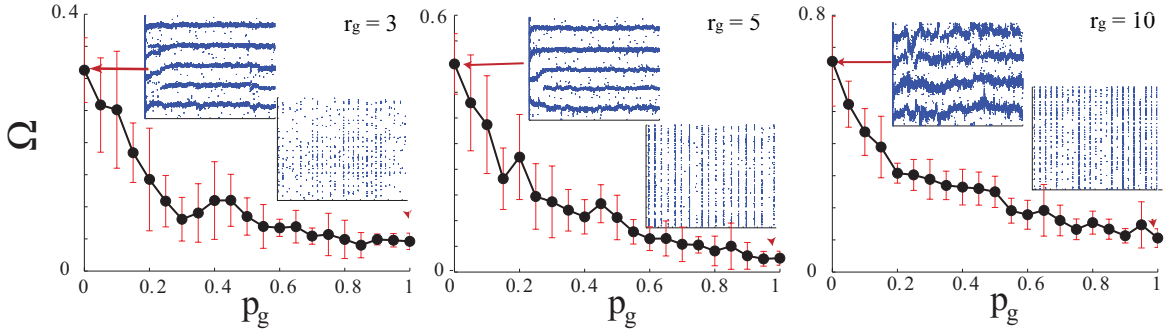

Figure 2.6: Changes in spatial patterning (Ω) as a function of topology (p_g) of GJ network, for r_g = 3, 5, 10 The connectivity of the inhibitory network is unchanged and is set to p_i = 0, r_i = 30. For r_g = 3, 5, 10, g_{gap} = 0.45, 0.21, 0.095 respectively, as chosen to give the highest Ω values (see Figure 2.5).

domains depend on the connectivity properties of both electrical and inhibitory networks. Moreover, the local, high activity pattern can be spatially stable (i.e. encompass the same group of cells) throughout the simulation, or change rapidly in time (see section 2.3.1.2 below).

For high values of electrical coupling, network activity becomes random and spatially uniform once again. In this case there is also significant reduction of the mean firing frequency, confirming previous findings in striatal FSI network simulations [117]. This is due to current shunting via GJs, which reduces the probability of neurons reaching action potential thresholds.

We then investigated the occurrence of the LAS, RAS and GSS as a function of electrical network connectivity (Figures 2.5 and Figures 2.6). We varied the GJ coupling, $g_{gap} \in [0, 0.5]$ and network topologies $p_g \in [0, 1]$ for three values of GJ connectivity, $r_g = 3$, 5, 10, 30.

The LAS patterning is clearly a function of locality of the electrical connections, with more local connections leading to the LAS state.

We observed that, as the total number of GJ connections (equal to $2r_g$ per cell) increases, non-uniform patterning is obtained for lower values of electrical connection strengths, g_{gap}, and the g_{gap} range for LAS significantly narrows (Figure 2.5). This is primarily due to the fact that the increased number of connections offsets the effects of coupling strength.

At the same time, as $p_{gap} \to 1$, the network transitions to the synchronized state and the spatially resolved patterns no longer form (Figure 2.6). The emergence of the GSS for more random connectivity patterns generally agrees with the in vitro experimental evidence observed in studies of interneurons in the cortex [81, 130, 39] as well as simulation studies [128, 139, 131, 132].

This transition seems to take place for lower values of rewiring when the network connectivity is sparser. Additionally, as the network connectivity increases, there is

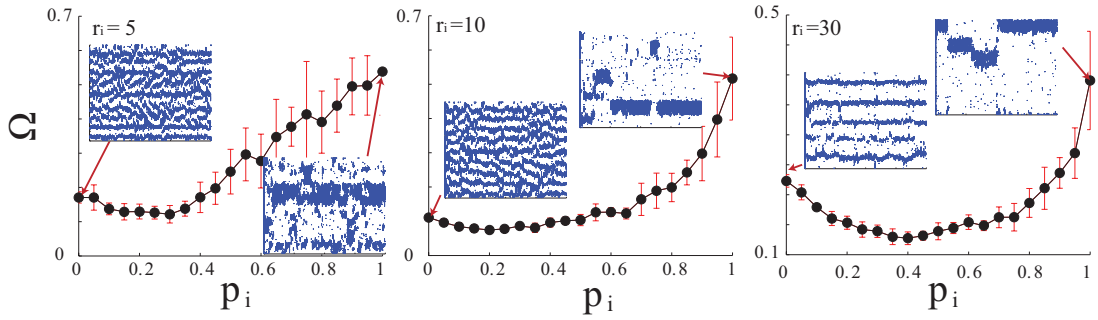

Figure 2.7: Spatial network patterning (Ω) as a function of inhibitory network topology (p_i) for $r_i = 5, 10, 30$. The connectivity of the GJ network is constant ($p_g = 0$, $r_g = 5$) and $w_{syn} = 2$. Local activation is observed for both local and random inhibitory coupling but its spatial characteristics change significantly.

an evident increase in the number of synchronously firing neurons per cycle (Figure 2.6).

2.4.1.2 Topological effects of inhibitory connectivity on network patterning

We also more closely examined the properties of the formed patterns as a function of the structure of the inhibitory network connectivity. We varied the rewiring parameter and the connection density of the inhibitory synapses (i.e., $p_i \in [0, 1]$ and $r_i = 3, 5, 10, 30$; Figure 2.7).

We observed a dramatic change of the patterning as a function of the topology of the inhibitory network. The multiple activated regions observed for both local GJ and synaptic connectivities, is replaced with a single active region when $p_i \to 1$. This is due to the fact that now activated regions generate global inhibition to rest of the network, providing competition to each other (Figure 2.7).

2.4.1.3 Excitatory chemical synapses do not support LAS formation

Finally, to confirm that the formation of the non-uniform spatio-temporal pattern is due to the sub-threshold equilibrating characteristic of electrical networks, and not

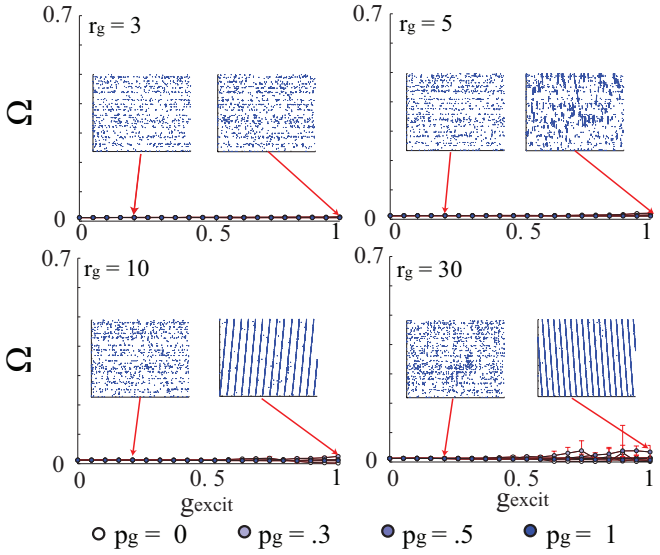

Figure 2.8: Excitatory chemical connections cannot substitute for GJ in the formation of local active zones. Ω vs. g_{excit} (excitatory connections instead of GJs) for varying the topology and connection strengths of the GJ network - r_i = 30, p_i = 1, r_g = 3, 5, 10, and p_g = 0, 0.3, 0.5, 1.0. There is no pattern formation, even as the connection strengths are increased to arbitrarily high values, twice the strength of the GJ networks.

primarily mediated by the chemical synapse excitatory-like interaction, we simulated networks with identical macrostructure properties and bi-directionality but with GJ connections replaced by excitatory connections (i.e. the sub-threshold equilibrating term was removed so that neural interactions were similar to these of the chemical synapses). We observed that, even for a significantly higher strength of connections (two-fold), these networks were unable to form the LAS patterns.(see insets Figure 2.8). This demonstrates that, despite the excitatory networks ability to depolarize locally connected neurons, the lack of any equilibration properties cannot generate a LAS.

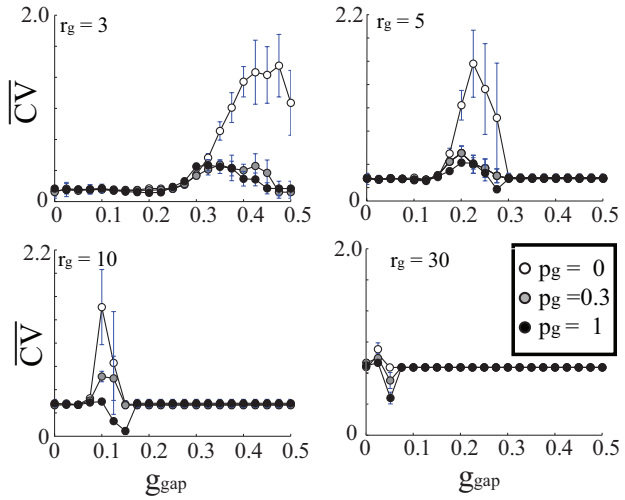

Figure 2.9: Measurement of stability ($C\bar{V}$) vs. GJ coupling strength (g_{gap}) for varying topology (p_g = 0.0 (white), = 0.3 (gray), = 1 (black) and connectivity (r_g = 3, 5, 10,30) of the GJ network. The connectivity of the inhibitory network remains unchanged and is set to $r_i = 30$ and $p_i = 1$. For small r_g the stability measure $C\bar{V}$ increases (the network becomes more unstable) as g_gap increases. As the number of GJ connections increases the network is stable over a wide range of GJ coupling strengths.

2.4.1.4 Temporal pattern stability of LAS as a function of electrical and inhibitory network connectivity

We also investigated the temporal stability of the observed patterns (Figure 2.9). The overall shift in the $C\bar{V}$ peak(s) follows that of the Ω metric: as r_{gap} increases, the width of the peak narrows and occurs for smaller values of g_{gap}. For low values of g_{gap} the network exhibits high stability (lower values of $C\bar{V}$). This is due to the fact that for the low coupling values the network activity is dominated by the input layer that provides random and uniform activation patterns (please refer to Figure 2.3 for raster plot examples).

For the higher values of GJ coupling, as the local regions of high activation form, the network shows decreased stability. This results from the rapid shifts of LAS regions Which in turn are due to random local fluctuations of spike frequency and their temporal correlations. These fluctuations cause rapid formation of new LAS regions while shutting down the old ones.

However, especially for the high and random GJ connectivity regime, there is a narrow parameter range that for which stability of the patterning is increased. The reasons are twofold: 1) for the lower connectivity range, low $C\bar{V}$ values indicate decreased spatial fluctuations in region of high activity (see bottom-right panel of (Figure 2.2), and 2) for the high connectivity regime, this is due to high activation of the whole network that leads to high frequency GSS firing patterns.

2.4.2 Stabilization of network dynamics in response to non-homogenous inputs

The results above were obtained with random, homogenous input to the interneuron network. We next investigated the consequences of perturbing this homogeneity, by increasing either input firing rate or input firing synchrony, in one region of the network (Figure 2.10). The panels A and C show an example of increasing the input

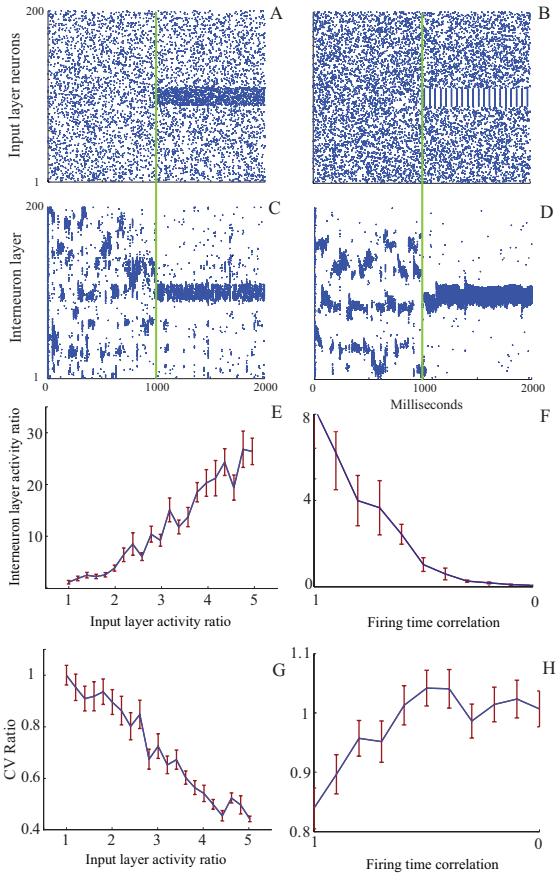

Figure 2.10: Response of the network to non-homogeneous input. The input layer is initially (0ms-1000ms) driven with homogenous input leading to unstable spatio-temporal interneuron dynamics. Then the network is either driven with input with locally increased frequency (A), or correlated input of the same firing frequency (B). (C and D) Both inputs elicit an increased frequency response in the corresponding interneurons, a decrease in firing rate in all other neurons, and an increase in the mean total stability of the network. (E) The input vs. network response as a function of the ratio of activity for neurons (90-110) over the activity of all other neurons. An input layer activity ratio of 1 returns uniform a uniformly random firing rate across the network. (F) The interneuron network response vs. the mean correlation of the firing pattern within the group of input neurons (1 means perfect correlation in firing and 0 correlation returns a random firing pattern). (G) The change in CV ratio, calculated from the actual CV divided by the CV obtained from uniform and uncorrelated input. The entire network stabilized as the interneuron layer activity ratio increased. (H) Similar to Figure G, the network stabilized as the temporal correlations were higher. Each data point is the average of 50 independent simulations and the standard error is the error bar. For these simulations $r_i = 30$, $p_i = 1$, $r_g = 5$, $p_g = 0$.

layer firing rate, in a specific region, without changing the firing rate elsewhere in the network, and the resultant interneuron layer activity. The panels B and D depict changes in interneuron activity due to the introduction of correlations in the firing of the input layer.

We found that relatively small manipulations of either parameter could produce a rapid stabilization of FSI network activity and a significant amplification of the response (firing rate) of the corresponding network region (Figure 2.10 E, F) accompanied by decrease in firing rate of other network regions. To quantify this effect we calculated the ratio of average firing frequency of neurons within the corresponding region and other parts of the network. In Figure 2.10 E a small 2-5 times increase in the noise level of specific input neurons can increase the ratio of FSI response 30 fold. In Figure 2.10F a temporal correlation (synchrony) increase, with no increase in firing rate of the input neurons, can induce an 8 fold FSI firing rate response. Both examples return expected ratio values of 1 when at nominal values (1 for noise ratio and 0 for the correlation, corresponding to random firing times). The ability of a GJ-coupled FSI network to detect and amplify small input asymmetries, in terms of a higher frequency or temporal coherence, and achieve a corresponding stable network activity pattern is a potentially highly useful feature. In the case of the striatum, it could be helpful in the selection and stabilization of planned courses of action. Decision-making involves the assessment of often equivocal or noisy evidence in order to make a commitment a highly non-linear, non-equivocal response (see Discussion).

Additionally, a shift in temporal stability (CV) accompanied changes in both these parameters. Figure 2.10G demonstrates that as the selected regions activity ratio increases, so does the stability (CV decreases). For the temporal correlation shifts (Figure 2.10H) we observed that this stabilization occurs at an even lower frequency response. This is not surprising however, as the nature of the temporally correlated input leads to a more temporally stable firing rate. In these figures we measured the

CV ratio or the relative CV shift as the actual CV value divided by the nominal CV value obtained from uniform and random input.

2.4.2.1 Stability analysis using experimental and simulated data from single neurons

To investigate whether such dynamics actually contribute to striatal function, we wished to compare our simulations to experimentally obtained spike trains from striatal neurons. We used a data set of FSIs recorded in rats performing a simple choice task (see Methods and [137]. We compared periods of time immediately before and after presentation of an auditory cue that instructs animals which way to move (at a later time). Thus, before the cue onset, both left and right actions are equally probable for the animal, but following cue onset rats know which way they need to go to receive a reward. We assume here that the cue, and/or preparation of a specific movement, corresponds to preferential input of specific subsets of cortical inputs to striatal networks.

Employing the same measures used in the network simulations above would require the simultaneous recording of many FSIs, which is not technically feasible at the current time. Instead we exploited the fact that we had many behavioral trials for each individually-recorded FSI and examined the stability of the firing pattern across repeated trials with the same instruction cue and movement. We also performed the same analysis for individual simulated FSIs over 100 independent trials. In both the model and experimental data, we observed a similar stabilization of firing pattern (Figure 2.11). Additionally, both experimental and simulated neurons accompanied stabilization with a range of firing rate increases or decreases.

We assessed the stabilization of firing for all experimentally recorded neurons (Figure 2.11) by comparing it to the surrogate generated trials (see section 2.2.3). The epochs were calculated as 250 ms before and after the cue. Although striatal

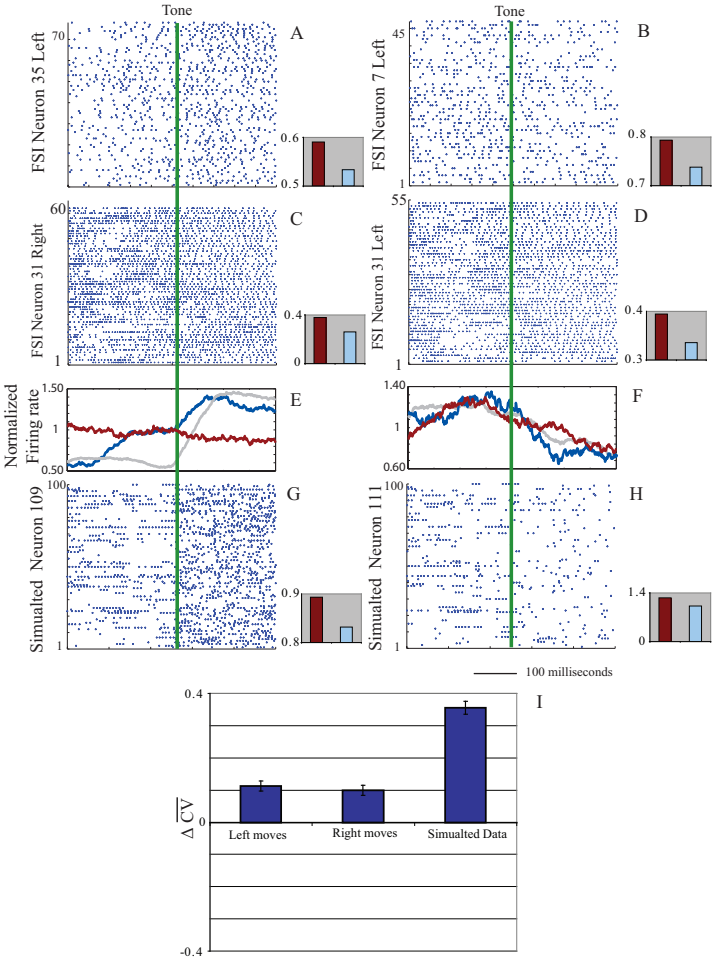

Figure 2.11: Stabilization of experimental and simulated data irrespective of firing rate changes. Experimental data from two neurons which showed an increase (A) and decrease (B) in firing rate. Additionally, we show an experimental neuron which demonstrates a clear stabilization in firing pattern (C and D). For these raster plots, lines represent the same neuron on different trials, rather than different neurons on a single trial. For comparison we show 100 trials from two simulated neurons which show an increase (inside the specific region) (G) and decrease (outside the specific region) (H) in firing rate. The sliding binned (100ms) firing rate is plotted in (E and F) for experimental (blue line neuron 35 and 7, red line neuron 31) and simulated (grey line) data. Inset bar plots show $\bar{CV}$ before (red) and after (light blue) the tone (or input shift for simulations) and are scaled to clearly see the differences. All individual examples show a stabilization (decrease in $\bar{CV}$) for all samples, regardless of the increase or decrease in firing rate. (I) Cumulative stabilization of all simulated neurons and simulated data $\bar{CV}$.

FSIs show diverse, behavior-linked, firing patterns in this and other tasks [28, 137], we still found overall increased stabilization in the FSI population.

For all leftward movements 8/39 neurons showed a significant stabilization, 2/39 neurons showed a significant destabilization, 6/39 neurons showed a statistically insignificant stabilization, 7/39 neurons showed a statistically insignificant destabilization, and 16/39 neurons had insufficient statistics. The mean shift for all 39 neurons was $\langle \Delta CV_{left} \rangle = 0.11$ and the surrogate trials gave $\langle \Delta CV_{surrogate,left} \rangle = 0.00 \pm 0.015$, giving a Z score = 7.3 and P value = $2.87 * 10^{-13}$. For all rightward movements 6/39 neurons showed a significant stabilization, 2/39 neurons showed a significant destabilization, 11/39 neurons showed a statistically insignificant stabilization, 5/39 neurons showed a statistically insignificant destabilization, and 15/39 neurons had insufficient statistics. The mean shift for all 39 neurons was $\langle \Delta CV_{right} \rangle = 0.10$ and the surrogate trials gave $\langle \Delta CV_{surrogate,right} \rangle = 0.00 \pm 0.016$, giving a Z score = 6.3 and P value = $2.98 * 10^{-10}$.

We also analyzed the simulated data using an identical method. Like the experimental data, simulated neurons may show an increase in firing rate if that neuron is within the stimulated region (neurons 90-110, Figure 2.10) or a decrease if it is located outside of it. Regardless of these firing rate changes however, the neurons exhibit an overall stabilization (left on right columns, Figure 2.11). This effect is demonstrated in panels C and D of Figure 2.10. For simulations, 1039/1352 trials showed a positive stability shift. The mean shift was $\langle \Delta CV_{sim} \rangle = 0.36$ and the surrogate trials gave $\langle \Delta CV_{surrogate,sim} \rangle = 0.00 \pm 0.020$, giving a Z score = 18 and P value =$4.44 * 10^{-16}$.

2.5 Discussion

We found that neuronal networks in which nodes are coupled by both inhibitory chemical synapses and gap junctions can support a wide range of dynamic states, that depend critically on network architecture. Although the random vs. local nature of

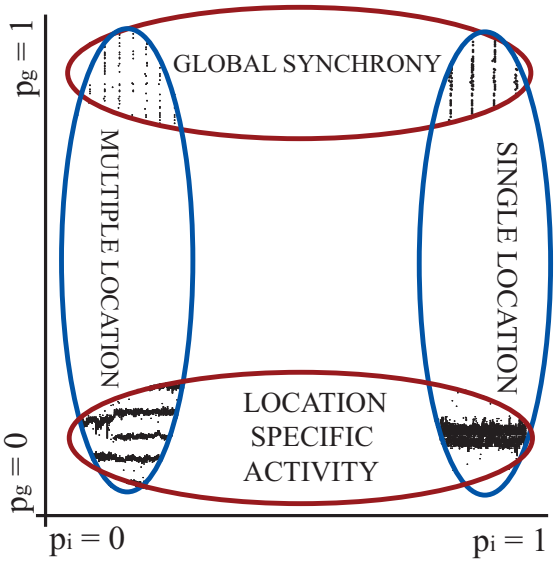

Figure 2.12: Summary of results on the interplay between topological conditions and LAS or GSS activity. Changes in structure of inhibitory connectivity is plotted on the X-axis, while structure of GJ connectivity is marked on Y-axis.

connectivity is a key parameter for both the chemical and electrical synapses, these two types of connection play non-interchangeable roles in setting network dynamics (schematically described in Figure 2.12). In particular, relatively local connectivity of the electrical network mediates the formation of discrete domains of highly active synchronized neurons (LAS state). This type of pattern formation is in stark contrast to the globally synchronized state that is created by a more widely distributed GJ connectivity in interneuron networks [129, 131, 132].

We further found that interneuron networks can show a sudden switch from unstable to stable temporal pattern formation, prompted by modest changes in the spatial distribution of input spiking rate or synchrony. We hypothesize that such dynamics may serve to support a search-and-select function of interneuron networks that could be useful in various brain networks. Finally we examined the activity patterns of real striatal FSIs and found evidence for a comparable switch from unstable to stable firing as actions were selected. These results both support a role for striatal FSI dynamics in decision-making, and begin to provide an functional explanation for

anatomical observations of local GJ connectivity in the striatum [40].

Interneuron network architectures vary between brain regions. For example, cortical and hippocampal CA1 GJ networks are much more uniformly distributed in structure without much variation along relevant spatial dimensions [36, 37]. In contrast, recent evidence shows that the striatal topology is highly irregular, with regions of higher and lower density and connectivity [40]. These differing network structures may result in distinctly different activity patterns of otherwise similar neurons. Our results support the idea that such structural differences result in distinct dynamic properties, that support distinct functional roles.

From a functional side, interneurons in the visual cortex [86, 37] and CA1 hippocampal formation [127, 35, 36] facilitate synchronization between their connected neurons by global population bursts [35, 132, 39]. Conversely, while striatal FSIs have similar intrinsic properties to FSIs elsewhere, they behave quite idiosyncratically in their firing rate, synchronization [28], and oscillatory entrainment [140]. Striatal FSIs may be participating in the formation of local microzones of enhanced activity, consistent with the idea that this structure processes information in a more parallel and fractured fashion than the integrated computational spaces established in hippocampus [60, 140].

These ideas will benefit from future studies on both the simulation and experimental sides. The conditions leading to spatial pattern formation should be further explored, for example by manipulating different parameters of inputs to simulated FSI networks and by incorporating features of projection neurons as well. Additional electrophysiological studies should reveal whether the stabilization of striatal FSIs occurs for a range of decision types, and by using a greater number of densely packed recording sites may be able to detect coordinated activity within very local microregions. New technologies are also opening the door to direct and selective manipulation of FSIs within networks (e.g. [30]) and thus will allow additional critical tests of the

relationships between FSI network pattern formation and behavior.

2.6 Acknowledgements

This work was supported by The Tourette Syndrome Association (JB), the Whitehall Foundation (JB), the National Institute on Drug Abuse (R01 014318; JB), the NIH Molecular Biophysics Training grant (T32 GM008270; TL) and NIH NIBIB grant EB008163 (MZ).

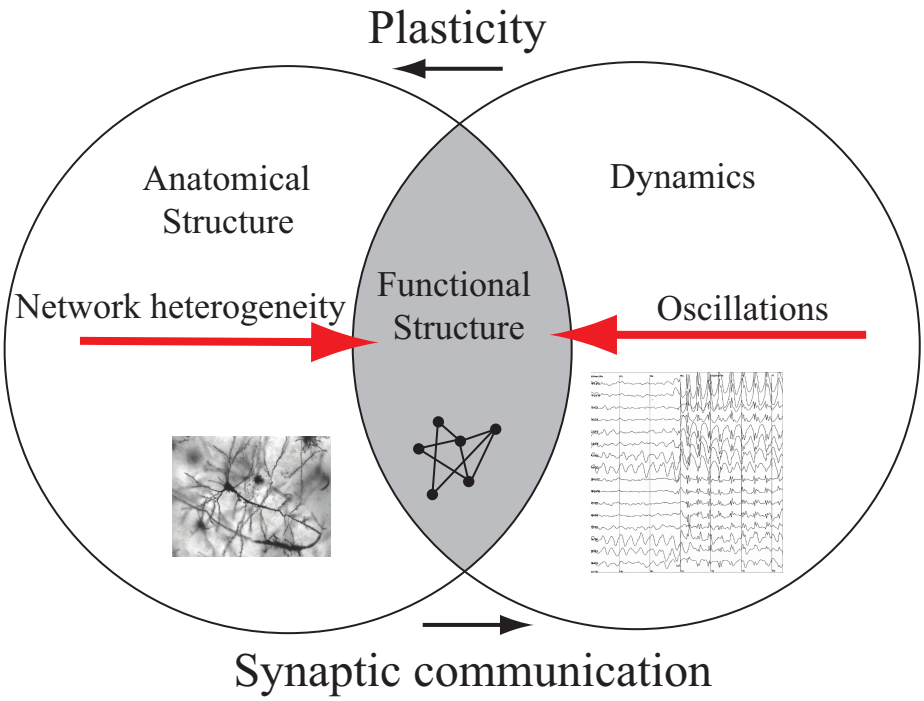
Plasticity
Anatomical
Structure
Dynamics
Network heterogeneity
Functional
Structure
Oscillations
Synaptic communication

CHAPTER III

Interaction between connectivity and oscillatory currents in a heterogeneous neuronal network

3.1 Introduction

The last chapter demonstrated how the network structure plays a critical role in the spatio-temporal dynamics of a neuronal network. In the brain however, more than just the network structure can influence the dynamics. In particular, external currents can interact with the network structure to elicit different types of activity. The dynamic characteristics of these currents play a significant role in the resultant activity of these structures, as they reflect the variety of things we learn, experience, and interact with throughout the day. This chapter therefore takes the next logical step, and combines network topologies with different characteristics of input currents. This is done in the context of oscillations, a very prevalent and important mechanism in the brain. As you will see in this chapter, the interaction between the network structure and input-dynamics greatly influence the output-dynamics in neuronal networks.

The oscillatory patterning of neural activity is ubiquitous and is thought to play a major role, in many functions, across nearly all regions of the brain [56, 57, 58, 59, 52, 56, 60, 61, 62, 63, 64]. Delta (1-4 Hz) [141], theta (4-10 Hz)[142, 59], alpha (8-12 Hz)[141], and gamma (25-100 Hz)[143, 57, 58, 144, 82, 145] frequencies are more

than just categorical denominations as each range is prominent and have independent functions in different areas. Accordingly, a considerable amount of work has been dedicated to the mechanisms involved in the generation of these oscillations (for example [81, 82, 123] and references therein). These mechanisms can be broadly divided into two groups: intrinsic cellular mechanisms and network based mechanisms. It is known that single cells can exhibit intrinsic oscillatory rhythms that are mediated by subthreshold voltage dependent currents or after hyperpolarization [123, 146, 54, 55, 82]. For example, certain neurons are postulated to classically resonate in response to subthreshold oscillatory current [68, 67]. From a network perspective, studies have shown that interacting cell assemblies can also mediate the formation of oscillatory patterning of their activity [80, 81, 82]. Recent work by Vervaeke et al. has demonstrated a (de)synchronization dependence on the local organization of the chemical synaptic connections in the Golgi interneuron network of the cerebellum [147].

An equally extensive amount of research has focused on the role of these oscillations during information processing. Various studies have suggested their role during learning [59], various stages of sleep [148], and recall [59] amongst many other processes. Oscillations are thought to act as a gating mechanism [124, 149], aid in enhancing connections via spike-timing dependent plasticity [144], or serve in the coordination of large separated groups of neurons [150]. From a more physical perspective, input frequencies have also been studied in the context of stochastic resonance, or the enhancement of an oscillatory signal in the presence of specific noise [151, 152, 153, 73].

Most of the work done until now has focused on the role of oscillations in homogeneous networks, i.e. networks having uniform structural and dynamical properties throughout their assembly [154, 155]. Brain networks however, are highly heterogeneous. Even within the same brain structures, such as the neocortex or hippocampus, the local network connectivity is being constantly altered by different processes. The

long-term potentiation or depression of synapses that underlie learning lead to the selective formation of cells ensembles with higher connectivity densities and increased synaptic connection strengths [156, 157]. In this chapter we focus on understanding how a uniform oscillatory drive interacts with structural heterogeneities in a neuronal network and how it may provide a dynamical backbone for information processing. Such an oscillatory drive is common throughout the brain both externally, as in the pacemaker medial septum leading the hippocampus [158], or from intrinsic sources, as in the slow-pyramidal and fast-basket cell interaction in the cortex [159]. We have found that the frequency of the input oscillation can act as a control parameter for the patterning of activity in the network. We show that for certain, large sets of network parameters, as well as specific ranges of frequency/amplitude of oscillation, the activity of the network region with modified structural properties can be selectively enhanced. This enhancement is in the form of an increase in total firing rate or in the increase of phase coherence of neuron spike times. Furthermore, the frequency ranges where the phase coherence of the heterogeneity are enhanced are significantly different than the frequency ranges where the firing rates are increased. These effects are modulated by the number of connections, synaptic coupling strength, and network structure.

Our results provide an insight into the possible dynamical underpinnings of the differential roles of oscillatory drive in the neural networks. We demonstrate that otherwise similar input oscillations can have drastically different effects depending on the properties of the network structure, and therefore different functional roles in the brain.

3.2 Modeling

3.2.1 Network architecture

We modeled a neuronal network consisting of groups of 200 excitatory and 200 inhibitory neurons. Both groups were arranged on a 1-D lattice with periodic boundary conditions forming a ring structure. The network elements were coupled using the Small-World paradigm [75] where neurons are initially connected to their nearest neighbors within a radius r, then randomly rewired anywhere within the network with probability p. Thus, $p = 0$ returns a uniform and locally coupled network and $p = 1$ returns a randomly and globally coupled network. A more realistic proportion of excitatory to inhibitory neurons is 80% - 20% and we have used the 50% - 50% ratio for symmetry purposes only. The results of this chapter are maintained for either ratio and we refer the reader to section 3.4.3 where we investigate a range of excitatory-inhibitory ratios. The use of a 1-D model was chosen to best suit the standard definitions of 'nearest neighbor distances' and other parameters in the Small-World paradigm [75] as well as in the interest of time, as more neurons are needed to model a 2-D architecture to the same accuracy. Previous work has also shown the neuronal dynamics are readily translatable from 1-2-3D cases [160, 161, 162]. To insure the robustness of our results however we briefly investigate a 2-D network in Section 3.4.4.

There were four connection topologies to consider for these two networks: the connections within the excitatory network (r_e, p_e), within the inhibitory network (r_i, p_i), from the excitatory to the inhibitory network (r_{e-i}, p_{e-i}), and from the inhibitory network to the excitatory network (r_{i-e} , p_{i-e}). The connectivity radius of connection types were set to be the same, $r_e = r_i = r_{e-i} = r_{i-e} = r$. We varied the connectivity structure emanating from the excitatory network (rewiring parameter $p_e = p_{e-i} = p$) and investigated rewiring parameter values $p \in [0, 1]$. We set the

connectivity emanating from inhibitory cells to be random $p_i = p_{i-e} = 1$ such that the inhibitory layer imparts global inhibition to the excitatory layer.

3.2.2 Integrate-and-Fire neuron model

It is known that neurons, and accordingly oscillator neuron models, can have distinct and complex interactions with oscillatory depolarizing currents. The goal of this work was to understand the interactions that result from the network itself and not on effects stemming from the dynamics of single neurons. Therefore we have used the leaky integrate-and-fire neuron model throughout most of our simulations. This model lacks a oscillating properties and a classical resonance frequency, therefore all frequency responses are direct properties of the network interactions themselves. This is not to say however, that the interaction between neuronal and network dynamics are not prevalent in real brain systems, quite the contrary is true, only that we seek to reduce the system to a network response to better understand this particular underlying mechanism. Sections 3.4.5 and 3.4.6 briefly cover the the interactions with more complex resonating neuron models.

$$C\frac{dV^j}{dt} = -\alpha_j(V - V^j_{rest}) + I_{ext} + \sum_k w^k_{syn} S^{jk} I^k_{syn} \tag{3.1}$$

Here, V^j is the membrane potential of the j^{th} neuron, α is a leakage coefficient which is different for every cell, $1/R_s = \alpha_j \in [0, 0.1]\mu S$; I^k_{syn} is the synaptic current generated at the time of the spike, w^j_{syn} defines the excitatory or inhibitory synaptic coupling strength and each element positive/negative for excitatory/inhibitory neurons; S^{jk} is the synaptic connectivity (adjacency) matrix; and I_{ext} is an external current (see next section). We investigated a range of synaptic couplings $w_{syn} \in [0, 0.3]$ increments of 0.1. For the simulations in this chapter the value of capacitance was $C = 0.5nF$ hence $\langle \tau_j \rangle = 10ms$ and $V_{rest} = -70mV$. We employed Eulers method to solve for the voltage with timesteps of $dt = 0.25ms$.

The synaptic current is activated after the presynaptic neuron reaches a threshold $V_{thresh} = -54mV$ and fires an action potential. The pre-synaptic neuron is then returned to V_{rest} and remains there for a refractory period $t_{ref} = 10ms$. The synaptic current is of the form:

$$I^k_{syn}(t) = (e^{\frac{-(t-t^k_{spike})}{\tau_s}} - e^{\frac{-(t-t^k_{spike})}{\tau_f}})I_{base} \tag{3.2}$$

where $I_{base} = 8nA$ scales the synaptic current, $(t - t^k_{spike})$ is the time since the last firing of the presynaptic neuron, $\tau_s = 3ms$ is the slow time constant, and $\tau_f = 0.3ms$ is the fast time constant. The variables τ_s and τ_f are chosen such that the post-synaptic potential lasts approximately 2 ms. There was a 2.5 ms synaptic delay between each neuron. We have investigated networks with different transmission delays and no major differences were detected.

To create the heterogeneity in the network, we selected a group of 20 adjacent neurons (usually IDs 90-110) and increased their synaptic coupling strength (w_{syn}) by 30% as compared to the rest of the network. This 30% increase was maintained when the overall w_{syn} was increased for the entire network. We also investigated a range of other connection strength enhancements and by designing the heterogeneity via added connections. We referred to this region as the structurally enhanced region. Varying the size of this region did not have a qualitative effect on our results.

Additionally, each neuron was individually exposed to a Poisson noise. The random probability of a neuron firing was set to 0.05% per time step, resulting in an average firing rate of 2 Hz in the absence of any other input.

3.2.3 External oscillating current

We controlled the oscillatory input into the network via the external current I_{ext}. Both the excitatory and inhibitory neurons were driven by the external oscillating current $\langle I_{ext} \rangle = 0$:

$$I_{ext} = A_{dr} sin(f_{dr} t + \delta), \tag{3.3}$$

where A_{oss} is the amplitude of the oscillation, f_{dr} is the driving frequency and δ is a random starting phase. We investigated $f_{dr} \in [3, 90] Hz$ in increments of 3 Hz and $A_{dr} \in [0.4, 1.2] nA$ in increments of 0.1 nA. This oscillation may be thought of as an external current source [158] or an intrinsically generated current source input into this specific population of neurons [147].

3.3 Analysis

We used two metrics to quantify the behavior of the network: regional firing rates (activity) and the mean phase coherence (MPC). The firing rate was defined as the number of firings per neuron per second and was calculated separately over the enhanced region and the rest of the network. To quantify how active the enhanced region was over the rest of the network, we defined the activity ratio as the firing rate of the enhanced region divided by the firing rate of the rest of the network.

We used the MPC to measure the amount of phase locking between cells [94, 71]. The MPC ranges between 0 (least coherent) and 1 (most coherent). The MPC is calculated pair-wise between neurons inter-spike-intervals via the equation, for the MPC between neuron n and m:

$$MPC_{nm} = \left| \frac{1}{S} \sum_{s=1}^{S} e^{i \phi_{nm_s}(j)} \right| \tag{3.4}$$

Here S is the total number of measurements of cell ms spike times within the first and last firing of cell n and ϕ_{nm_s} is the phase between cell n and m for interval j containing s. The phase is defined as

$$\phi_{nm_s}(j) = 2\pi \frac{\tau_{n_j,m_s}}{\tau_{n_j}}, \tag{3.5}$$

where

$$\tau_{n_j} = t_{n_{j+1}} - t_{n_j}; \tag{3.6}$$

is the inter-spike-interval j for neuron n containing s and

$$\tau_{n_j,m_s} = t_{m_s} - t_{n_j}; \tag{3.7}$$

is the time difference between the initial firing of neuron n, on interval j, and the firing s, of neuron m, with the condition,

$$t_{n_j} \leq t_{m_s} \leq t_{n_{j+1}} \tag{3.8}$$

Finally, to calculate total MPC we take the average of all MPC pairs across all neurons,

$$MPC = \frac{1}{NM} \sum_{n}^{N} \sum_{m}^{M} MPC_{nm} \tag{3.9}$$

where N = M = 200 are the total number of neurons.

As before, we also computed the MPC of the enhanced region, outside region, and the MPC ratio to determine the difference in coherence. Because the MPC is a pair-wise calculation, and can be very time intensive, the outside region was defined as a random subset of 20 adjacent neurons not in the enhanced region.

3.3.1 Power spectral density

To compute the power spectral density (PSD) plots, we binned the total spiking output (10 ms bins) of the enhanced and outside region. This was simply a sum

of ones (if the neuron fired) and zeros (if it did not). We then used the MATLAB Fast-Fourier Transform function on the complete 2000 ms simulation.

3.3.2 Resonate and fire neuron model

To better understand the generality of our results, we investigated the basic phenomena for two other classes of neurons: the resonate-and-fire and Hodgkin-Huxley Type I models. The resonate-and-fire neuron was based off the model presented by Izhikevich [71]. We selected the model because the classical resonance frequency/condition was easily modified and achieved. The model is a 2-D linear system where x is the current like internal variable and y is the voltage like internal variable. Here

$$\frac{dx}{dt} = -x - \omega y + I_{ext} + w_{syn,j} \sum_k S^{jk} I^k_{syn} \tag{3.10}$$

and

$$\frac{dy}{dt} = -\omega x - y \tag{3.11}$$

For a full discussion refer to [71]. For our analysis, we adjusted the parameters of the neuron, $\omega = 0.2, 0.3$, and 0.4 (all other values remain the same), to resonate at roughly 30, 45, and 60 Hz respectively.

3.3.3 Hodgkin Huxley neuron model

We selected a Type-I non-resonating Hodgkin Huxley interneuron neuron based off a model by Wang and Busaki [123] and generalized by Pfeuty et al. [132]. These neurons had two compartments (somatic and dendritic) with sodium, potassium, and leak currents, along with an excitatory and inhibitory coupling in the same manner as our simulations. A brief summary is provided below; for the detailed description

we refer you to [132, 123]. The model is divided into a somatic compartment (s) and dendritic compartment (d). The dynamics of the somatic compartment are given by:

$$C\frac{dV^s}{dt} = -I_L - I_{Ns} - I_{Kdr} - g_c(V^s - V^d) + I_{noise}, \tag{3.12}$$

the dendritic compartment is described by:

$$C\frac{dV^d}{dt} = -I_{L,d} - g_c(V^d - V^s) + I_{ext}, \tag{3.13}$$

where the currents are $I_L = g_L(V^s - V_L)$, $I_{L,d} = g_L(V^d - V_L)$, $I_{Na} = g_{Na}m_\infty^3 h(V^s - V_{Na})$, and $I_K = g_K n^4(V^s - V_K)$.

I_L is the leak current, I_{Na} transient sodium current and I_{Kdr} is the delayed rectifier potassium current, m, h, n are voltage dependent conductances. We implemented these equations with following parameters: $g_{Na} = 35mS/cm^2, V_{Na} = 55mV, g_K = 9mS/cm^2, V_k = -75mV, g_L = 0.1mS/cm^2, g_c = 0.3mS/cm^2, V_L = -65mV, C = 1F/cm^2$

3.4 Interaction of network properties and oscillations

Our goal was to understand the interaction between network topology and oscillatory input on the dynamics of a heterogeneous neuronal network. For this reason we have created a network that has a localized region of increased connectivity (w_{syn} is fixed to 30% higher than the rest of the network). To investigate the differences of network response within the synaptically enhanced region, we measured the spiking activity and MPC within the region and within the rest of the network, and took the ratio of the two values. Throughout this chapter we monitored these values as a function of the driving frequency f_{dr} of input.

We first studied the change of activity for the enhanced region, the outside region, and the ratio of these two while changing the oscillatory input frequency f_{dr}

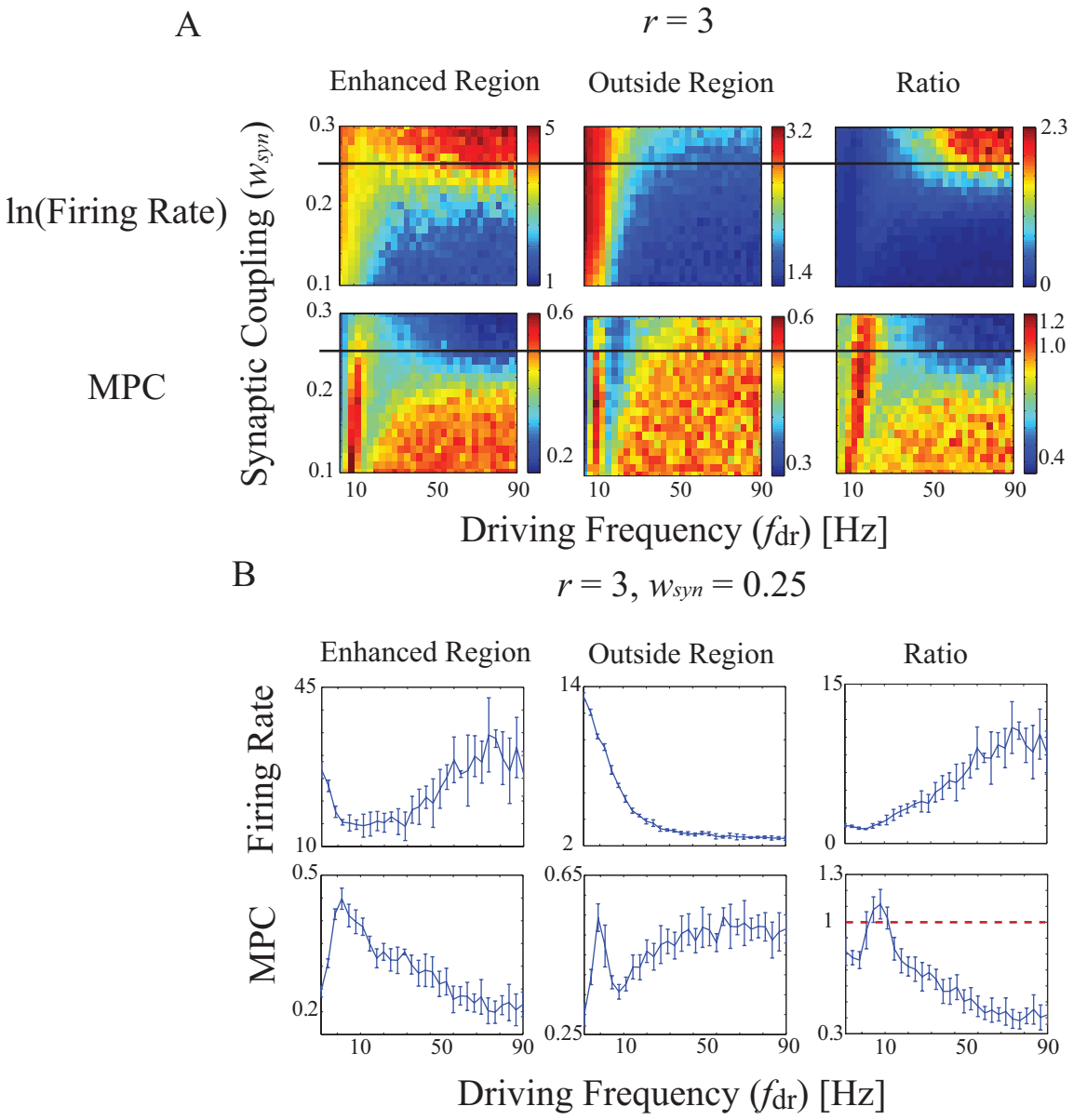

Figure 3.1: Comparison of activity patterns between the structurally enhanced region and rest of the network. A) Top - The natural log of the firing rates for the enhanced region, rest of the network, and the natural log of ratio of the two. Bottom - the mean phase coherence for the corresponding regions. We varied the synaptic coupling and oscillation frequency while keeping the oscillation amplitude $A_{dr} = 0.8nA$ and connection radius $r = 3$ fixed. B) The same measures as before but for a specific value of synaptic coupling $w_{syn} = 0.25$. Parameter values correspond to the line drawn through the figure on the left. The red dotted line signifies a MPC ratio of 1.

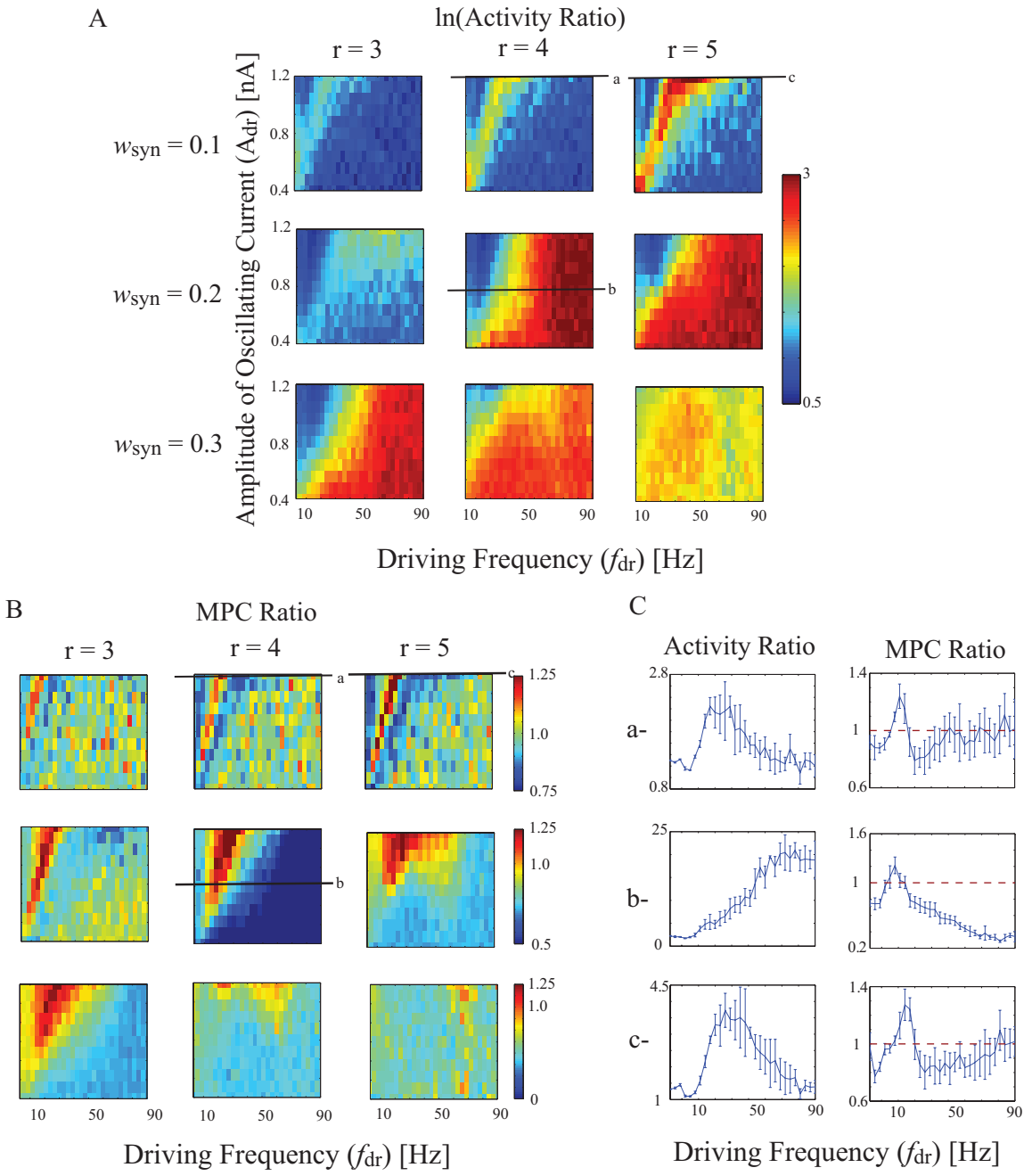

Figure 3.2: Frequency dependent enhancement of the activity of the enhanced region. A) The natural log of the activity ratio and B) the MPC ratio. We vary the amplitude of the input oscillation $A_{dr} \in [0.4, 1.2]nA$ and driving frequency $f_{dr} \in [3, 90]Hz$ for three different $w_{syn} = 0.1, 0.2, 0.3$ and $r = 3, 4, 5$. C) Selected line plots for parameter values as denoted on the color figures (a): $r = 4$, $w_{syn} = 0.1$, $A_{oss} = 1.2nA$; (b): $r = 4$, $w_{syn} = 0.2$, $A_{dr} = 0.8nA$ and (c): $r = 5$, $w_{syn} = 0.1$, $A_{dr} = 1.2nA$.

and the network coupling strength w_{syn}. Figure 3.1 shows vastly different spatio-temporal activity patterns depending on these parameters. At lower frequencies, for the whole range of synaptic couplings, the entire network is active due to the peaks of the slow oscillations acting as 'almost constant' depolarizing currents. At higher frequencies, and higher synaptic coupling strengths, only the enhanced region is able to maintain spiking activity. This increase in activity is generated and sustained by the enhanced region's increased synaptic coupling strength, causing each excitatory pre-synaptic spike to have a stronger post-synaptic depolarization. This is then inherently a network effect, and will be dependent on the connectivity properties (w_{syn} and r). Figure 3.1 further suggests however, that the network properties interact with individual neuron input properties (f_{dr} and A_{dr}). This will be expanded upon and explained in the following sections.

Overall, the network activity displayed three gross behaviors as a function of driving frequency: a random state where the oscillation is not sufficient to stimulate the network and the activity is primarily driven by external noise; a network-wide bursting state typically mediated by slow oscillations; and a state where the enhanced region is predominantly active, typically mediated by higher frequency oscillations. Additionally we observed changes in the mean phase coherence within the heterogeneity. That enhancement typically occurred for lower frequencies, just before the transition from the global bursting to increased activity of the enhanced region.

Figure 3.2 depicts an overall summary of the obtained results for changing characteristics of the input current. The color plots in Figure 3.2A depict the natural logarithm of the activity ratio between the enhanced region and rest of the network for different values of connectivity ($r = 3, 4, 5$). Figure 3.2B represents the MPC ratio for the two regions. The three rows represent three different values of overall network coupling strength. The x-axis on the color plot represents the driving frequency f_{dr}, while the y-axis is the amplitude (A_{dr}).

For weak network coupling strength (Figure 3.2, $w_{syn} = 0.1$, all r) we observed a narrow band of increased activity ratio that is highly dependent on the driving amplitude. The changes in MPC ratio are largely insignificant, showing minimal enhancement for frequencies just preceding the activity enhancement. For the intermediate and high network coupling strength regime (for all r) we observed a significant shift of the activity increase towards the high frequency regime for all oscillatory amplitude values. Furthermore, we also observed a large frequency regime where the network heterogeneity displays an increased MPC. This occurs for low frequencies preceding the transition to enhanced region activity enhancement (Figure 3.2, $w_{syn} = 0.2$, $r = 4$).

The observed changes in the activity ratios and MPCs are due to two competing processes. In the weak coupling regime the enhanced region displays a increase of its activity for a discrete low frequency range. This occurs because the oscillations are slow enough that the peaks of the oscillation provide a sufficient time window to sustain network induced activity. This activity is only maintained in the enhanced region because the increased excitatory synaptic potentials depolarize neighboring neurons sufficiently. This can be see in Figure 3.3 where for low $< 20Hz$ frequencies both the enhanced region and the outside network can sustain activity. Above this frequency however, only the enhanced region can sustain activity. This frequency range is preceded by a phase locking of the neurons to a slow ($< 20Hz$) oscillatory drive and invokes synchronous activity within the enhanced region. This synchronous activity further increases the enhanced region's ability to maintain activity because the excitatory post-synaptic potentials are highly coincident.

For the intermediate and high values of network coupling, the resonance effect is superseded by the enhanced region's propensity to easily enter a highly active, reverberatory regime with natural frequencies around 70 Hz. This reverberation is generated by the enhanced region's neurons integration time (controlled by the leak-

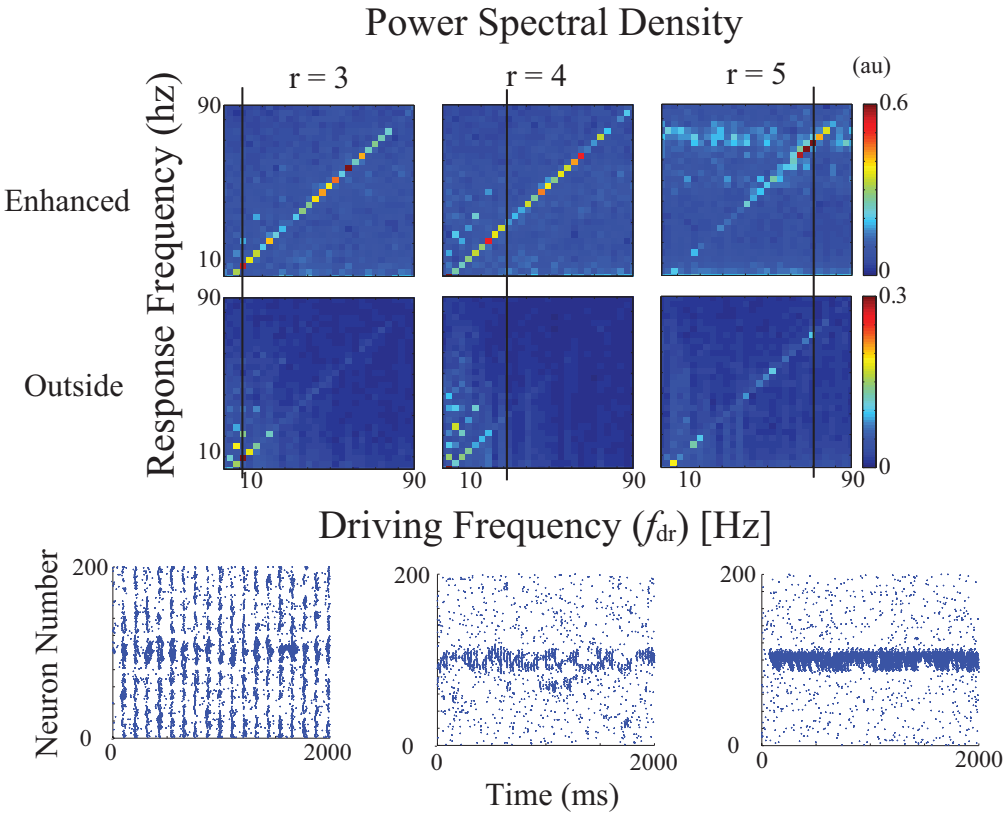

Figure 3.3: Spectral Density analysis of the total network response to oscillatory drive. We plotted the PSD of the averaged activity for the enhanced (top) and outside (bottom) regions vs. the driving frequency $f_{dr} \in [3, 90]Hz$. For $r = 3, 4$, and 5 the synaptic coupling is fixed at $w_{syn} = 0.3, 0.2$, and 0.15 respectively. $A_{dr} = 0.8nA$ for all simulations. The bottom row depicts raster plots for driving frequency denoted by the black lines for $r = 3$ (left), $r = 4$ (middle), and $r = 5$ (right).

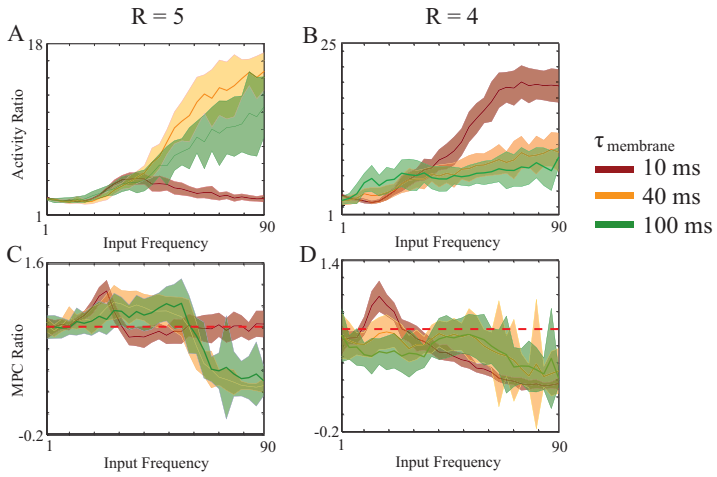

Figure 3.4: Changing the membrane time constant $\tau_{membrane}$ adjusts the Frequency Response of the Network. The activity ratio and MPC ratio for increasing membrane time constants. A and C. Oscillation amplitude is fixed at $A_{dr} = 1.2nA$, $r = 5$, and $w_{syn} = 0.1$ B and D. Oscillation amplitude is fixed at $A_{dr} = 0.8nA$, $r = 4$, and $w_{syn} = 0.1$

age current and synaptic input), synaptic delay, and refractory period matching the frequency of the oscillation, allowing sustained activity to quickly pass back and forth throughout the enhanced region. Basically each neuron is ready to integrate up and fire again at the peaks of each oscillation inducing a network resonance effect. Concurrently, the rest of the network is strongly inhibited by the inhibitory network receiving increased input from the enhanced region. Figure 3.3 also shows the network's propensity to fire at this rate (top right) and the drastically increased activity when the input frequency is in this range. Additionally Figure 3.3 shows how the number of connections (changing the synaptic current each neuron receives) affects the frequency dependencies. From this it is clear that increasing the number of connections decreases the integration time of the neuron, generating a stronger band of activity in the high frequency 70-80 Hz range.

We also investigated the effects the refractory period and membrane time constants had on the frequency dependence. Figure 3.4 shows the effects of varying membrane time constants (on the neuron). Not surprisingly, as we decrease the leak-

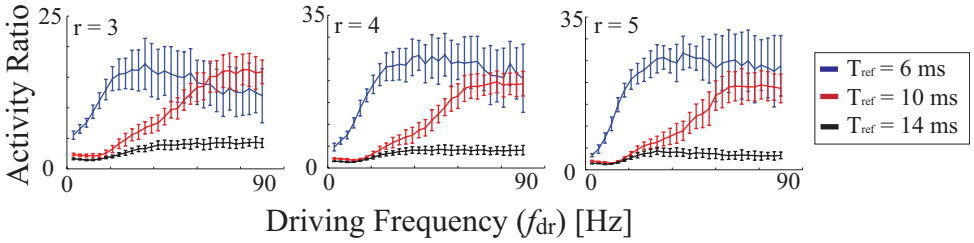

Figure 3.5: Changing the Refractory Period (T_{ref}) adjusts the Frequency Response of the Network. Oscillation amplitude is fixed at $A_{dr} = 0.8nA$ and $w_{syn} = 0.3, 0.2$, and 0.15 for $r = 3$, 4, and 5 respectively.

age, decreasing the time the neuron takes to integrate up, the natural resonance frequency of the network increases. Figure 3.4 A shows the $\tilde{4}0$ Hz peak we achieved for our standard $\tau = 10ms$, a shift to a peak of about 70 Hz for $\tau = 40ms$, and a maximal frequency response of 80-90 Hz for $\tau = 100ms$. Accordingly the activity ratio increases because the enhanced region is firing at a higher frequency and there is increased excitation. It is also interesting to note that the MPC peaks only for the lower frequency current induced activity. This implies a trade off between high and low frequency induced network resonances. The higher frequencies generate the highest activity ratios, but the lower frequencies generate high activity ratios as well with increased coherence, a possibly important property for numerous brain functions.

Figure 3.5 demonstrates the effect the refractory period has on the frequency dependence. From what we have discussed above it is not surprising that a faster refractory time actually benefits slower oscillations. The faster refractory periods allow neurons to fire more than once under a single slow oscillation, important for sustaining activity under each peak. A 10 ms refractory period however is ideal for the high frequency regime because each neuron is simply recharging when the oscillation is in its trough. A 14 ms refractory period is too slow for either of these processes.

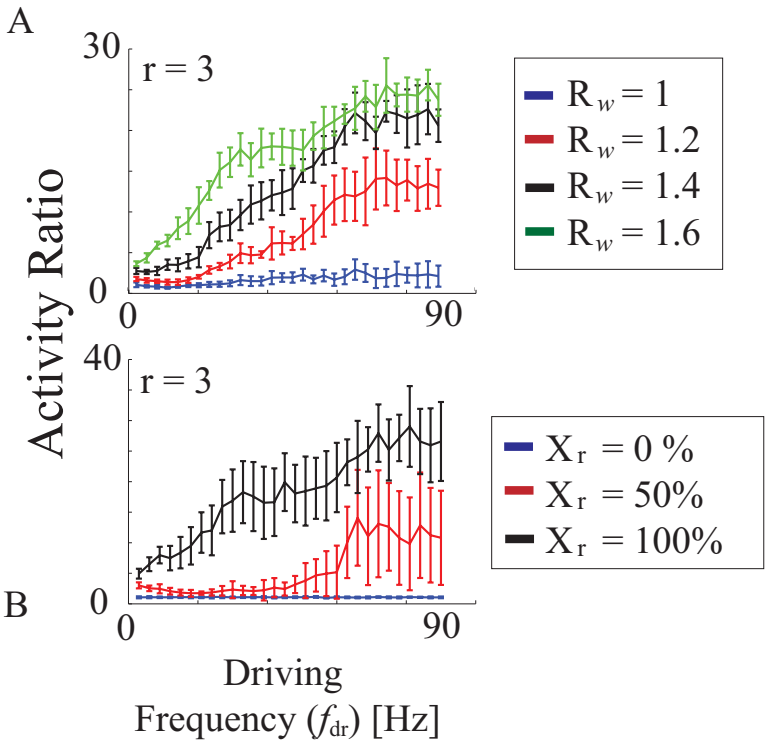

Figure 3.6: Changing the connectivity in the enhanced region. A: the ratio of synaptic coupling strength (R_w) of the enhanced region vs. the rest of the network is varied. B: The enhanced region is built by randomly adding a percentage local connections within the radius $(r + 2)$ for neurons in the enhanced region. For example if $X_r = 50\%$ and $r = 3$ then the neurons within the enhanced region are 100% connected from $r = 1$ through $r = 3$ and 50% connected for $r = 4$ through $r = 5$. For all simulations shown: the connectivity radius of the base network is $r = 3$, $A_{dr} = 0.8nA$ and $w_{syn} = 0.3$.

3.4.1 Different designs of the enhanced region

We then investigated how significant the heterogeneous enhancement needs to be to observe the robust activation differences. We did this by increasing/decreasing the synaptic coupling of the enhanced region by changing the excitatory coupling strength while keeping all other excitatory and inhibitory connections the same (Figure 3.6A). We observed that a relatively small increase in excitatory connection strengths within the enhanced region (around 20% over the rest of the network) allows for a significant increase in activity. This is in comparison to experimentally observed effects of spike timing dependent plasticity which can be on the order of 200%. This change in the excitatory balance provides an adaptive mechanism for the network to respond differently, depending on the overall strength of synaptic heterogeneities.

We also investigated changes in activity when we built the enhanced region through the addition of connections within the region while keeping w_{syn} the same as the rest of the network. We added connections by inserting a random fraction of additional local connections for and increased radius $(r + 2)$. Figure 3.6B demonstrates that a 50% increase in the number of connections was enough to increase the activity ratio. It is important to note however that this 50% increase in number of connections was significantly higher than the 20% increase in w_{syn} needed to increase the activity ratio.

3.4.2 Activity enhancement and network topology

Next we investigated how the network topology affects the enhanced region activity ratio. To do this we have varied the rewiring parameter $p \in [0, 1]$ from local $(p = 0)$ to random $(p = 1)$. We observe that as the connectivity becomes more global the activity ratio attenuates (Figure 3.7). This is due to the fact that as local connections are abolished the network becomes more homogeneous and random and thus the differentiation between the enhanced region ceases to exist. We still however

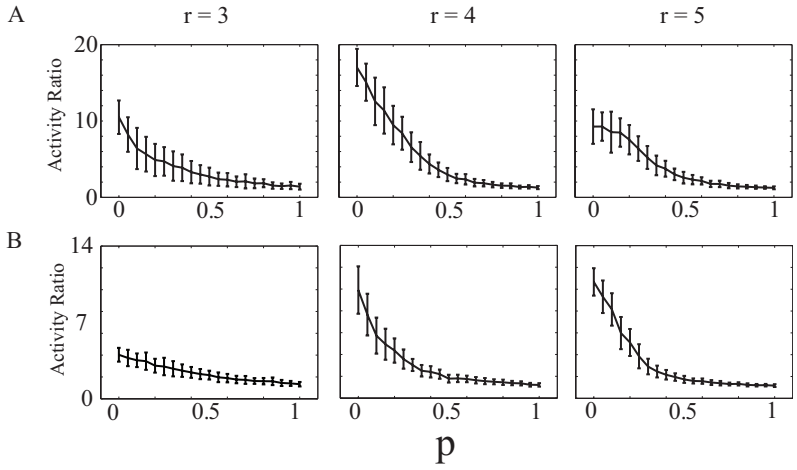

Figure 3.7: Activity ratio dependence on network topology. We changed the value of the rewiring parameter p from 0 and 1 for different parameter values. Values and error bars are averaged over 50 simulations. A) $f_{dr} = 70Hz$; $A_{dr} = 0.8nA$; $w_{syn} = 0.25$; B) $f_{dr} = 30Hz$; $A_{dr} = 0.8nA$; $w_{syn} = 0.25$.

observed significant activity enhancement for intermediate rewiring topologies near the small-world regime.

3.4.3 Changing the number of inhibitory neurons

In this section we investigate the effect the number of inhibitory neurons has on the overall observed behaviors. The overall connectivity parameters remain the same for these simulations but a random percentage of inhibitory neurons are removed from the nominal 200. If in/out connections happen to land on the removed neuron the conenction(s) accordingly cease. Figure 3.8 shows the activity and MPC ratio for two prevalent ranges. Interestingly we observe that the activity ratio increases slightly as the number of inhibitory neurons decreases for the 40 Hz peak parameter range and decreases for the 80 Hz peak parameter range. This occurs because the enhanced region, already firing at its maximal firing rate, at 80 Hz, drives the inhibitory region, which randomly inhibits the rest of the network (Figure 3.8B). When the overall number of excitatory neurons/connections is decreased there is less inhibition to the excitatory network, increasing the activity outside the enhanced region

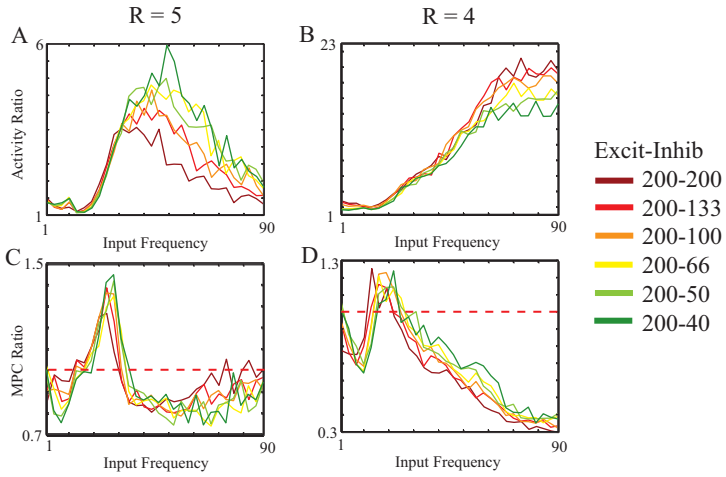

Figure 3.8: Changing the ratio of excitatory to inhibitory neurons. The different ratios of excitatory to inhibitory neurons are plotted in different colors. The error bars have been eliminated for clarity. A,C) $r = 5$, $A_{dr} = 1.2nA$; $w_{syn} = 0.1$; B,D) $r = 4$ $A_{dr} = 1.2nA$; $w_{syn} = 0.2$.

only, hence lowering the activity ratio. Conversely, for the lower activity ratio 40 Hz peak, less inhibition allows the enhanced region to fire at a slightly higher firing rate and frequency peak Figure 3.8A. Recent computational work by Fisher et al. [163] has shown that target spiking rates can be achieved in networks with different balances of excitatory and inhibitory neurons. Such a system might also respond variably to different input frequencies, as this result would suggest. Aside from this slight shift however, the frequency dependent transitions remain largely the same for the activity ratio, and identical for the MPC ratio. This is not surprising because the inhibitory network layer acts only as regulator to the inhibitory network layer. It is unable to self-sustain activity because $\langle I_{ext} \rangle = 0$ and the synaptic input is hyperpolarizing. The only driver of this network then, besides noise, is the activity of the excitatory network, which is in-turn limited by the activity of the inhibitory network. Therefore a steady baseline state of activity is easily achieved and even a large reduction in the inhibitory population has a negligible effect. This result is important because it demonstrates that the frequency dependent activity shifts are robust across a wide range of excitatory-to-inhibitory neuron ratios.

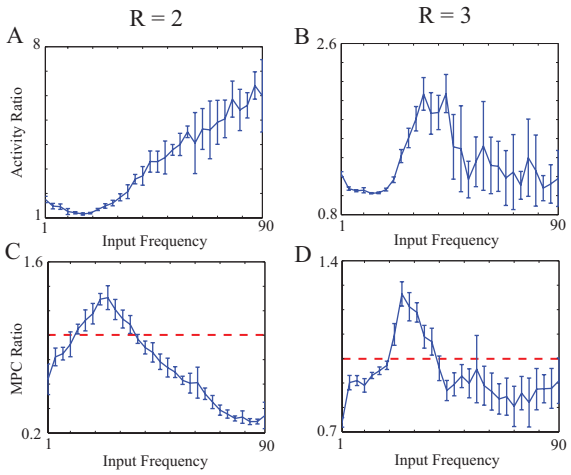

Figure 3.9: Simulation for a 2-D network. A,C - $r = 2$, $A_{dr} = 1.2nA$; $w_{syn} = 0.2$. (B,D) - $r = 4$, $A_{dr} = 1.2nA$, $w_{syn} = 0.065$.

3.4.4 Frequency response of a 2-D network

1-D simulations of neuronal networks are widely used across much of neuroscience research. Though unlikely, here we wanted to ensure that these results were not just artifacts of a 1-D network simulation. Here we simulated a $20 * 10$ periodic 2-D network where the synaptic coupling strengths were necessarily modified to account for the increased connections for a given connection radius (Figure 3.10A). We clearly see that we can recover both the low frequency and high frequency activity ratio responses, and the MPC dependence remained similar to the previous result.

3.4.5 Comparison to a resonate-and-fire neuron

We have specifically chosen a non-resonating neuron model for this chapter to most clearly interpret the impact of the network properties, as opposed to the resonant properties of an individual neuron. A full analysis of the interaction between a single neurons resonance and network properties will be left to another work In this section however, we briefly compare our results to that of a networked Izhikevich resonate-and-fire model (RAF) [71], to ensure that the responses we have observed are ubiquitous.

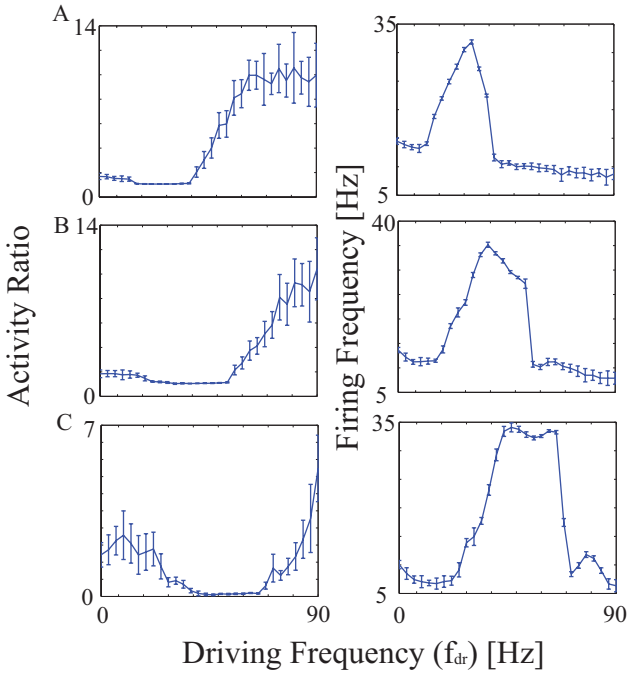

Figure 3.10: Driving frequency vs. activity ratio and overall firing frequency for a RAF neuron. Row A network response for RAF neuron of resonance frequency around 30 Hz. Row B network response for RAF neuron of resonance frequency around 45 Hz. Row C network response for RAF neuron of resonance frequency around 60 Hz. The first column is the enhanced region activity ratio and the second is the overall network firing frequency.

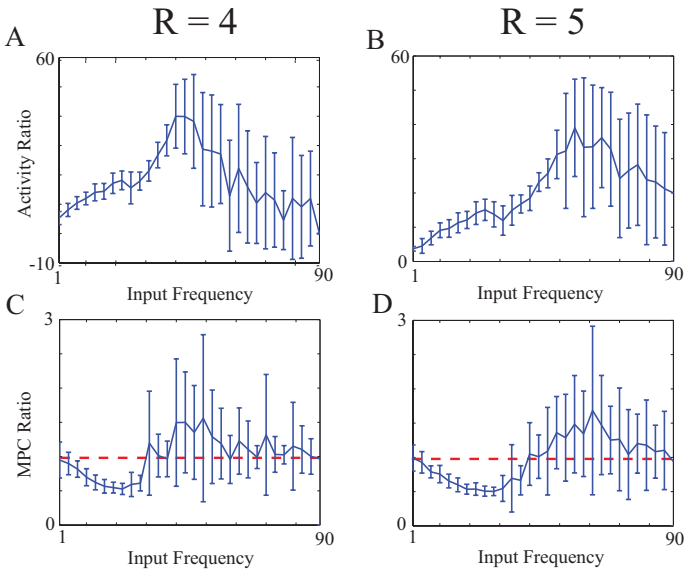

Figure 3.11: Driving frequency vs. activity ratio and MPC ratio for a non resonating Hodgkin Huxley neuron. A - $r = 4$, $w_{syn} = 3$, $A_{dr} = 1.2nA$. B - $r = 35$, $w_{syn} = 2.5$, $A_{dr} = 1nA$ Simulations are averaged over 25 trials.

Here we adjusted the parameters of the RAF neuron, $w = 0.2, 0.3$, and 0.4 (all other values remain the same), to resonate at roughly 30, 45, and 60 Hz respectively. We then performed an identical analysis as previous sections with $w_{syn} = 0.3$, $A_{dr} = 1.2nA$, $r = 4$. Figure 3.10 shows the activity ratio and overall firing frequency of these networks RAF neurons and each frequency. We clearly see the same enhancement in the activity ratio for higher and lower frequencies (Figure 3.10, Column 1). The only part of the activity ratio curve that is affected is the range where single neuron resonance occurs, where the entire network is active, and the activity ratio accordingly goes to 1. We can see this range in Figure 3.10, Column 2.

From these results it is clear that the single neuron dynamical properties superimpose onto the network response. The network response is therefore maintained.

3.4.6 Comparison to a Hodgkin and Huxley neuron

Finally we compared our results to a more biologically realistic Hodgkin-Huxley (HH) neuron. We used a two compartment (soma and dendrite) neuron to contrast

to our integrate-and-fire results Figure 3.11 demonstrates the activity ratio response of these neurons to the varying input frequencies. The HH model neuron did not resonate at any frequency between 1-90Hz, but did have increased impedance at higher frequencies, indicating a weak frequency preference. It is clear that a network of HH neurons with an enhanced region allows for the same frequency-specific selective activation of the enhanced region in similar coupling and current ranges. Additionally we see a shift of the MPC to the frequency range is enhanced. This is not surprising however, because the individual neurons' frequency preference, in this range, causes the firing rate to be modulated at this frequency, therefore enhancing the MPC. What likely occurs in the brain is a balance between these two behaviors.

While this analysis of HH neurons is by no means a thorough investigation of the possible interactions between oscillations and network in a complex neuronal model system, it proves that the observed phenomenon is network driven and independent of the specific dynamical equations of the individual cells.

3.5 Discussion

Oscillations are believed to have important and distinct functions in numerous regions of the brain [57, 149, 144, 59]. Their implicated roles also vary widely as a function of their amplitude and frequency [62, 164]. While high frequency gamma oscillations are thought to play an important role during focused attention and recall [59, 57], slower theta/beta band oscillations are thought to be important for learning [165, 126]. We have shown that, for a network with a heterogeneous connectivity structure, the frequency and amplitude of oscillations can play a crucial role in determining activity patterns within different network regions. While higher frequency oscillations may be optimal for the enhancements in activity of structural heterogeneities, lower frequency oscillations mediate phase locking within these heterogeneities.

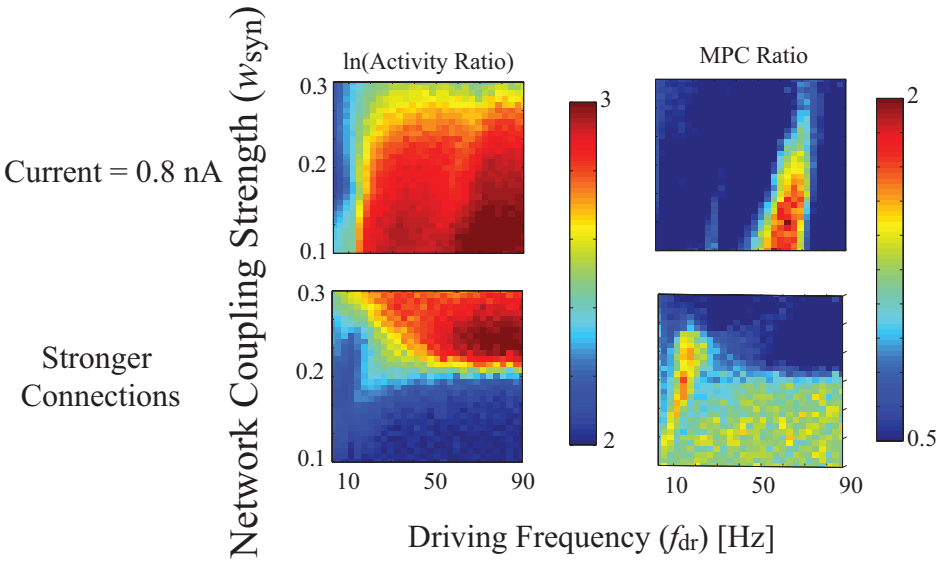

Figure 3.12: Creating network heterogeneity through local depolarization. The natural log of the activity ratio (left) and the MPC ratio (right). We vary the synaptic coupling $w_{syn} \in [0.1, 0.3]$ and oscillation frequency $f_{dr} \in [0, 90]$. We investigated a depolarizing current of 0.2, for a $A_{dr} = 0.8nA$, and r = 4. We compare these results with these obtained for the structural heterogeneity.

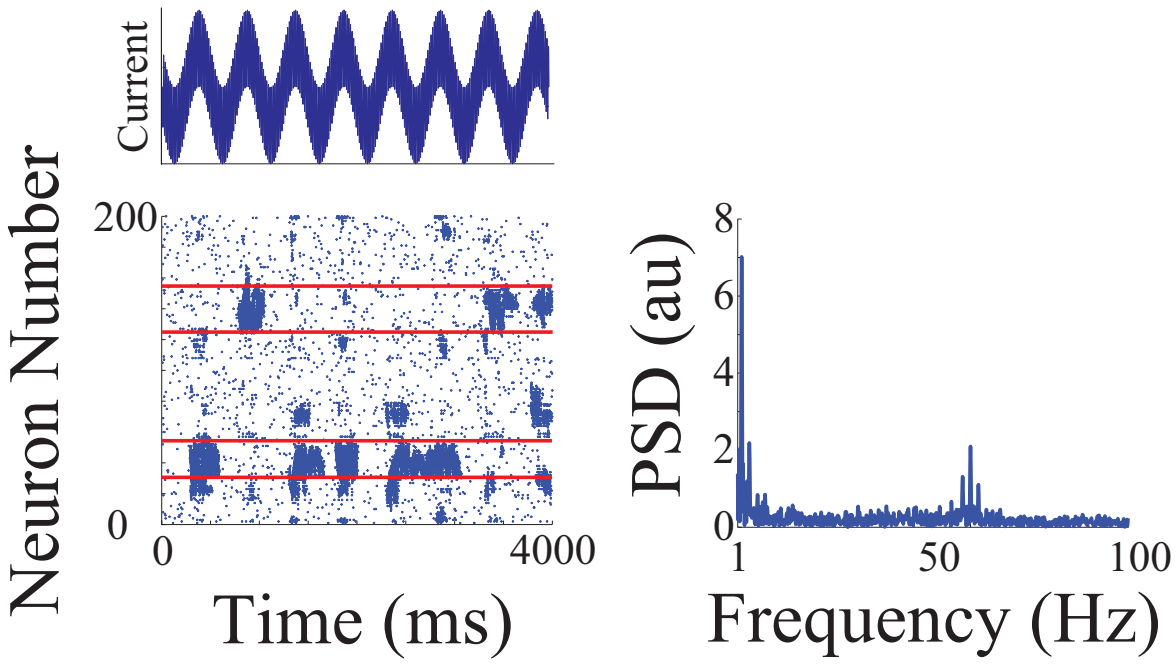

Figure 3.13: A Slow + Fast Oscillatory input allows for switching between two enhanced regions. Enhanced regions are in red. Strong 2 Hz and 60 Hz frequency component is maintained in the activity. Here $r = 5$, $w_{syn} = 0.2$ and $A_{oss} = 0.4nA$. The power spectral density shows frequency activity at low and high frequencies.

This is due to the fact that the additional network mediated current changes, in a nonlinear fashion, the response properties of the enhanced region. These local changes to network properties can be activated by an oscillatory current within specific frequency ranges. The specific ranges depend on the neuronal refractory periods, synaptic communication times, and intrinsic current response, creating an optimal range of frequency responses.

A different response can be obtained by creating a network heterogeneity through the addition of a depolarizing current to a group of cells. Here significant enhancement is obtained throughout most the entire range of driving frequencies and the mean phase coherence increase is shifted towards higher frequencies (Figure 3.12), with no activity ratio peaks at specific frequencies.This suggests that a mere change of balance between excitatory and inhibitory currents due to formation of additional synapses [166] or background spikes rates [163], cannot generate the same results achieved otherwise in this chapter.

One set of processes which might employ this frequency response mechanism are those that involve higher frequency oscillations concurrent with lower frequency oscillations. A commonly observed example is gamma rhythms riding on theta rhythms during encoding and recall in the hippocampus [142]. Additionally, in recent work by Colgin et al. [57] they demonstrated that the specific frequency of a gamma oscillations was routed differentially through either the CA1 or CA3 at different phases of a theta oscillation. Another well documented use is during playback in sleep [122]. In any of these process, pre-developed short-term memory traces are reactivated for recall and/or long term encoding. This reactivation is limited to a small number of traces at a time, not global reactivation of the entire network. If we consider the enhanced region to be analogous to a short term memory trace, then the selective frequency response shown in this chapter provides a mechanism allowing a input frequency to selectively reactivate that memory alone without involving other neurons

and traces in the process. Figure 3.13 demonstrates a model system we have designed to exhibit the possible use of the interaction between fast and slow oscillations when more than one heterogeneity is present. Here we have two enhanced regions, (neuron IDs 40-60 and IDs 140-160) and we input an oscillatory current of 2 Hz and a concurrent oscillatory current of 60 Hz. At the peaks of the 2 Hz oscillation the network randomly activates one of the enhanced regions, while the other is inhibited due to the activity from the inhibitory network. When the 2 Hz oscillation is in a trough the entire network is quiet before either of the enhanced regions are randomly activated again by the peak. Figure 3.13 may be representative of playback of multiple newly formed memories during REM sleep as it provides a mechanism to randomly cycle through memory traces while only activating/encoding one at a time.

In conclusion, the effects that we have discussed in this chapter may provide the dynamical underpinnings to a number of brain functions that are mediated by intrinsic oscillatory patterning. For example, the increased re-activation of an already enhanced region can affect the strength of memory recall or playback during sleep [59, 148]. Additionally, increases in the coherence of neuronal activity can influence spike timing dependent plasticity between neurons, enhancing the network heterogeneity [59, 63].

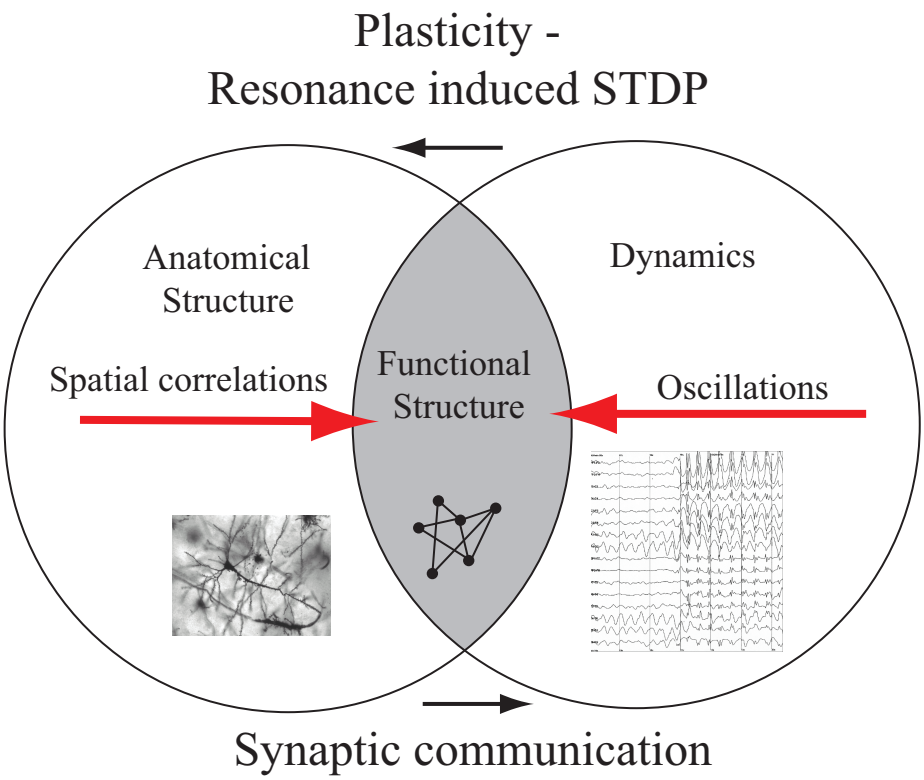
Plasticity -
Resonance induced STDP
Anatomical
Structure
Dynamics
Spatial correlations
Functional
Structure
Oscillations
Synaptic communication

CHAPTER IV

The resonance frequency shift, pattern formation, and enhanced network reorganization via sub-threshold input

4.1 Introduction

The first two chapters of this thesis investigated how both network topology and the dynamical properties of the the input current can influence the spatio-temporal dynamics of the resultant neuronal activity. This final chapter comes full circle and studies how the properties of the input current, coupled with the dynamical properties of the neuron and neuronal network, can influence the synaptic topology of the network. Like chapter III, this is done in the context of current oscillations in the brain, except here we include the resonant properties of the neuron (as opposed to specifically omitting it in chapter III). We also show how an initially randomly coupled network, like that used in Chapter II, can transform into a heterogeneously coupled network, like that used in Chapter III, through spike-timing dependent plasticity mechanisms. Most importantly, we show that this transformation is mediated by the specific input current pattern, for the first time employing current inputs to mimic real cognitive inputs.

Sub-threshold brain oscillations have long been thought to play an important role

in learning and the encoding of memories [81, 59, 126]. For example, measured theta rhythms (6-10Hz) have been shown to correspond to the 'active learning' state of the hippocampus [124, 149]. These oscillations, along with synaptic modification via spike-timing-dependent plasticity (STDP) provide the necessary basis for the formation and changes of memory traces in neuronal networks of the brain [126, 18, 157]. The exact mechanisms by which these changes occur however, has been an area of considerable research and debate.

At the same time it has been demonstrated that certain types of neurons have the ability to resonate [52, 54] and fire in response to a specific sub-threshold oscillatory current. Furthermore, it has also been recently shown that this natural frequency can shift in response to changes in the neuron's membrane potential [167, 141]. Here we propose a novel mechanism linking these three experimentally observed phenomena in which a neuronal network may utilize intrinsic oscillatory patterning, together with cell's ability to resonate and dynamically shift its resonant frequency, as a means to encode patterns based on the characteristics of a **sub-threshold** signal current. We show that changing the magnitude of the sub-threshold input can shift the cells' natural frequency into, and out of, the sub-threshold oscillatory current's range. This causes the neuron to resonate and phase lock to the period of the oscillation when the signal current is within a certain range. We use a network of resonate-and-fire (RAF) [71] neurons to demonstrate that this mechanism generates a highly selective spatio-temporal firing pattern. We compare the response properties of this network to a supra-threshold stimulated RAF network and to a network of supra-threshold stimulated integrate and fire neurons (IAF), all receiving sub-threshold oscillatory currents. We show that the RAF frequency adaptation mechanism is far superior at resolving temporal correlations/differences than the other models. This property, in conjunction with spike timing dependent plasticity (STDP), can be utilized to store temporal correlations between different input. Finally, we use this natural

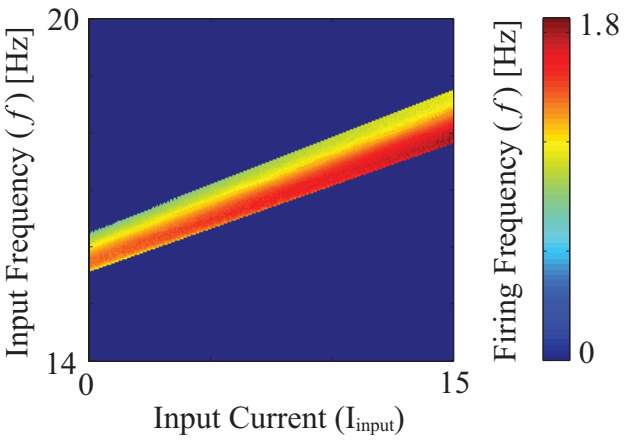

Figure 4.1: Firing frequency response of a single neuron to varying strengths of the signal current and frequencies of the oscillatory current. The oscillating current amplitude is fixed at $A = 3$ and $\delta = 1$. The color scale denotes the firing frequency of a neuron

frequency shift mechanism to explain two experimentally observed phenomena in the hippocampus: the phase precession [168, 169] along theta oscillation observed in the firing of hippocampal place cells as animal traverses its place field, and the dynamic changes in phase locking observed between the medial prefrontal cortex and the ventral or dorsal hippocampus during fear or a working memory task respectively [170, 171].

4.2 Methods

4.2.1 Resonate and fire neuron

To investigate the performance of proposed resonance adaptation mechanism we used a network of 200 randomly coupled, excitatory, resonate-and-fire neurons [71, 172]. The neurons are described by a set of two ordinary differential equations representing the internal current (x) and voltage (y) of the cell.

$$\frac{dx^j}{dt} = bx^j - \omega y^j + I^j_{ext} \tag{4.1}$$

$$\frac{dy^j}{dt} = \omega x^j + by^j \tag{4.2}$$

Where, for neuron j, $\omega = 100$ modifies the natural oscillation frequency, $b = -1$ defines the attraction of the voltage to it's resting potential, and I_{ext} is the external current defined as

$$I^j_{ext} = C_{syn} \sum_k S^{jk} I^k_{syn} + I^j_{input}. \tag{4.3}$$

Here, the first term is the synaptic current received from other firing neurons; $C_{syn} = 5$ is the synaptic coupling strength, S^{jk} is the synaptic connectivity matrix. The synaptic coupling is defined as

$$I^k_{synaptic} = e^{\frac{-(t-t^k_{spike})}{\tau_s}} - e^{\frac{-(t-t^k_{spike})}{\tau_f}}. \tag{4.4}$$

Here, $t - t^k_{spike}$ is the time since the pre-synaptic neuron firing, $\tau_s = 3$ and $\tau_f = .3$. The variables τ_s and τ_f are chosen such that the post synaptic potential has a pulse shape and lasts approximately $2ms$. The second term, I^j_{input}, denotes external current.

After each neuron fires at $x = 1$, x is reset to 0 and held there for 10ms – the duration of the refractory period.

Based on experimental results [167, 141] the resonant frequency shift is set to be a linear function of the total external current received by the given cell,

$$\omega^j = \omega^j_0 + \delta I^j_{ext}. \tag{4.5}$$

Here ω^j_0 is the oscillation frequency in the absence of any external currents, and δ is a scaling factor. Figure 4.1 demonstrates the resonance response of the neuron for different signal currents and sub-threshold current frequencies. Experimental studies have demonstrated both positively and negatively sloped responses to neuron

depolarizations ($\pm\delta$) [167, 141]. We have chosen $\delta = 1$, however both responses will produce similar results.

The input current consists of two components and is defined as

$$I_{input} = A_f sin(ft) + I_{signal}. \tag{4.6}$$

The first component is a sub-threshold oscillatory current of amplitude $A_f = 3$. For $b = -1$ and $\omega = 100$ the resonance frequency is between f =15-19 Hz (see above figure) thus we used $f = 17$ Hz as our primary input frequency. This frequency can be easily adjusted without changes to the described behavior. The second component was a sub-threshold (except when compared with **supra-threshold** resonate and fire network) current input to the network (e.g. a sensory input). The specific properties of the input signal are defined in detail in the next section, however note that the maximum magnitude of $I_{input} < 10$, whereas the current threshold needed for the cell to fire, defined by Equation 4.1, is around $I = 35$. Thus, for the sub-threshold resonate and fire network, the total input current is well in sub-threshold regime at all times.

4.2.2 Integrate and fire neuron

To compare the results from the RAF model to another easily tractable model we used the leaky integrate-and-fire neuron model:

$$\tau_m \frac{dV^j}{dt} = -\alpha_j V^j + R_s I - \sum_k w_{syn}^{jk} S^{jk} I_{syn}^k \tag{4.7}$$

Here, V^j is the membrane potential of the j^{th} neuron, $\tau_m = 0.5$ms is the time constant; α is a leakage coefficient which is different for every cell, $\alpha \in$ [1:1.3]; I_{syn}^k is the synaptic current generated at the time of the spike, w_{syn}^{jk} defines the chemical synapse coupling strength; S^{jk} is the synaptic connectivity (adjacency) matrix; I is

a uniform external current which keeps the neurons readily excitable, $I = 0.5$; R_s is the neuron resistance $R_s = 1$.

The synaptic current is activated after the pre-synaptic neuron reaches a threshold $V_{thresh} = 1$ and fires an action potential. The pre-synaptic neuron is then returned to $V = 0$ and remains there for a refractory period $t_{ref} = 10$ms. The synaptic current is of the form

$$I^k_{syn}(t) = e^{\frac{-(t-t^k_{spike})}{\tau_s}} - e^{\frac{-(t-t^k_{spike})}{\tau_f}} \tag{4.8}$$

where $(t - t^k_{spike})$ is the time since the last firing of the presynaptic neuron, $\tau_s = 3$ms is the slow time constant, and $\tau_f = 0.3$ms is the fast time constant. The variables τ_s and τ_f are chosen such that the post-synaptic potential lasts approximately 2ms.

4.2.3 Measuring temporal pattern properties: mean phase coherence

We used the mean phase coherence (MPC) to measure the amount of phase locking between cells [94, 71]. The MPC ranges between 0 (no phase locking) and 1 (maximal phase locking). The MPC is calculated pair-wise between neurons n and m:

$$MPC_{nm} = \left| \frac{1}{S} \sum_{s=1}^{S} e^{i\phi_{nm_s}(j)} \right| \tag{4.9}$$

Here S is the total number of spikes of cell m and ϕ_{nm_s} is the phase between cell n and m for interval j containing s. This phase is defined as:

$$\phi_{nm_s}(j) = 2\pi \frac{\tau_{n_j,m_s}}{\tau_{n_j}}, \tag{4.10}$$

where

$$\tau_{n_j} = t_{n_{j+1}} - t_{n_j}; \tag{4.11}$$

is the inter-spike-interval j for neuron n containing spike s of the m-th cell and

$$\tau_{n_j,m_s} = t_{m_s} - t_{n_j}; \tag{4.12}$$

is the time difference between the initial firing of neuron n, on interval j, and the firing s, of neuron m, with the condition,

$$t_{n_j} \leq t_{m_s} \leq t_{n_{j+1}} \tag{4.13}$$

Finally, we take the average of all MPC pairs across all neurons,

$$MPC = \frac{1}{N(N-1)} \sum_{n}^{N} \sum_{m \neq n}^{N} MPC_{nm} \tag{4.14}$$

where $N = 200$ are the total number of neurons.

4.2.3.1 Signal Phase Coherence

We also measure phase coherence of the neurons with respect to the oscillatory drive. Here the phase of the oscillatory signal at which given cell fired was obtained directly. The signal phase coherence was calculated in a similar fashion to the MPC.

Mean minimal interneuron interspike interval

To further quantify the temporal spiking pattern between the neurons we calculated mean minimal interneuron interspike interval (mISI). Namely we calculated the ISI length for the nearest firing times between every neuron:

$$ISI_{nm} = \frac{1}{S} \sum_{s=1}^{S} |t_{n_s} - t'_{m_s}| \tag{4.15}$$

where, t'_{m_s} is the nearest firing of cell m to t_{n_s}.

Then

$$|ISI| = \frac{1}{N(N-1)} \sum_{n}^{N} \sum_{m}^{M} ISI_{nm} \tag{4.16}$$

is the mean inter-neuron ISI.

4.3 Results

We compared the performance of the RAF resonant frequency adaptive network with two other network realizations: an identical RAF network driven by a supra-threshold signal current, and a non-resonating IAF [173] network driven by a supra-threshold signal current. All networks received a fixed sub-threshold oscillatory current with a frequency of f =17 Hz and an amplitude of $A_f = 3$.

4.3.1 Comparison of neuronal and signal phase locking properties

First we examined the response of the networks to a range of different input currents. We do this by investigating the degree of selectivity and locking of network activity as a function of the variance of the input (I_{signal}). Here, the magnitude of the input current was drawn from a random Gaussian distribution to vary the signal currents into each neuron. For each simulation, the specific value of the signal current was kept constant over time. We computed the mean phase coherence, phase locking of activity to the oscillatory current, and the mean inter-neuron ISI for the three types of networks.

Figure 4.2A depicts the phase locking of neuronal activity to the network oscillatory drive as a function of the input variance. One can observe that the phase locking for the frequency adaptation network is nearly perfect for most of the range, tailing off for high values of input variance. This indicates that the neurons are locked to specific phases on the oscillatory current. This is due to the fact that the active neurons (i.e those that receive appropriate current shifting their natural frequency towards

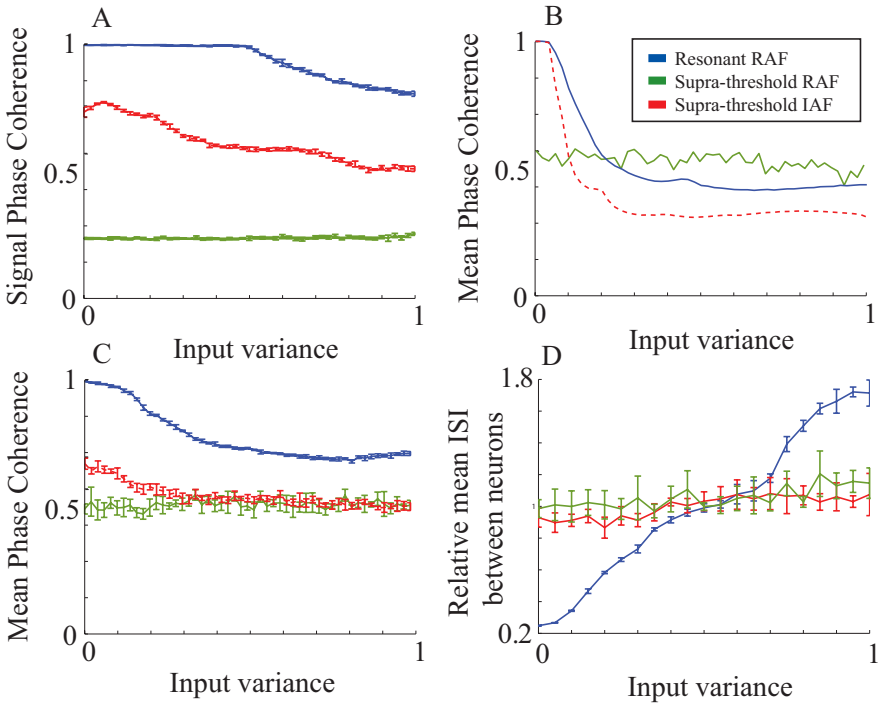

Figure 4.2: Response of neurons to a range of input signal currents. The RAF resonance adaptation mechanism with sub-threshold input is denoted by blue, RAF with supra-threshold input by red, and IAF with supra-threshold by green. a) The phase coherence of the network firing times with the oscillatory current v.s increasing ranges of signal currents. b) The MPC response of an uncoupled network to increasing ranges of signal currents. c) The MPC response of a coupled network to increasing ranges of signal currents. d) The mean inter-spike interval (ISI) calculated between neurons vs. increasing ranges of signal currents for a coupled network. Errors are calculated over five simulations.

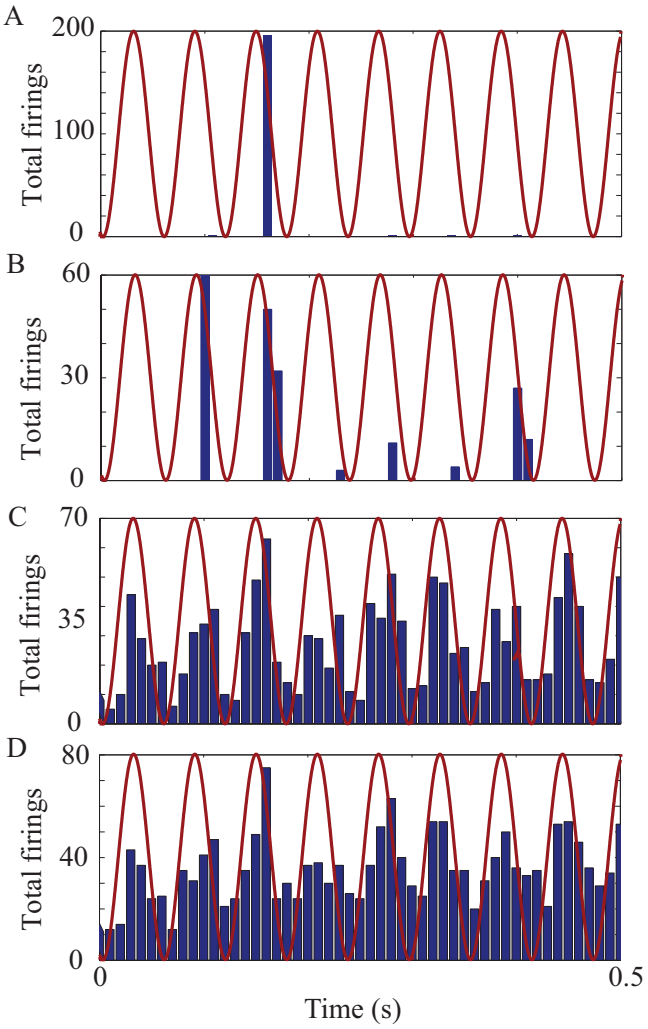

Figure 4.3: Histogram of firing times on oscillation. Histogrammed firing times of neuronal network for A) Resonant RAF, Variance = 0. B) Resonant RAF, Variance = 0.3. C) Suprathreshold RAF, Variance = 0.3. D) Suprathreshold IAF, Variance = 0.3.

the frequency of the oscillatory drive), being effectively oscillators, phase synchronize with the oscillatory current [174, 175, 71]. Other neurons remain quiescent as they do not resonate (i.e. their natural frequency is significantly different from that of the oscillatory drive) and the total input signal they receive is sub-threshold. This effect is significantly diminished for the RAF network with supra-threshold input, and almost completely absent in the IAF network. It occurs because the neurons' firings are effectively driven by the supra-threshold inputs with the cell firing frequency determined by the amplitude of this input.

Figures 4.2B and 4.2C depict the MPC changes of uncoupled neurons and coupled networks. The MPC is an indicator of the stability of the phase relationships between the neurons themselves. This, in turn, determines stability and selectivity of the generated network activity pattern. The MPC for the uncoupled adaptive RAF network is shown in blue in Figure 4.2B. Here the MPC is high for low input variance but declines quickly as the input variance is increased. This is in contrast to the signal coherence in 4.2A because, even though the neurons are locked to the phase of the individual oscillatory cycle, they fire at different cycles, depending on the signal current magnitude. When the neurons are coupled Figure 4.2C, the excitatory connections mediate increased neuronal interactions and firing at the same oscillatory cycle leading to a higher MPC. By comparison, for both the coupled and uncoupled case, the supra-threshold RAF and IAF networks have lower MPC. For the supra-threshold RAF neurons the MPC remains high for a narrow range of signal currents because of the phase locking of the cells receiving similar input, however for larger values of the variance the differences in the I_{signal} lead to significantly different firing frequencies and thus abolition of phase locking. For the IAF model MPC remains low over all input variance range.

Figure 4.2D depicts the modulation of the inter-neuron inter-spike intervals (ISI) as a function of variance of input currents. The mean ISI changes significantly for

the resonance adaptation mechanism, while it remains constant for other two models. This indicates an increased signal current selectivity (in terms of spiking coincidence), as a function of input variance, for the adaptive resonance mechanism compared with supra-threshold input for both RAF and IAF models. This occurs because, for small values of variance, the active cells fire within narrow time windows. When the variance is increased the cells are still locked to the oscillation phase but are firing on different oscillatory cycles, rapidly increasing the mean ISI value. This effect is abolished for the other two network realizations as the supra-threshold inputs inhibit cells from phase locking and thus the specific variance of input has little effect on the ISI. As we will show below this phenomenon has a large effect on the efficiency of the STDP driven synaptic modifications.

Finally, Figure 4.3 exhibits the basis for these observations via histograms of the neuronal firing times. Here we have the total firing for the network on the $y - axis$ and the time on the $x - axis$. Panel A shows the resonant RAF model with an input variance of 0. Here all the neurons fire simultaneously at a phase of $\pi/3$ from the peak of the oscillation. Panel B shows the resonant RAF model with an input variance of 0.3. Here the neurons fire at a phase near $\pi/3$ and on completely different cycles. Panels C and D are for the suprathreshold RAF and IAF cases respectively and show that the firings are modulated under the oscillations instead of being phase locked.

4.3.2 Enhanced STDP driven synaptic modifications and the spatio-temporal correlation of inputs

The results described above indicate that the resonance frequency shift provides a superior mechanism to translate differences in the input signal characteristics to distinct patterns of spatio-temporal neuronal activity. Next we investigate how well these neuronal activity patterns translate to STDP modified network connections. To do this we used a standard symmetric decaying exponential learning rule to model the

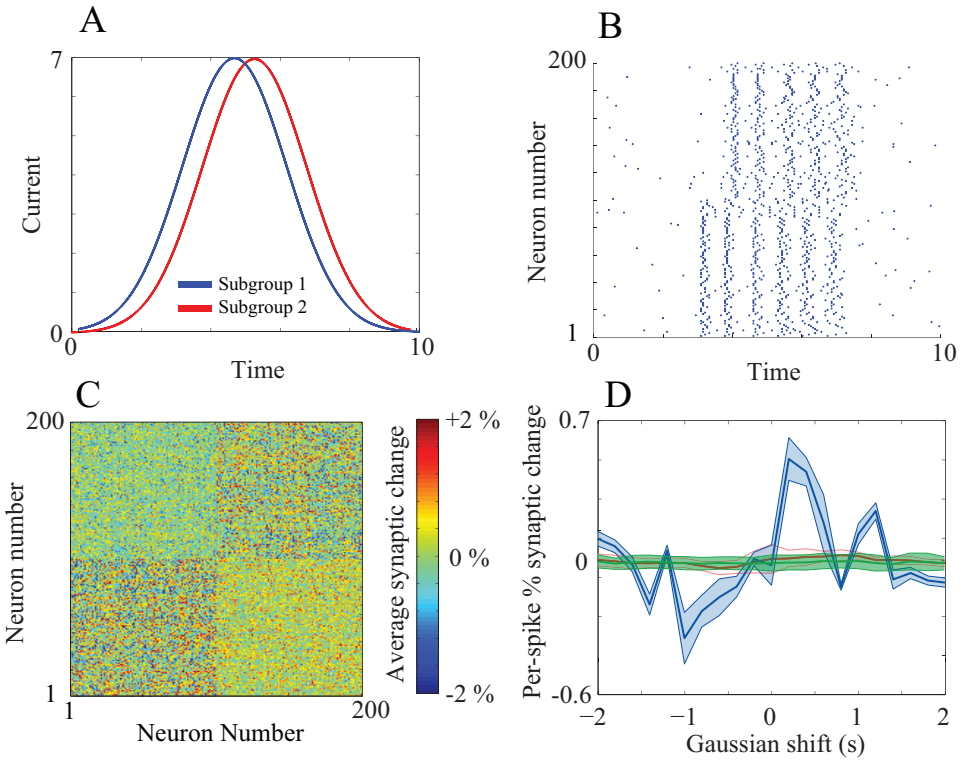

Figure 4.4: STDP network connectivity changes due to the correlation of Gaussian inputs. A) The Gaussian profile and temporal shift of the signal currents into each region. B) Example of the activity raster plot of neuronal activity. C) The pattern of modified connectivity strengths between the neurons at the end of the simulation (10s), averaged over 100 trials, for all possible connections. x-axis is from, y-axis it to. D) Comparison of mean, directional connectivity changes between the two network subgroups as a function of the input shift. The different colors are a comparison between the RAF adaptive resonance network, supra-threshold RAF network, and supra-threshold IAF network.

effects of STDP on the network. Here the synapses may be strengthened (depressed) by a factor C if the presynaptic neuron fires shortly before (after) the postsynaptic cell:

$$C^j(t_{diff}) = \Delta \frac{T_{diff}}{|T_{diff}|} e^{\frac{-T_{diff}}{\tau}}, \tag{4.17}$$

where t_{post} and t_{pre} denote time before and after synaptic modification, respectively; T_{diff} is the time difference between the presynaptic and postsynaptic neuron firing, $\Delta = 0.1$ scales the STDP strength, and $\tau = 15$ms is the STDP time constant defining the relevant timescale for synaptic changes.

The network was divided into two sub-groups each receiving a signal current with time-shifted Gaussian profile,

$$I_{signal} = D \exp -(t - t_{shift})^2/\sigma^2, \tag{4.18}$$

where $\sigma = 1.5$s, $D = 10$ for sub-threshold input and $D = 80$ for supra-threshold input, Figure 4.4A. For the data depicted on Figure 4.4A-C the time shift between the two sub-groups was fixed at 0.5s. Figure 4.4B depicts the spike timing raster of the network, and Figure 4.4C shows the resultant connectivity matrix, obtained at the end of the simulation (t = 10s), averaged over 100 trials. We see that, within each sub-region, where neurons receive identical inputs, strong increases or decreases occur in the synaptic strengths. These changes are symmetrical (the net changes average to zero), with the specific patterning of STDP changes governed by the initial random connectivity. More importantly however, one can observe a strong unidirectional strengthening (weakening) of connections from regions with the leading(following) Gaussian. This is shown by the increased red connections for connections from 1-100 $\rightarrow$ 101-200 and increased blue connections from 101-200 $\rightarrow$ 1-100

Finally, we investigated how the unidirectional coupling changed as a function of

the temporal shift between the Gaussian signal currents. We did this for all three neuron/network models by computing the difference between the mean couplings of both regions. This will directly measure the extent to which the changes in the network topology reflect the correlation between the signal currents. Figure 4.4D depicts the normalized (per spike) changes in directional connectivity between the two neuronal sub-groups for the RAF frequency adaptation network with sub-threshold input (blue), supra-threshold input (red), and the IAF network with supra-threshold input (green). Clearly the sub-threshold input, together with the resonant frequency adaptation mechanism, provides the most supportive dynamical environment for the network reorganization. The changes are reflected in directional connectivity between the two regions, correlating the time dependence of the signal currents to the strengthening of connections.

4.4 Discussion

Based on the above results it is clear that the sub-treshold driven neurons exhibiting voltage dependent natural frequency shifts provide very efficient dynamical substrate for formation of input driven spatio-temporal patterns of activity. This, coupled with STDP learning, provides an efficient mechanism that underlies the formation of a connectivity topology that maps the characteristics of the input signal(s) - more so than supra-threshold input driven networks. This effectiveness arises from the enhanced phase and signal locking, due to the resonance frequency shift response, and the higher sensitivity in spike timing due to resonance induced firing. In short, the neurons' firing times are consistently mapped onto specific, current dependent, phases of the input oscillation, rather than just being modulated by a supra-threshold oscillating current.

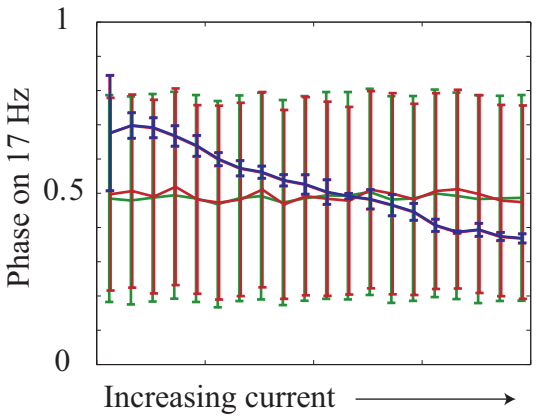

Figure 4.5: Phase precession as a function of input strength. The lines denote average phase of neuronal firing with respect to the oscillatory current (blue – sub-threshold resonance adaptation mechanism; green - supra-threshold input driven RAF; red – supra–threshold driven IAF).

4.4.1 Input dependent phase precession

This input-dependent phase locking and phase precession has been observed experimentally in nearly all parts of the brain involved in learning [57, 122, 126], and specifically during hippocampal place cell firing [168, 169] when the animal is traversing the place field associated with that cell. While it is relatively difficult to explain this phenomenon using supra-threshold network realizations, it is an intrinsic property of the sub-threshold resonance adaptation mechanism we described Figure 4.5.

4.4.2 Dynamic modulation of information transfer between brain modalities

Finally, the voltage dependent natural frequency shift may explain recently observed dynamic changes in information flow between different brain modalities. It has been shown that the medial prefrontal cortex synchronizes with the ventral hippocampus (vHPC) during anxiety [170] and with the dorsal hippocampus (dHPC) during working memory tasks [171],specifically in the theta (4-12 Hz) range in both cases. It is also known that the dHPC and vHPC have slightly different preferred frequencies of theta that route the flow of information in different states. Such a

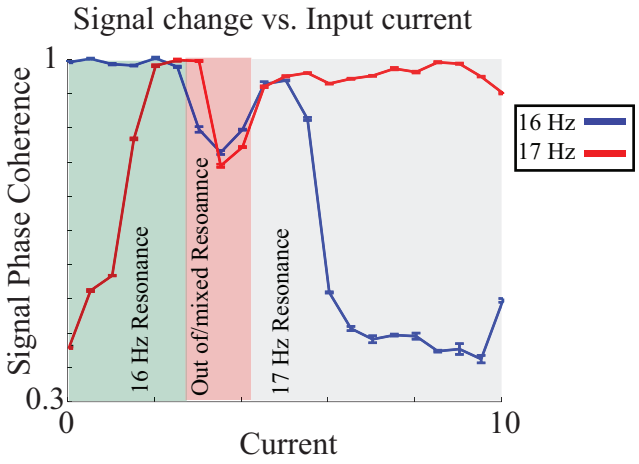

Figure 4.6: Dynamic changes in phase locking between two oscillatory inputs. The network is driven by two oscillatory inputs having different frequencies (16 Hz and 17 Hz). Signal coherence is measured with respect to both signals (red and blue lines). As the I_{signal} is increased the network switches locking from one to other signal.

dynamic change in frequency preference between modalities is easily explained within our model. Different neuromodulatory processes or lower frequency oscillations may change the membrane depolarization for large number of neurons within a modality simultaneously, causing a shift in their natural frequencies. This, in turn, may lead to altered patterns of locking when two oscillatory inputs are present. Figure 4.6 depicts such a transition for the frequency ranges we used earlier. Here the network receives two oscillatory inputs with slightly different frequencies. As the cells' membranes are progressively depolarized the network shifts from being locked to the lower frequency input to the the higher frequency one, as reported by the signal coherence.

To the best of our knowledge, we are the first to demonstrate the use of oscillations and the sub-threshold frequency shift as a mechanism which provides brain networks with the enhanced ability to encode input patterns.

CHAPTER V

Conclusions

We have shown that the brain's complexity lies well beyond its complicated anatomical structure. This complexity begins with the arrangement of connections between these neurons, forming an immensely complex structure. Furthermore, networks of neurons are connected in a specific manner at different scales in the brain, each providing different levels of integration and computation. By changing the types of neurons involved, the number of neurons, or the arrangement of connections between them (to name a few factors), these networks can elicit vastly different patterns of spatio-temporal activity that result in very different functionality. These functions arise from the wide and diverse range of dynamics that the networks are capable of. From synchrony, phase synchrony, oscillations, resonance, and pattern formation, the spatial and temporal dynamics of these networks reflect both the input they receive, the properties of the cells and connections, and the the outputs they provide. To make matters even more complicated, the brain is not fixed. The dynamical relationships between neurons go back and influence the structure of the brain network itself, via synaptic plasticity mechanisms, and constantly alter the connectivity landscape of the brain. Through all these mechanisms the brain becomes a reflection of the experiences and personality of the individual that posseses it, allowing it to interact and change the environment around it.

This thesis has covered three topics which exemplify these properties. Chapter II studied the electrically connected gap-junction networks in the brain, concurrent with an inhibitory network, and the spatio-temporal patterns of activity their interactions produce. Here the short-range gap-junctions supplied the means for local synchrony generation while the long-range inhibitory connections provided a global inhibition mechanism. Provided the correct range of connectivity parameters were used, the resultant activity was a state of locally sustained pattern formation. The changing of the electrical connectivity from local to random transitioned the network from a confined, locally synchronous state to a global one. In contrast, the changing of the inhibitory connections from local to random changed the number of active regions from a single isolated one to multiple regions, depending on the wiring parameters of the inhibitory connections. The results were then compared to striatal *in vivo* data from the Berke lab, and it was shown that the dynamics resulting from the local gap-junction connectivity matched well with the experimentally recorded data. Both the computational and experimental results were novel, and provided insight into how the patterns of activity supplied by the striatum may contribute to the decision making process in the basal ganglia.

Chapter III extended the interaction of structure and dynamics to investigate homogeneous networks. It also introduced oscillatory dynamics into the fold, and investigated how these oscillations can interact with the network structure to generate a new kind of dynamics. Here I investigated the ability of a particular oscillatory current frequency to elicit a selective response from a topologically 'enhanced' region of a network. By changing the strength of connections within the network, the amplitude, and the frequency of the oscillation, I was able to selectively activate the enhanced region, activate the entire network, or quiet the entire network. In particular, the selective activation of the enhanced region was due to a network generated frequency preference and a corresponding resonant response at higher frequencies. Addition-

ally, at lower frequencies, the enhanced region showed an increased phase coherence. These network derived frequency responses further expand our understanding and speculation to the purpose of oscillations throughout the brain. They also suggest that otherwise similar oscillations may have completely different functional purposes, depending on the state of the network.

Chapter IV expands our study of oscillations and proposes a mechanism via which resonant oscillations can be used in learning through STDP. Here we utilize the fact that some neurons have the ability to classically resonate, and shift this resonance frequency due to a sub-threshold depolarizing current. This resonance frequency shift is translated into stable and highly selective spatio-temporal patterns of activation in response to varying sub-threshold input currents. These responses are then combined with a simple and widely used model of STDP to show that the patterns of activation map to the network topology. To my knowledge, this is the first work to demonstrate the use of sub-threshold oscillations and resonance to translate spatio-temporal correlations of input into temporal patterns of activity and a spatial mapping of learning.

The goal of this work was not to capture every brain dynamic, all of its individual components, and form an exact model of the resulting activity. Instead, as it is a thesis in physics, it was to identify the underlying neuronal and network mechanisms that govern the overarching patterns of activity observed throughout the brain. This was done by first identifying the cellular and network properties that have the strongest influence on a particular activity. Then, by examining large parameter spaces of network variables, I was able to understand the interplay between the different properties and characteristics that arise from each. By doing this, the underlying principles behind particular mechanisms were established. Also, by studying large parameter spaces and using simplified non-specific models, the results of each chapter could be translated to numerous regions and functions of the brain. In future work, by both myself and others in this field, I see the field of computational and physical neuroscience only

expanding and becoming more diverse. Particularly, as computing power continues to grow, even the most basic models will include complexity and scale not possible ten years ago; however, I do have reservations as simulations become more complex, that they will begin to resemble, perhaps too much, the brain structures which they model. When this becomes the case, I believe some of the inherent simplicity and tractability of these models will accordingly be lost.

The brain is so complex that not only does it take a wide range of experimental techniques to investigate it, but it also takes a plethora of different approaches and viewpoints to even begin to understand it. These range from the physiological, psychological, and cellular to the mathematical and physical methods employed in this thesis, each with their own strengths and weaknesses. The brain is obviously a biological system first, and accordingly, a large number of neurobiologist study the molecular and cellular mechanisms in the brain. Another well established (and likely the oldest) approach is that of the biopsychologists, and their linking of the behavioral and physiological understandings of the brain. As part of a relatively new and emerging field employing methods combining biology, complex systems, mathematics, and physics this body of work has ventured to understand the brain from a range of non-classical perspectives. These approaches have incorporated measures and methodologies that were previously limited to areas outside of neuroscience. It is my hope that, by combining these fields, this paper has brought a unique physical and mathematical perspective to the brain.

BIBLIOGRAPHY

BIBLIOGRAPHY

[1] Nicola J Allen and Ben A Barres. Neuroscience: Glia - more than just brain glue. *Nature*, 457(7230):675–677, Feb 2009.

[2] Mariana Alonso, Inmaculada Ortega-Prez, Matthew S Grubb, Jean-Pierre Bourgeois, Pierre Charneau, and Pierre-Marie Lledo. Turning astrocytes from the rostral migratory stream into neurons: a role for the olfactory sensory organ. *J Neurosci*, 28(43):11089–11102, Oct 2008.

[3] Lili-Naz Hazrati, B. K. Kleinschmidt-DeMasters, Michael H Handler, Mary Lou Smith, Ayako Ochi, Hiroshi Otsubo, James T Rutka, Cristina Go, Shelly Weiss, and Cynthia E Hawkins. Astrocytic inclusions in epilepsy: expanding the spectrum of filaminopathies. *J Neuropathol Exp Neurol*, 67(7):669–676, Jul 2008.

[4] A. Verkhratsky and E. C. Toescu. Neuronal-glial networks as substrate for cns integration. *J Cell Mol Med*, 10(4):826–836, 2006.

[5] David Stellwagen and Robert C Malenka. Synaptic scaling mediated by glial tnf-alpha. *Nature*, 440(7087):1054–1059, Apr 2006.

[6] Chung-Chuan Lo and Xiao-Jing Wang. Cortico-basal ganglia circuit mechanism for a decision threshold in reaction time tasks. *Nat Neurosci*, 9(7):956–963, Jul 2006.

[7] P. Redgrave, T. J. Prescott, and K. Gurney. The basal ganglia: a vertebrate solution to the selection problem? *Neuroscience*, 89(4):1009–1023, 1999.

[8] Adam R Aron, Sarah Durston, Dawn M Eagle, Gordon D Logan, Cathy M Stinear, and Veit Stuphorn. Converging evidence for a fronto-basal-ganglia network for inhibitory control of action and cognition. *J Neurosci*, 27(44):11860–11864, Oct 2007.

[9] John G McHaffie, Terrence R Stanford, Barry E Stein, Vronique Coizet, and Peter Redgrave. Subcortical loops through the basal ganglia. *Trends Neurosci*, 28(8):401–407, Aug 2005.

[10] Mary C Whitman and Charles A Greer. Adult neurogenesis and the olfactory system. *Prog Neurobiol*, 89(2):162–175, Oct 2009.

[11] Angelique Bordey. Enigmatic gabaergic networks in adult neurogenic zones. *Brain Res Rev*, 53(1):124–134, Jan 2007.

[12] P. S. Eriksson, E. Perfilieva, T. Bjrk-Eriksson, A. M. Alborn, C. Nordborg, D. A. Peterson, and F. H. Gage. Neurogenesis in the adult human hippocampus. *Nat Med*, 4(11):1313–1317, Nov 1998.

[13] Henriette van Praag, Alejandro F Schinder, Brian R Christie, Nicolas Toni, Theo D Palmer, and Fred H Gage. Functional neurogenesis in the adult hippocampus. *Nature*, 415(6875):1030–1034, Feb 2002.

[14] Hong jun Song, Charles F Stevens, and Fred H Gage. Neural stem cells from adult hippocampus develop essential properties of functional cns neurons. *Nat Neurosci*, 5(5):438–445, May 2002.

[15] G. A. Cecchi, L. T. Petreanu, A. Alvarez-Buylla, and M. O. Magnasco. Unsupervised learning and adaptation in a model of adult neurogenesis. *J Comput Neurosci*, 11(2):175–182, 2001.

[16] April E Hebert and Pramod K Dash. Plasticity in the entorhinal cortex suppresses memory for contextual fear. *J Neurosci*, 24(45):10111–10116, Nov 2004.

[17] Yang Dan and Mu-Ming Poo. Spike timing-dependent plasticity: from synapse to perception. *Physiol Rev*, 86(3):1033–1048, Jul 2006.

[18] S. Song, K. D. Miller, and L. F. Abbott. Competitive hebbian learning through spike-timing-dependent synaptic plasticity. *Nat Neurosci*, 3(9):919, Sep 2000.

[19] S. Song and L. F. Abbott. Cortical development and remapping through spike timing-dependent plasticity. *Neuron*, 32(2):339–350, Oct 2001.

[20] Wim Ramadan, Oxana Eschenko, and Susan J Sara. Hippocampal sharp wave/ripples during sleep for consolidation of associative memory. *PLoS One*, 4(8):e6697, 2009.

[21] Mattias P Karlsson and Loren M Frank. Awake replay of remote experiences in the hippocampus. *Nat Neurosci*, 12(7):913–918, Jul 2009.

[22] Adrien Peyrache, Mehdi Khamassi, Karim Benchenane, Sidney I Wiener, and Francesco P Battaglia. Replay of rule-learning related neural patterns in the prefrontal cortex during sleep. *Nat Neurosci*, 12(7):919–926, Jul 2009.

[23] David R Euston, Masami Tatsuno, and Bruce L McNaughton. Fast-forward playback of recent memory sequences in prefrontal cortex during sleep. *Science*, 318(5853):1147–1150, Nov 2007.

[24] S. C. Ponten, F. Bartolomei, and C. J. Stam. Small-world networks and epilepsy: graph theoretical analysis of intracerebrally recorded mesial temporal lobe seizures. *Clin Neurophysiol*, 118(4):918–927, Apr 2007.

[25] Shuzo Sakata and Tetsuo Yamamori. Topological relationships between brain and social networks. *Neural Netw*, 20(1):12–21, Jan 2007.

[26] Changsong Zhou and et al. Structure-function relationship in complex brain networks expressed by hierarchical synchronization. *New Journal of Physics*, 9:178, 2007.

[27] Troy Lau, Gregory J Gage, Joshua D Berke, and Michal Zochowski. Local dynamics of gap-junction-coupled interneuron networks. *Phys Biol*, 7:16015, 2010.

[28] Joshua D Berke. Uncoordinated firing rate changes of striatal fast-spiking interneurons during behavioral task performance. *J Neurosci*, 28(40):10075–10080, Oct 2008.

[29] Maria Victoria Puig, Mika Ushimaru, and Yasuo Kawaguchi. Two distinct activity patterns of fast-spiking interneurons during neocortical up states. *Proc Natl Acad Sci U S A*, 105(24):8428–8433, Jun 2008.

[30] Jessica A Cardin, Marie Carln, Konstantinos Meletis, Ulf Knoblich, Feng Zhang, Karl Deisseroth, Li-Huei Tsai, and Christopher I Moore. Driving fast-spiking cells induces gamma rhythm and controls sensory responses. *Nature*, 459(7247):663–667, Jun 2009.

[31] A. L. Hodgkin and A. F. Huxley. Propagation of electrical signals along giant nerve fibers. *Proc R Soc Lond B Biol Sci*, 140(899):177–183, Oct 1952.

[32] A. L. Hodgkin and A. F. Huxley. A quantitative description of membrane current and its application to conduction and excitation in nerve. *J Physiol*, 117(4):500–544, Aug 1952.

[33] A. L. Hodgkin and A. F. Huxley. The components of membrane conductance in the giant axon of loligo. *J Physiol*, 116(4):473–496, Apr 1952.

[34] W. Schultz. Predictive reward signal of dopamine neurons. *J Neurophysiol*, 80(1):1–27, Jul 1998.

[35] Barry W Connors and Michael A Long. Electrical synapses in the mammalian brain. *Annu Rev Neurosci*, 27:393–418, 2004.

[36] T. Fukuda and T. Kosaka. Gap junctions linking the dendritic network of gabaergic interneurons in the hippocampus. *J Neurosci*, 20(4):1519–1528, Feb 2000.

[37] Takaichi Fukuda, Toshio Kosaka, Wolf Singer, and Ralf A W Galuske. Gap junctions among dendrites of cortical gabaergic neurons establish a dense and widespread intercolumnar network. *J Neurosci*, 26(13):3434–3443, Mar 2006.

[38] Jay R Gibson, Michael Beierlein, and Barry W Connors. Functional properties of electrical synapses between inhibitory interneurons of neocortical layer 4. *J Neurophysiol*, 93(1):467–480, Jan 2005.

[39] G. Tams, E. H. Buhl, A. Lrincz, and P. Somogyi. Proximally targeted gabaergic synapses and gap junctions synchronize cortical interneurons. *Nat Neurosci*, 3(4):366–371, Apr 2000.

[40] Takaichi Fukuda. Network architecture of gap junction-coupled neuronal linkage in the striatum. *J Neurosci*, 29(4):1235–1243, Jan 2009.

[41] Nathan W Gouwens, Hugo Zeberg, Kunichika Tsumoto, Takashi Tateno, Kazuyuki Aihara, and Hugh P C Robinson. Synchronization of firing in cortical fast-spiking interneurons at gamma frequencies: a phase-resetting analysis. *PLoS Comput Biol*, 6(9), 2010.

[42] M. Galarreta and S. Hestrin. Electrical synapses between gaba-releasing interneurons. *Nat Rev Neurosci*, 2(6):425–433, Jun 2001.

[43] L. Goldman and J. S. Albus. Computation of impulse conduction in myelinated fibers; theoretical basis of the velocity-diameter relation. *Biophys J*, 8(5):596–607, May 1968.

[44] X. Xi, W. C. Randall, and R. D. Wurster. Electrophysiological properties of canine cardiac ganglion cell types. *J Auton Nerv Syst*, 47(1-2):69–74, Apr 1994.

[45] T. Tateno, A. Harsch, and H. P C Robinson. Threshold firing frequency-current relationships of neurons in rat somatosensory cortex: type 1 and type 2 dynamics. *J Neurophysiol*, 92(4):2283–2294, Oct 2004.

[46] Douglas McLelland and Ole Paulsen. Neuronal oscillations and the rate-to-phase transform: mechanism, model and mutual information. *J Physiol*, 587(Pt 4):769–785, Feb 2009.

[47] R. Hennig and T. Lmo. Firing patterns of motor units in normal rats. *Nature*, 314(6007):164–166, 1985.

[48] Attila Losonczy, Boris V Zemelman, Alipasha Vaziri, and Jeffrey C Magee. Network mechanisms of theta related neuronal activity in hippocampal ca1 pyramidal neurons. *Nat Neurosci*, 13(8):967–972, Aug 2010.

[49] Edward O Mann and Istvan Mody. Control of hippocampal gamma oscillation frequency by tonic inhibition and excitation of interneurons. *Nat Neurosci*, 13(2):205–212, Feb 2010.

[50] Carien S Lansink, Pieter M Goltstein, Jan V Lankelma, and Cyriel M A Pennartz. Fast-spiking interneurons of the rat ventral striatum: temporal coordination of activity with principal cells and responsiveness to reward. *Eur J Neurosci*, 32(3):494–508, Aug 2010.

[51] M. Galarreta and S. Hestrin. A network of fast-spiking cells in the neocortex connected by electrical synapses. *Nature*, 402(6757):72–75, Nov 1999.

[52] B. Hutcheon and Y. Yarom. Resonance, oscillation and the intrinsic frequency preferences of neurons. *Trends Neurosci*, 23(5):216–222, May 2000.

[53] Eugene M Izhikevich. Resonance and selective communication via bursts in neurons having subthreshold oscillations. *Biosystems*, 67(1-3):95–102, 2002.

[54] N. Wu, C. F. Hsiao, and S. H. Chandler. Membrane resonance and subthreshold membrane oscillations in mesencephalic v neurons: participants in burst generation. *J Neurosci*, 21(11):3729–3739, Jun 2001.

[55] P. Parmananda, Claudia H Mena, and Gerold Baier. Resonant forcing of a silent hodgkin-huxley neuron. *Phys Rev E Stat Nonlin Soft Matter Phys*, 66(4 Pt 2):047202, Oct 2002.

[56] Mark D Bevan, Peter J Magill, David Terman, J. Paul Bolam, and Charles J Wilson. Move to the rhythm: oscillations in the subthalamic nucleus-external globus pallidus network. *Trends Neurosci*, 25(10):525–531, Oct 2002.

[57] Laura Lee Colgin, Tobias Denninger, Marianne Fyhn, Torkel Hafting, Tora Bonnevie, Ole Jensen, May-Britt Moser, and Edvard I Moser. Frequency of gamma oscillations routes flow of information in the hippocampus. *Nature*, 462(7271):353–357, Nov 2009.

[58] Yasemin M Akay, Andrei Dragomir, Chuanze Song, Jie Wu, and Metin Akay. Hippocampal gamma oscillations in rats. *IEEE Eng Med Biol Mag*, 28(6):92–95, 2009.

[59] Daria Osipova, Atsuko Takashima, Robert Oostenveld, Guilln Fernndez, Eric Maris, and Ole Jensen. Theta and gamma oscillations predict encoding and retrieval of declarative memory. *J Neurosci*, 26(28):7523–7531, Jul 2006.

[60] Gyorgy Buzsaki. *Rhythms of the Brain*. Oxford University Press, New York, 2006.

[61] Alfons Schnitzler and Joachim Gross. Normal and pathological oscillatory communication in the brain. *Nat Rev Neurosci*, 6(4):285–296, Apr 2005.

[62] Stan Gielen, Martin Krupa, and Magteld Zeitler. Gamma oscillations as a mechanism for selective information transmission. *Biol Cybern*, 103(2):151–165, Aug 2010.

[63] Maoz Shamir, Oded Ghitza, Steven Epstein, and Nancy Kopell. Representation of time-varying stimuli by a network exhibiting oscillations on a faster time scale. *PLoS Comput Biol*, 5(5):e1000370, May 2009.

[64] Sam M Doesburg, Jessica J Green, John J McDonald, and Lawrence M Ward. Rhythms of consciousness: binocular rivalry reveals large-scale oscillatory network dynamics mediating visual perception. *PLoS One*, 4(7):e6142, 2009.

[65] Hua Hu, Koen Vervaeke, and Johan F Storm. Two forms of electrical resonance at theta frequencies, generated by m-current, h-current and persistent na+ current in rat hippocampal pyramidal cells. *J Physiol*, 545(Pt 3):783–805, Dec 2002.

[66] W-T. Wang, Y-H. Wan, J-L. Zhu, G-S. Lei, Y-Y. Wang, P. Zhang, and S-J. Hu. Theta-frequency membrane resonance and its ionic mechanisms in rat subicular pyramidal neurons. *Neuroscience*, 140(1):45–55, Jun 2006.

[67] Y. Gutfreund, Y. yarom, and I. Segev. Subthreshold oscillations and resonant frequency in guinea-pig cortical neurons: physiology and modelling. *J Physiol*, 483 (Pt 3):621–640, Mar 1995.

[68] B. Hutcheon, R. M. Miura, and E. Puil. Subthreshold membrane resonance in neocortical neurons. *J Neurophysiol*, 76(2):683–697, Aug 1996.

[69] Akifumi Enomoto, Juliette M Han, Chie-Fang Hsiao, and Scott H Chandler. Sodium currents in mesencephalic trigeminal neurons from nav1.6 null mice. *J Neurophysiol*, 98(2):710–719, Aug 2007.

[70] N. Brunel and S. Sergi. Firing frequency of leaky intergrate-and-fire neurons with synaptic current dynamics. *J Theor Biol*, 195(1):87–95, Nov 1998.

[71] E. M. Izhikevich. Resonate-and-fire neurons. *Neural Netw*, 14(6-7):883–894, 2001.

[72] S. Boccaletti, V. Latora, Y. Moreno, M. Chavez, and D. U Hwang. Complex networks: Structure and dynamics. *Physics Reports*, 2006.

[73] Matja Perc. Stochastic resonance on excitable small-world networks via a pacemaker. *Physical Review E*, 76(6):066203, 2007. Copyright (C) 2010 The American Physical Society Please report any problems to prola@aps.org PRE.

[74] R. Pastor-Satorras and A. Vespignani. Epidemic spreading in scale-free networks. *Phys Rev Lett*, 86(14):3200–3203, Apr 2001.

[75] D. J. Watts and S. H. Strogatz. Collective dynamics of 'small-world' networks. *Nature*, 393(6684):440–442, Jun 1998.

[76] Jeffrey Travers and Stanley Milgram. An experimental study of the small world problem. *Sociometry*, 32:425–443, 1967.

[77] Ed Bullmore and Olaf Sporns. Complex brain networks: graph theoretical analysis of structural and functional systems. *Nat Rev Neurosci*, 10(3):186–198, Mar 2009.

[78] Kai Yuan, Wei Qin, Jixin Liu, Qian Guo, Minghao Dong, Jinbo Sun, Yi Zhang, Peng Liu, Wei Wang, Yarong Wang, Qiang Li, Weichuan Yang, Karen M von

Deneen, Mark S Gold, Yijun Liu, and Jie Tian. Altered small-world brain functional networks and duration of heroin use in male abstinent heroin-dependent individuals. *Neurosci Lett*, 477(1):37–42, Jun 2010.

[79] C. J. Stam. Characterization of anatomical and functional connectivity in the brain: a complex networks perspective. *Int J Psychophysiol*, 77(3):186–194, Sep 2010.

[80] Reinoud Maex and Erik De Schutter. Resonant synchronization in heterogeneous networks of inhibitory neurons. *J Neurosci*, 23(33):10503–10514, Nov 2003.

[81] Marlene Bartos, Imre Vida, and Peter Jonas. Synaptic mechanisms of synchronized gamma oscillations in inhibitory interneuron networks. *Nat Rev Neurosci*, 8(1):45–56, Jan 2007.

[82] Jorge N Brea, Leslie M Kay, and Nancy J Kopell. Biophysical model for gamma rhythms in the olfactory bulb via subthreshold oscillations. *Proc Natl Acad Sci U S A*, 106(51):21954–21959, Dec 2009.

[83] T. Hattori, E. G. McGeer, and P. L. McGeer. Fine structural analysis of the cortico-striatal pathway. *J Comp Neurol*, 185(2):347–353, May 1979.

[84] Floris G Wouterlood, Amber J Boekel, Riichi Kajiwara, and Jeroen A M Belin. Counting contacts between neurons in 3d in confocal laser scanning images. *J Neurosci Methods*, 171(2):296–308, Jun 2008.

[85] M. P. Witter, P. A. Naber, T. van Haeften, W. C. Machielsen, S. A. Rombouts, F. Barkhof, P. Scheltens, and F. H. Lopes da Silva. Cortico-hippocampal communication by way of parallel parahippocampal-subicular pathways. *Hippocampus*, 10(4):398–410, 2000.

[86] Yael Amitai, Jay R Gibson, Michael Beierlein, Saundra L Patrick, Alice M Ho, Barry W Connors, and David Golomb. The spatial dimensions of electrically coupled networks of interneurons in the neocortex. *J Neurosci*, 22(10):4142–4152, May 2002.

[87] P. E. Patton and B. McNaughton. Connection matrix of the hippocampal formation: I. the dentate gyrus. *Hippocampus*, 5(4):245–286, 1995.

[88] J. F. Staiger, R. Ktter, K. Zilles, and H. J. Luhmann. Connectivity in the somatosensory cortex of the adolescent rat: an in vitro biocytin study. *Anat Embryol (Berl)*, 199(4):357–365, Apr 1999.

[89] Nuno Maarico da Costa and Kevan A C Martin. Whose cortical column would that be? *Front Neuroanat*, 4:16, 2010.

[90] Wei Liao, Zhiqiang Zhang, Zhengyong Pan, Dante Mantini, Jurong Ding, Xujun Duan, Cheng Luo, Guangming Lu, and Huafu Chen. Altered functional connectivity and small-world in mesial temporal lobe epilepsy. *PLoS One*, 5(1):e8525, 2010.

[91] Greg D Field, Jeffrey L Gauthier, Alexander Sher, Martin Greschner, Timothy A Machado, Lauren H Jepson, Jonathon Shlens, Deborah E Gunning, Keith Mathieson, Wladyslaw Dabrowski, Liam Paninski, Alan M Litke, and E. J. Chichilnisky. Functional connectivity in the retina at the resolution of photoreceptors. *Nature*, 467(7316):673–677, Oct 2010.

[92] Christophe Habas, Rmy Guillevin, and Abdelouhad Abanou. Functional connectivity of the superior human temporal sulcus in the brain resting state at 3t. *Neuroradiology*, Oct 2010.

[93] Jonathan D Power, Damien A Fair, Bradley L Schlaggar, and Steven E Petersen. The development of human functional brain networks. *Neuron*, 67(5):735–748, Sep 2010.

[94] Mormann Florian, Lehnertz Klaus, David Peter, and E. Elger Christian. Mean phase coherence as a measure for phase synchronization and its application to the eeg of epilepsy patients. *Phys. D*, 144(3-4):358–369, 2000. 361033.

[95] Jack Waddell, Rhonda Dzakpasu, Victoria Booth, Brett Riley, Jonathan Reasor, Gina Poe, and Michal Zochowski. Causal entropies–a measure for determining changes in the temporal organization of neural systems. *J Neurosci Methods*, 162(1-2):320–332, May 2007.

[96] Giulio Tononi and Olaf Sporns. Measuring information integration. *BMC Neurosci*, 4:31, Dec 2003.

[97] S. Feldt, J. Waddell, V. L. Hetrick, J. D. Berke, and M. Zochowski. Functional clustering algorithm for the analysis of dynamic network data. *Phys Rev E Stat Nonlin Soft Matter Phys*, 79(5 Pt 2):056104, May 2009.

[98] Schreiber. Measuring information transfer. *Phys Rev Lett*, 85(2):461–464, Jul 2000.

[99] D. Puthankattil Subha, Paul K Joseph, Rajendra Acharya U, and Choo Min Lim. Eeg signal analysis: a survey. *J Med Syst*, 34(2):195–212, Apr 2010.

[100] David A Leopold. Neuroscience: fmri under the spotlight. *Nature*, 465(7299):700–701, Jun 2010.

[101] Florinda Ferreri, Patrizio Pasqualetti, Sara Mtt, David Ponzo, Fabio Ferrarelli, Giulio Tononi, Esa Mervaala, Carlo Miniussi, and Paolo Maria Rossini. Human brain connectivity during single and paired pulse transcranial magnetic stimulation. *Neuroimage*, 54(1):90–102, Jan 2011.

[102] Maria Boersma, Dirk J A Smit, Henrica M A de Bie, G. Caroline M Van Baal, Dorret I Boomsma, Eco J C de Geus, Henriette A Delemarre van de Waal, and Cornelis J Stam. Network analysis of resting state eeg in the developing young brain: Structure comes with maturation. *Hum Brain Mapp*, May 2010.

[103] Jaroslav Hlinka, Charilaos Alexakis, Ana Diukova, Peter F Liddle, and Dorothee P Auer. Slow eeg pattern predicts reduced intrinsic functional connectivity in the default mode network: an inter-subject analysis. *Neuroimage*, 53(1):239–246, Oct 2010.

[104] Juliane Britz, Dimitri Van De Ville, and Christoph M Michel. Bold correlates of eeg topography reveal rapid resting-state network dynamics. *Neuroimage*, 52(4):1162–1170, Oct 2010.

[105] Martin Havlicek, Jiri Jan, Milan Brazdil, and Vince D Calhoun. Dynamic granger causality based on kalman filter for evaluation of functional network connectivity in fmri data. *Neuroimage*, 53(1):65–77, Oct 2010.

[106] Ngoc Jade Thai, Olivia Longe, and Gina Rippon. Disconnected brains: what is the role of fmri in connectivity research? *Int J Psychophysiol*, 73(1):27–32, Jul 2009.

[107] Maria Blatow, Ernst Nennig, Anita Durst, Klaus Sartor, and Christoph Stippich. fmri reflects functional connectivity of human somatosensory cortex. *Neuroimage*, 37(3):927–936, Sep 2007.

[108] C. M. Gray, P. E. Maldonado, M. Wilson, and B. McNaughton. Tetrodes markedly improve the reliability and yield of multiple single-unit isolation from multi-unit recordings in cat striate cortex. *J Neurosci Methods*, 63(1-2):43–54, Dec 1995.

[109] Woodrow L Shew, Timothy Bellay, and Dietmar Plenz. Simultaneous multi-electrode array recording and two-photon calcium imaging of neural activity. *J Neurosci Methods*, 192(1):75–82, Sep 2010.

[110] Andrew J Hill, Nicholas A Jones, Claire M Williams, Gary J Stephens, and Benjamin J Whalley. Development of multi-electrode array screening for anti-convulsants in acute rat brain slices. *J Neurosci Methods*, 185(2):246–256, Jan 2010.

[111] H. Markram and M. Segal. Long-lasting facilitation of excitatory postsynaptic potentials in the rat hippocampus by acetylcholine. *J Physiol*, 427:381–393, Aug 1990.

[112] H. Yao and Y. Dan. Stimulus timing-dependent plasticity in cortical processing of orientation. *Neuron*, 32(2):315–323, Oct 2001.

[113] Masahiko Yoshioka. Spike-timing-dependent learning rule to encode spatiotemporal patterns in a network of spiking neurons. *Phys Rev E Stat Nonlin Soft Matter Phys*, 65(1 Pt 1):011903, Jan 2002.

[114] Gal Chechik. Spike-timing-dependent plasticity and relevant mutual information maximization. *Neural Comput*, 15(7):1481–1510, Jul 2003.

[115] J. J. Hopfield and Carlos D Brody. Learning rules and network repair in spike-timing-based computation networks. *Proc Natl Acad Sci U S A*, 101(1):337–342, Jan 2004.

[116] Eugene M Izhikevich, Joseph A Gally, and Gerald M Edelman. Spike-timing dynamics of neuronal groups. *Cereb Cortex*, 14(8):933–944, Aug 2004.

[117] Johannes Hjorth, Kim T Blackwell, and Jeanette Hellgren Kotaleski. Gap junctions between striatal fast-spiking interneurons regulate spiking activity and synchronization as a function of cortical activity. *J Neurosci*, 29(16):5276–5286, Apr 2009.

[118] Michal Rivlin-Etzion, Odeya Marmor, Gali Heimer, Aeyal Raz, Asaph Nini, and Hagai Bergman. Basal ganglia oscillations and pathophysiology of movement disorders. *Curr Opin Neurobiol*, 16(6):629–637, Dec 2006.

[119] Roger L Albin. Neurobiology of basal ganglia and tourette syndrome: striatal and dopamine function. *Adv Neurol*, 99:99–106, 2006.

[120] Jane S Paulsen, Peggy C Nopoulos, Elizabeth Aylward, Christopher A Ross, Hans Johnson, Vincent A Magnotta, Andrew Juhl, Ronald K Pierson, James Mills, Douglas Langbehn, Martha Nance, P. R. E. D. I. C. T-H. D. Investigators, and Coordinators of the Huntington's Study Group (HSG). Striatal and white matter predictors of estimated diagnosis for huntington disease. *Brain Res Bull*, 82(3-4):201–207, May 2010.

[121] T. Kos and J. M. Tepper. Inhibitory control of neostriatal projection neurons by gabaergic interneurons. *Nat Neurosci*, 2(5):467–472, May 1999.

[122] Z. Clemens, B. Weiss, A. Szucs, L. Eross, G. Rsonyi, and P. Halsz. Phase coupling between rhythmic slow activity and gamma characterizes mesiotemporal rapid-eye-movement sleep in humans. *Neuroscience*, 163(1):388–396, Sep 2009.

[123] X. J. Wang and G. Buzski. Gamma oscillation by synaptic inhibition in a hippocampal interneuronal network model. *J Neurosci*, 16(20):6402–6413, Oct 1996.

[124] M. K. Sun, W. Q. Zhao, T. J. Nelson, and D. L. Alkon. Theta rhythm of hippocampal ca1 neuron activity: gating by gabaergic synaptic depolarization. *J Neurophysiol*, 85(1):269–279, Jan 2001.

[125] Joseph T Gwin, Klaus Gramann, Scott Makeig, and Daniel P Ferris. Removal of movement artifact from high-density eeg recorded during walking and running. *J Neurophysiol*, 103(6):3526–3534, Jun 2010.

[126] Ueli Rutishauser, Ian B Ross, Adam N Mamelak, and Erin M Schuman. Human memory strength is predicted by theta-frequency phase-locking of single neurons. *Nature*, 464(7290):903–907, Apr 2010.

[127] Michael V.L. Bennett and R. Suzanne Zukin. Electrical coupling and neuronal synchronization in the mammalian brian. *Neuron*, 41:495–511, 2004.

[128] Hideo Hasegawa. Synchronization in small-world network of spiking neurons:diffusive versus sigmoid couplings. *Physical Review E*, 72(056139), 2005.

[129] Nancy Kopell and Bard Ermentrout. Chemical and electrical synapses perform complementary roles in the synchronization of interneuronal networks. *Proc Natl Acad Sci U S A*, 101(43):15482–15487, Oct 2004.

[130] Elliott B Merriam, Theoden I Netoff, and Matthew I Banks. Bistable network behavior of layer i interneurons in auditory cortex. *J Neurosci*, 25(26):6175–6186, Jun 2005.

[131] Srdjan Ostojic, Nicolas Brunel, and Vincent Hakim. Synchronization properties of networks of electrically coupled neurons in the presence of noise and heterogeneities. *J Comput Neurosci*, 26(3):369–392, Jun 2009.

[132] Benjamin Pfeuty, David Golomb, Germn Mato, and David Hansel. Inhibition potentiates the synchronizing action of electrical synapses. *Front Comput Neurosci*, 1:8, 2007.

[133] Alexander B Wiltschko, Gregory J Gage, and Joshua D Berke. Wavelet filtering before spike detection preserves waveform shape and enhances single-unit discrimination. *J Neurosci Methods*, 173(1):34–40, Aug 2008.

[134] Sankari Ramanathan, Jason J Hanley, Jean-Michel Deniau, and J. Paul Bolam. Synaptic convergence of motor and somatosensory cortical afferents onto gabaergic interneurons in the rat striatum. *J Neurosci*, 22(18):8158–8169, Sep 2002.

[135] H. Kita, T. Kosaka, and C. W. Heizmann. Parvalbumin-immunoreactive neurons in the rat neostriatum: a light and electron microscopic study. *Brain Res*, 536(1-2):1–15, Dec 1990.

[136] Paul S A Kalanithi, Wei Zheng, Yuko Kataoka, Marian DiFiglia, Heidi Grantz, Clifford B Saper, Michael L Schwartz, James F Leckman, and Flora M Vaccarino. Altered parvalbumin-positive neuron distribution in basal ganglia of individuals with tourette syndrome. *Proc Natl Acad Sci U S A*, 102(37):13307–13312, Sep 2005.

[137] Alexander B Wiltschko, Gregory J Gage, and Joshua D Berke. Wavelet filtering before spike detection preserves waveform shape and enhances single-unit discrimination. *J Neurosci Methods*, 173(1):34–40, Aug 2008.

[138] Joshua D Berke, Murat Okatan, Jennifer Skurski, and Howard B Eichenbaum. Oscillatory entrainment of striatal neurons in freely moving rats. *Neuron*, 43(6):883–896, Sep 2004.

[139] Johannes Hjorth, Alex Hanna Elias, and Jeanette Hellgren Kotaleski. The significance of gap junction location in striatal fast spiking interneurons. *Neurocomputing*, 70(2007):1887–1891, 2006.

[140] J. D. Berke. Fast oscillations in cortical-striatal networks switch frequency following rewarding events and stimulant drugs. *Eur J Neurosci*, 30(5):848–859, Sep 2009.

[141] Birgit Mathes, Ulrich Pomper, Peter Walla, and Canan Basar-Eroglu. Dissociation of reversal- and motor-related delta- and alpha-band responses during visual multistable perception. *Neurosci Lett*, 478(1):14–18, Jun 2010.

[142] Anton Sirota, Sean Montgomery, Shigeyoshi Fujisawa, Yoshikazu Isomura, Michael Zugaro, and Gyrgy Buzski. Entrainment of neocortical neurons and gamma oscillations by the hippocampal theta rhythm. *Neuron*, 60(4):683–697, Nov 2008.

[143] Edward O Mann and Istvan Mody. Control of hippocampal gamma oscillation frequency by tonic inhibition and excitation of interneurons. *Nat Neurosci*, 13(2):205–212, Feb 2010.

[144] Christoph S Herrmann, Ingo Frnd, and Daniel Lenz. Human gamma-band activity: a review on cognitive and behavioral correlates and network models. *Neurosci Biobehav Rev*, 34(7):981–992, Jun 2010.

[145] Pascal Fries. Neuronal gamma-band synchronization as a fundamental process in cortical computation. *Annu Rev Neurosci*, 32:209–224, 2009.

[146] Matthew H Higgs and William J Spain. Conditional bursting enhances resonant firing in neocortical layer 2-3 pyramidal neurons. *J Neurosci*, 29(5):1285–1299, Feb 2009.

[147] Koen Vervaeke, Andrea Lorincz, Padraig Gleeson, Matteo Farinella, Zoltan Nusser, and R. Angus Silver. Rapid desynchronization of an electrically coupled interneuron network with sparse excitatory synaptic input. *Neuron*, 67(3):435–451, Aug 2010.

[148] Matthias Molle, Lisa MArchall, Steffen Gais, and Jan Born. Grouping of spindle activity during slow oscillations in human no-rapid eye movement sleep. *The Journal of Neuroscience*, 22(24):10941–10947, 2002.

[149] S. Raghavachari, M. J. Kahana, D. S. Rizzuto, J. B. Caplan, M. P. Kirschen, B. Bourgeois, J. R. Madsen, and J. E. Lisman. Gating of human theta oscillations by a working memory task. *J Neurosci*, 21(9):3175–3183, May 2001.

[150] Wolf Singer. Distributed processing and temporal codes in neuronal networks. *Cogn Neurodyn*, 3(3):189–196, Sep 2009.

[151] Y. Wang, D. T. Chik, and Z. D. Wang. Coherence resonance and noise-induced synchronization in globally coupled hodgkin-huxley neurons. *Phys Rev E Stat Phys Plasmas Fluids Relat Interdiscip Topics*, 61(1):740–746, Jan 2000.

[152] Frank Moss, Lawrence M. Ward, and Walter G. Sannita. Stochastic resonance and sensory information processing: a tutorial and review of application. *Clinical Neurophysiology*, 115(2):267, 2004. 1388-2457 doi: DOI: 10.1016/j.clinph.2003.09.014.

[153] Mark D McDonnell and Derek Abbott. What is stochastic resonance? definitions, misconceptions, debates, and its relevance to biology. *PLoS Comput Biol*, 5(5):e1000348, May 2009.

[154] Y. Yu, W. Wang, J. Wang, and F. Liu. Resonance-enhanced signal detection and transduction in the hodgkin-huxley neuronal systems. *Phys Rev E Stat Nonlin Soft Matter Phys*, 63(2 Pt 1):021907, Feb 2001.

[155] Okyu Kwon and Hie-Tae Moon. Coherence resonance in small-world networks of excitable cells. *Physics Letters A*, 298(5-6):319, 2002. 0375-9601 doi: DOI: 10.1016/S0375-9601(02)00575-3.

[156] Tobias Kalenscher, Carien S Lansink, Jan V Lankelma, and Cyriel M A Pennartz. Reward-associated gamma oscillations in ventral striatum are regionally differentiated and modulate local firing activity. *J Neurophysiol*, 103(3):1658–1672, Mar 2010.

[157] Shane Lee, Kamal Sen, and Nancy Kopell. Cortical gamma rhythms modulate nmdar-mediated spike timing dependent plasticity in a biophysical model. *PLoS Comput Biol*, 5(12):e1000602, Dec 2009.

[158] Balzs Hangya, Zsolt Borhegyi, Nra Szilgyi, Tams F Freund, and Viktor Varga. Gabaergic neurons of the medial septum lead the hippocampal network during theta activity. *J Neurosci*, 29(25):8094–8102, Jun 2009.

[159] Kenji Morita, Rita Kalra, Kazuyuki Aihara, and Hugh P C Robinson. Recurrent synaptic input and the timing of gamma-frequency-modulated firing of pyramidal cells during neocortical "up" states. *J Neurosci*, 28(8):1871–1881, Feb 2008.

[160] Theoden I Netoff, Robert Clewley, Scott Arno, Tara Keck, and John A White. Epilepsy in small-world networks. *J Neurosci*, 24(37):8075–8083, Sep 2004.

[161] Hoi Fei Kwok, Peter Jurica, Antonino Raffone, and Cees van Leeuwen. Robust emergence of small-world structure in networks of spiking neurons. *Cogn Neurodyn*, 1(1):39–51, Mar 2007.

[162] Cornelis J Stam and Jaap C Reijneveld. Graph theoretical analysis of complex networks in the brain. *Nonlinear Biomed Phys*, 1(1):3, 2007.

[163] Nicholas Fisher, Sachin S Talathi, Paul R Carney, and William L Ditto. Effects of phase on homeostatic spike rates. *Biol Cybern*, 102(5):427–440, May 2010.

[164] Olaleke O Oke, Andor Magony, Himashi Anver, Peter D Ward, Premysl Jiruska, John G R Jefferys, and Martin Vreugdenhil. High-frequency gamma oscillations coexist with low-frequency gamma oscillations in the rat visual cortex in vitro. *Eur J Neurosci*, 31(8):1435–1445, Apr 2010.

[165] Iezzi Ennio, Suppa Antonio, Conte Antonella, Agostino Rocco, Nardella Andrea, and Berardelli Alfredo. Theta-burst stimulation over primary motor cortex degrades early motor learning. *European Journal of Neuroscience*, 31(3):585–592. 10.1111/j.1460-9568.2010.07090.x.

[166] Pawel Kudela, Piotr J Franaszczuk, and Gregory K Bergey. Changing excitation and inhibition in simulated neural networks: effects on induced bursting behavior. *Biol Cybern*, 88(4):276–285, Apr 2003.

[167] Magdalena Sanhueza and Juan Bacigalupo. Intrinsic subthreshold oscillations of the membrane potential in pyramidal neurons of the olfactory amygdala. *Eur J Neurosci*, 22(7):1618–1626, Oct 2005.

[168] Andrew P Maurer and Bruce L McNaughton. Network and intrinsic cellular mechanisms underlying theta phase precession of hippocampal neurons. *Trends Neurosci*, 30(7):325–333, Jul 2007.

[169] George Dragoi and Gyrgy Buzski. Temporal encoding of place sequences by hippocampal cell assemblies. *Neuron*, 50(1):145–157, Apr 2006.

[170] Avishek Adhikari, Mihir A Topiwala, and Joshua A Gordon. Synchronized activity between the ventral hippocampus and the medial prefrontal cortex during anxiety. *Neuron*, 65(2):257–269, Jan 2010.

[171] Torfi Sigurdsson, Kimberly L Stark, Maria Karayiorgou, Joseph A Gogos, and Joshua A Gordon. Impaired hippocampal-prefrontal synchrony in a genetic mouse model of schizophrenia. *Nature*, 464(7289):763–767, Apr 2010.

[172] Keiji Miura and Masato Okada. Pulse-coupled resonate-and-fire models. *Phys Rev E Stat Nonlin Soft Matter Phys*, 70(2 Pt 1):021914, Aug 2004.

[173] J. Feng. Is the integrate-and-fire model good enough?–a review. *Neural Netw*, 14(6-7):955–975, 2001.

[174] Arkady Pikovsky, Michael Zaks, Michael Rosenblum, Grigory Osipov, and Jurgen Kurths. Phase synchronization of chaotic oscillations in terms of periodic orbits. *Chaos*, 7(4):680–687, Dec 1997.

[175] Rosenblum, Pikovsky, and Kurths. Phase synchronization of chaotic oscillators. *Phys Rev Lett*, 76(11):1804–1807, Mar 1996.